The Dissertation Committee for Ayou Hao Certifies that this is the approved version of the following dissertation:

Mechanical and Thermal Properties of Kenaf/Polypropylene Nonwoven Composites

Committee:

Jonathan Y. Chen, Supervisor

Joseph H. Koo, Co-Supervisor

Desiderio, Kovar

Mourad, Krifa

Li, Shi

Bugao, Xu

Mechanical and Thermal Properties of Kenaf/Polypropylene Nonwoven Composites

by

Ayou Hao, B.Textile.E.

Dissertation

Presented to the Faculty of the Graduate School of

The University of Texas at Austin

in Partial Fulfillment

of the Requirements

for the Degree of

Doctor of Philosophy

The University of Texas at Austin

May 2013

Dedication

To my grandmother Xingyuan Yin

Acknowledgements

I would like to thank my advisor, Dr. Jonathan Y. Chen, for his help and support. Dr. Chen gave me the freedom to explore areas interest with a great amount of independence.

I would also like to thank my co-advisor, Dr. Joseph H. Koo, for teaching me to be a successful person and providing valuable guidance along the way.

I would like to acknowledge my committee members: Dr. Desiderio Kovar, Dr. Mourad Krifa, Dr. Li Shi, and Dr. Bugao Xu for their valuable suggestions to strengthen this work.

Appreciations also extend to my collaborators providing me with pleasant cooperation experience over these last four and a half years at UT Austin. In particular, I would like to thank Dr. Haifeng Zhao for his great support and mentorship in the area of engineering mechanics. In addition, I thank Lin Yuan and Si Chon Lao for their valuable technical discussion about this research.

I would also like to express my gratitude to my undergraduate advisor, Dr. Bohong Gu, from Department of Textiles at Donghua University and the other mentor, Dr. Qun Xu, from Department of Materials Science and Engineering at Zhengzhou University for starting me down the road towards the area of polymeric composites.

I would also like to thank my friends: Xinran, Yuming, Jingjing, Tianyi, Sally Bernie, and other friends in life group for giving me the cherished memories.

Finally, I'd like to thank my family. I'm grateful to my parents for their continuous encouragement and patience. I'm especially grateful to my husband, Yizhuo Chen, for his support, dedication and endless love.

Mechanical and Thermal Properties of Kenaf/Polypropylene Nonwoven Composites

Ayou Hao, Ph.D.

The University of Texas at Austin, 2013

Supervisor: Jonathan Y. Chen

Co-supervisor: Joseph H. Koo

The objectives of this research are to characterize the mechanical and thermal performance of natural fiber nonwoven composites and to predict the composite strength and long-term creep performance. Three natural fibers: kenaf, jute, and sunn hemp as potential candidates were compared in terms of physical, thermal and mechanical properties. In order to see the effects of fiber surface chemical treatment, sunn hemp fiber was treated with sodium hydroxide (NaOH) agent. Kenaf fiber was selected for the following study due to the higher specific modulus and the moderate price of kenaf fiber. After alkaline treatment, the moisture content, glass-transition temperature, and decomposition temperature of sunn hemp fiber increased but not significantly.

The mechanical performance of kenaf/polypropylene nonwoven composites (KPNCs) in production of automotive interior parts was investigated. The uniaxial tensile, three-point bending, in-plane shearing, and Izod impact tests were performed to evaluate the composite mechanical properties. The thermal properties were evaluated using TGA, DSC, and DMA. An adhesive-free sandwich structure was found to have excellent impact resistance performance. Based on the evaluation of mechanical and

thermal properties, manufacturing conditions of 230 C and 120 s for 6 mm thick sample and 230 C and 60 s for 3 mm thick samples were selected.

The open-hole and pin filled-hole effects on the tensile properties of KPNCs in production of automotive interior parts were investigated. Three specimen width -to-hole diameter (W/D) ratios of 6, 3 and 2 were evaluated. A preliminary model by extended finite element method (XFEM) was established to simulate the composite crack propagation. Good agreement was found between experimental and simulation results. Mechanical properties of the KPNCs in terms of uniaxial tensile, open-hole tensile (OHT), and pin filled-hole tensile (FHT) were measured experimentally. By calculating the stress concentration factor Kt for brittle materials, the net section stress factor Kn for ductile materials, and the strength reduction factor Kr, it was found that KPNC was relatively ductile and insensitive to the notch.

The strain rate effects on the tensile properties of KPNC were studied. The strain rate effects confirmed the time-dependence of KPNCs. Afterward, the creep behavior of KPNC and PP performed by DMA was investigated extensively. The linear viscoelastic limit (LVL) was found to be 1 MPa in this study. The long-term creep behavior of KPNC compared to virgin PP plastic was predicted using the time-temperature superposition (TTS) principle. Three-day creep tests were also conducted to verify the effectiveness of TTS prediction. It was found that the master curve for PP fit better with the three-day creep data than KPNC, due to the multiphase thermo-rheological complexity of KPNC. The creep recovery, stress effects and cyclic creep performance were also evaluated. Two popular creep models: the four-element Burgers model and the Findley power law model were used to simulate the creep behavior in this study. It was found that KPNC had higher creep resistance and better creep recoverability than virgin PP plastics.

Table of Contents

List of Tables

List of Figures

Chapter 1: Introduction

1.1 Literature Review

1.1.1 Natural Fibers

Industrial uses of natural fibers have increasingly gained attention from various manufacturing sectors due to the public concern for energy security and environmental protection (Hao et al., 2008a; Hao et al., 2010; Jiang et al., 2011). Lignocellulosic natural fibers such as kenaf, jute, sunn hemp, ramie, sisal and coir fibers have many technical and environmental advantages over synthetic fiber materials. These fibers have specifically desirable properties such as stiffness (Eichhorn et al., 2001; Sherman, 1999), impact resistance (Sydenstricker et al., 2003), and flexibility (Nair et al., 1996). In addition, they are available in large quantities (Maldas et al., 1988), and are renewable, biodegradable, and almost CO_2-neutral in production (Pervaiz & Sain, 2003). Other desirable properties include low cost, low density, less equipment abrasion (Nair et al., 1996; Toriz et al., 2002), less skin and respiratory irritation (Karnani et al., 1997), vibration damping (Sherman, 1999; Sydenstricker et al., 2003) and enhanced energy recovery (Karnani et al., 1997; Mohanty et al., 2000). The hydrophilicity of natural fibers results high moisture absorption. The physical properties of natural fibers are mainly determined by the structure, cellulose content, and degree of polymerization. Fiber structure can be modified using physical and/or chemical treatments.

Kenaf (*Hibiscus cannabinus*) is the bast of the kenaf plant, which constitutes 40% of the plant. It contains cellulose (44–57%), hemi-cellulose (22–23%), lignin (15–19%) ash (2–5%), and other elements (~6%) (Kozłowski & Władyka-Przybylak, 2008). Kenaf yields 6 to 10 tons of dry fiber per acre per year. It is estimated that the annual output of kenaf fiber is 330 thousand tons worldwide (Chen & Liu, 2010). Mechanical properties

of kenaf fiber are similar to those of jute fiber, but kenaf fiber is stronger, whiter, and more lustrous. Kenaf has been used for thousands of years as cordage, canvas, sacking, and fish net due to its mildew resistance (Cook, 1984). Due to a worldwide shortage of forestry resources, a major application of kenaf in the 1980s was in the pulp and paper industry as a substitution of wood (Kador et al., 1990). Kenaf can also be used to make building materials such as particleboards or fiber boards in the furniture and interior decoration industry. Kenaf was one of the main components to build a special three layer structure flame-resistant lignocellulosic particleboard (Kozlowski et al., 1999). In addition, the woody core of kenaf has a potential application for low-density panels used for thermal resistance or sound absorption building materials (Sellers Jr et al., 1993). As an abundant source of natural fiber, kenaf also has been increasingly used in the fiber reinforced composites in recent decades.

White jute (*Corchorus capsularis*) and tossa jute (*Corchorus olitorius*) are the second most important vegetable fibers after cotton, in terms of global consumption and availability. The annual worldwide yield of jute fiber is about ten times that of kenaf fiber. But almost all jute production in the world is from India and Bangladesh. Jute fiber is finer than kenaf fiber and is mostly used in the agricultural and industrial fields (IJSG, 2013).

Sunn hemp (*Crotalaria juncea L.*) is one of the earliest fibers of India. It has been utilized as a green manure, livestock feed, and as a non-wood fiber crop. Sunn hemp can produce over 5,604 kg/ha of biomass and over 112 kg/ha of nitrogen when grown as a summer annual. When closely spaced, the sunn hemp plants grow to a height of 3 m, with a stem diameter of up to 25 mm. The plant produces 2–4% by wt of dry fiber. The fiber is actually a bundle of sub-fibers. Fiber walls are reinforced with spirally oriented cellulose in a hemi-cellulose and lignin matrix. The chemical composition of sunn hemp fiber is

67.8 wt% cellulose, 16.6 wt% hemi-cellulose, 0.3 wt% pectin, 3.5 wt% lignin, 1.4 wt% soluble, 0.4% wt% waxes, and 10 wt% water (Lewin, 2006). Apart from ramie, sunn hemp fiber has the highest amount of α-cellulose compared to all other bast and leaf fibers. Past research showed that the soft, lignified sunn hemp fiber has a shiny luster, fine texture and high tensile strength, but it is coarser and stiffer than jute fiber. Therefore, its end-uses are limited to canvas, sailcloth, industrial ropes, nets and twines (Lewin, 2006). More recent efforts have indicated that other potential products can be developed from sunn hemp fiber such as commercial nursery application, newsprint, and specialty papers (Cook & White, 1996). Additional characteristics that enhance the potential value of sunn hemp as a non-wood fiber crop are low nitrogen fertilization requirements, the ability to fix nitrogen and to grow in marginal soils, and drought resistance.

1.1.2 Natural Fiber Reinforced Polymer Matrix Composites (PMCs)

The use of natural fibers in PMCs is growing rapidly to meet diverse end uses in transportation, geotextiles, low cost building, and other construction industries (Chapman, 2010; Singh & Gupta, 2005). Natural fibers play an important role in developing biodegradable composites to substitute for glass or carbon fiber-reinforced plastics because of the growing concerns of global warming and the rising price of petroleum-based products (Joshi et al., 2004; Wambua et al., 2003). Natural fiber reinforced PMCs from renewable natural resources offer several advantages such as high specific strength and modulus (Edeerozey et al., 2007), impact resistance (Sydenstricker et al., 2003), and bending flexibility (Nair et al., 1996), low cost, low density (Zampaloni et al., 2007), renewable nature (Jiang et al., 2011), biodegradability, no health hazards, and low CO_2 emission in production (Pervaiz & Sain, 2003). PMCs based on kenaf fiber

and matrices of thermosets such as epoxy (Xue et al., 2009) and polyester resin (Aziz & Ansell, 2004), and thermoplastics such as polypropylene (Hao et al., 2012a; Hao et al., 2012b; Hao et al., 2012c), polylactic acid (PLA) (Hao et al., 2008a; Yussuf et al., 2010), and polyvinyl alcohol (PVA) (Chen et al., 2005b) have been reported.

The mechanical properties of natural fiber reinforced PMCs have been investigated over the past few decades. Davoodi (Davoodi et al., 2010) studied the hybrid kenaf/glass reinforced epoxy composite for use in car bumper beams. Shinji (Shinji, 2008) investigated kenaf/PLA composites and found out the mechanical properties of such composites increase with increasing kenaf fiber volume fraction up to 70%. Kenaf fiber was also proven to have a higher reinforcing effect on natural rubber compared with that of synthetic polyester fibers, and improved the rheological properties of the rubber (El-Sabbagh et al., 2001). Shibata (Shibata et al., 2008) evaluated a composite with randomly oriented fibers that was made from biodegradable resin and kenaf fibers and established a Cox's model to predict the flexural properties. The major problem with the natural fiber reinforced composites is the low adhesion between the surface of the fiber and the matrix. The possible treatments of the fiber surface were therefore studied by researchers. Herrera-Franco (Herrera-Franco & Valadez-González, 2004; Herrera-Franco & Valadez-González, 2005) evaluated the mechanical properties of short and continuous henequen fiber reinforced high density polyethylene composites after silane coupling agent treatment. Jacobs (Jacob et al., 2004) concluded that the alkali treated sisal/oil palm hybrid fiber reinforced rubber composites exhibited better tensile properties than untreated composites. Because the interface modification methods can improve the fiber–matrix adhesion, composite strength is ultimately increased.

1.1.3 Natural Fiber Nonwoven Composites

The nonwoven fabric, which is defined as a sheet or web of directionally or randomly oriented fibers, bonded by friction, cohesion or adhesion, provides low-cost reinforcement for composites. Due to this lack of fiber orientation, nonwoven fabrics are usually bulkier than woven or knitted fabrics and the density of nonwoven fabric varies with fiber type and construction (Wang & Li, 1995).

The needle-punching technique uses an array of barbed needles repeatedly penetrating through the nonwoven fiber web to form fiber entanglements and results in a 3D fiber orientation. The fiber webs become more compact after needle-punching due to the friction of entangled fibers. A number of fibers are oriented vertically to the fiber web plane after the needles are removed, making these fiber bundles act as "nails" punching into the fiber web. Therefore, the out-of-plane strength of nonwoven felts is enhanced. In addition, needle-punching helps prevent the fiber-fiber slipping when the nonwoven felt is subject to tension in plane. Needle-punched nonwoven composites offer good interlaminar, shear and compressive properties (Wang, 1999). Because fiber is laid randomly in the fabric plane for most nonwoven felts, the in-plane properties of such nonwoven composites are less anisotropic than other types of fiber composites such as a woven composites (Song et al., 2012).

Kenaf/polypropylene nonwoven composites (KPNCs) are ideal for producing bio-based auto interior parts because they can reduce vehicle weight for higher fuel efficiency; lower production cost by time and energy saving; enhance vehicle acoustical performance; and improve passenger safety (Chapman, 2010). Consequently, KFNC is nowadays increasingly used as a substitute for petroleum based injection molded plastics and glass fiber-reinforced composites in auto interior manufacture, such as passenger carpet, door panel trim, headliner, trunk trim and so on (Chapman, 2010). Expanded use

of these green materials will bring environmental benefits in terms of carbon sequestration (Mohanty et al., 2002), green house gas reduction (Dornburg et al., 2003), and an increase of vehicle fuel efficiency (Pervaiz & Sain, 2003).

Nonwoven fabrication followed by compression molding has some advantages over resin transfer molding and injection molding. It is a one-shot process with reduced processing time for thermoplastic polymers, energy saving, and cost effectiveness. However, little attention has been paid to the nonwoven fabrication and compression molding technique for producing KPNCs used in this research. There is also little work on characterization of the nonwoven composite mechanical and thermal behavior that is distinct from traditional metal or plastic materials. Most prevalent counterparts to KPNCs are natural fiber reinforced PMCs. PMCs are normally processed using resin transfer molding and injection molding technique (Hao et al., 2008b; Keller, 2003; Rouison et al., 2006; Xie et al., 2002). The fiber content in PMCs is usually up to 30% by weight, meaning that the polymer matrix takes up a higher fraction of the composite. In contrast, the fiber content of KPNCs is 50–70% by weight (Hao et al., 2012b). With such a high fiber fraction, kenaf fiber is therefore the dominant material and most load-bearing component in KPNCs. Besides, the higher the natural fiber content, the more environmental friendly is the composite. The melt polypropylene (PP) fiber works like glue that bonds the intersected kenaf fiber. Due to the nature of nonwoven fabrication, natural fibers are randomly oriented in-plane. In this nonwoven web structure, natural fiber and polymer bonding fiber are intersected with overlap points. This gives KPNC a porous structure, instead of a continuous polymer matrix structure. Therefore, this nonwoven fabrication followed by compression molding allows KPNCs to have a higher natural fiber content that tends to improve composite biodegradability.

Kenaf fiber varies in physical structure (diameter, shape), chemical content and mechanical properties due to the intrinsic inhomogeneous nature. The plant variety, growing environment and processing conditions will greatly affect the fiber properties. Thus, the testing results of KPNC have relatively larger variations than homogeneous materials. Due to the limitation of lab-scale manufacture, samples were not fabricated at the same time in Chapters 3, 4 and 5. Therefore, a maximum of 20% difference on composite Young's moduli of samples used in different chapters was expected in this dissertation. However, samples within a given chapter exhibited less variation.

1.2 RESEARCH OBJECTIVES

The objectives of the research are to investigate the processability of natural fibers in making nonwoven composites for automotive interior parts; to characterize the composites' mechanical and thermal performance; and to predict the composite strength and long-term creep performance. The current end-use performance criteria of automotive interior parts are determined by the properties of PP plastics. By evaluating composites' end-use performance, the manufacturing conditions that improve the performance can be obtained. For industrial mass production, end-use performance of natural fiber nonwoven composites needs to be predictable, so that auto makers' various requirements can be incorporated in the stage of interior design. One of the research goals is to identify testing methods and techniques that allow assessment of nonwoven composite end-use performance based on the mechanical and thermal characteristics.

1.3 RESEARCH INNOVATIONS

This research has several innovations comparing with previous results from our research group and also with other researchers' work. First, manufacture conditions like temperature, pressure and time are controlled precisely and consistently by a compression molding machine unlike previously published research (Chen et al., 2005a; Chen et al., 2007; Chen et al., 2005b) . The influence of manufacture conditions on the mechanical and thermal behavior of KPNCs was investigated. Secondly, the previous research in our lab has drawn some conclusions by statistically analyzing the experimental data, but these specific conclusions cannot be applied to general models. Therefore, the finite element method (FEM) was utilized to model the mechanical properties of 2D nonwoven composite panels. This well-fit model can be extended to be applied on the 3D composites for future studies. In addition, the notch effects on the tensile properties of KPNCs were also evaluated. The notch effects have a very significant meaning in the composite pin joint design application. The failure strength prediction and crack propagation simulation were also performed using extended finite element method (XFEM). There are limited studies on the crack propagation analysis by XFEM because this method was firstly introduced in 2000. An extensive study on the creep behavior of KPNCs was also carried out and compared with virgin PP plastics to see if KPNC was applicable to substitute PP plastics. Finally, a sandwich structure was designed to have a superior impact resistant performance. All this research work is original.

1.3 DISSERTATION OVERVIEW

Chapter 2 starts with the research on natural fiber selection. Three natural fibers: kenaf, jute, and sunn hemp as potential candidates were compared in terms of physical,

thermal and mechanical properties. Combining with literature data, kenaf fiber without chemical treatment was selected in subsequent chapters.

In Chapter 3, the influence of manufacturing conditions on the mechanical and thermal properties of KPNCs was investigated. The best process condition combinations among the samples tested in this chapter was found. Two sample thicknesses: 3 mm and 6 mm were selected. The 3 mm thick samples have twice the density than that of 6 mm thick samples in this chapter. Two samples, one has the highest modulus and the other has the largest elongation at break were used for the study in Chapter 4.

In Chapter 4, notch effects on the tensile properties of KPNCs were studied by performing open-hole and pin filled-hole tensile tests. A preliminary XFEM model was established to simulate crack propagation near the notch. Two sample thicknesses of 3 mm and 6 mm were selected. The 3 mm thick samples have the same density with 6 mm thick samples in this chapter.

In Chapter 5, the strain rate effects on KPNC were first investigated. It was found that KPNC is sensitive to strain rate, indicating a viscoelastic behavior of this composite. Therefore, the creep behavior of KPNCs in comparison with solid virgin PP plastics was investigated. The long-term service performance of KPNCs was predicted based on the time-temperature superposition (TTS) principle.

1.4 REFERENCES

Aziz, S.H., Ansell, M.P. 2004. The effect of alkalization and fibre alignment on the mechanical and thermal properties of kenaf and hemp bast fibre composites: Part 1 – polyester resin matrix. *Composites Science and Technology*, **64**(9), 1219-1230.

Chapman, R.A. 2010. Applications of nonwovens on technical textiles. in: *Nonwoven textiles in automotive interiors*, (Ed.) Y. Chen, CRC Press LLC. Boca Raton.

Chen, J., Liu, F. 2010. Bast fibers: from plants to products 1ed. in: *Industrial Crops and Uses*, (Ed.) B.P. Singh, CABI. Cambridge, UK, pp. 308-325.

Chen, Y., Chiparus, O., Sun, L., Negulescu, I., Parikh, D.V., Calamari, T.A. 2005a. Natural fibers for automotive nonwoven composites. *Journal of Industrial Textiles*, **35**(Compendex), 47-62.

Chen, Y., Sun, L., Negulescu, I., Wu, Q., Henderson, G. 2007. Comparative Study of Hemp Fiber for Nonwoven Composites. *Journal of Industrial Hemp*, **12**(1), 27 - 45.

Chen, Y., Sun, L.F., Chiparus, O., Negulescu, I., Yachmenev, V., Warnock, M. 2005b. Kenaf/ramie composite for automotive headliner. *Journal of Polymers and the Environment*, **13**(2), 107-114.

Cook, C.G., White, G.A. 1996. *Crotalaria juncea: a potential multi-purpose fiber crop*. ASHS Press, Arlington, VA.

Cook, J.G. 1984. *Handbook of textile fibers*. Merrow Publishing Co. Ltd.

Davoodi, M.M., Sapuan, S.M., Ahmad, D., Ali, A., Khalina, A., Jonoobi, M. 2010. Mechanical properties of hybrid kenaf/glass reinforced epoxy composite for passenger car bumper beam. *Materials & Design*, **31**(10), 4927-4932.

Dornburg, V., Lewandowski, I., Patel, M. 2003. Comparing the land requirements, energy savings, and greenhouse gas emissions reduction of biobased polymers and bioenergy. *Journal of Industrial Ecology*, **7**(3 - 4), 93-116.

Edeerozey, A.M.M., Akil, H.M., Azhar, A.B., Ariffin, M.I.Z. 2007. Chemical modification of kenaf fibers. *Materials Letters*, **61**(10), 2023-2025.

Eichhorn, S.J., Baillie, C.A., Zafeiropoulos, N., Mwaikambo, L.Y., Ansell, M.P., Dufresne, A., Entwistle, K.M., Herrera-Franco, P.J., Escamilla, G.C., Groom, L., Hughes, M., Hill, C., Rials, T.G., Wild, P.M. 2001. Review: Current international research into cellulosic fibres and composites. *Journal of Materials Science*, **36**(9), 2107-2131.

El-Sabbagh, S., El-Hariri, D., El-Ghaffar, M. 2001. Effect of kenaf fibres on the properties of natural rubber vulcanizates. *Polymers & polymer composites*, **9**(8), 549-560.

Hao, A., Geng, Y., Xu, Q., Lu, Z., Yu, L. 2008a. Study of different effects on foaming process of biodegradable PLA/starch composites in supercritical/compressed carbon dioxide. *Journal of Applied Polymer Science*, **109**(4), 2679-2686.

Hao, A., Jiang, W., Chen, J. 2010. Sunn hemp fiber physical and thermal properties in comparison with kenaf and jute fibers. in: *Plant Fibers as Renewable Feedstocks for Biofuel and Bio-based Products*, (Ed.) F. Liu, CCG International Inc., pp. 2-15.

Hao, A., Sun, B., Qiu, Y., Gu, B. 2008b. Dynamic properties of 3-D orthogonal woven composite T-beam under transverse impact. *Composites Part A: Applied Science and Manufacturing*, **39**(7), 1073-1082.

Hao, A., Yuan, L., Zhao, H., Jiang, W., Chen, J.Y. 2012a. Notch effects on the tensile property of kenaf/polypropylene nonwoven composites in: *American Society of Mechanical Engineers IMECE2012-87108* Houston, TX.

Hao, A., Zhao, H., Jiang, W., Chen, J.Y. 2012b. Kenaf fiber nonwoven composites as automotive interior material: mechanical, thermal, and acoustical performance. in: *Society for the Advancement of Material and Process Engineering (SAMPE)*. May 21-24, Baltimore, MD.

Hao, A., Zhao, H., Jiang, W., Yuan, L., Chen, J. 2012c. Mechanical properties of kenaf/polypropylene nonwoven composites. *Journal of Polymers and the Environment*, **20**(4), 959-966.

Herrera-Franco, P.J., Valadez-González, A. 2004. Mechanical properties of continuous natural fibre-reinforced polymer composites. *Composites Part A: Applied Science and Manufacturing*, **35**(3), 339-345.

Herrera-Franco, P.J., Valadez-González, A. 2005. A study of the mechanical properties of short natural-fiber reinforced composites. *Composites Part B: Engineering*, **36**(8), 597-608.

IJSG. 2013. International Jute Study Group. Available from: http://www.jute.org/index.php Access on January 27, 2013.

Jacob, M., Thomas, S., Varughese, K.T. 2004. Mechanical properties of sisal/oil palm hybrid fiber reinforced natural rubber composites. *Composites Science and Technology*, **64**(7–8), 955-965.

Jiang, W., Sun, L., Hao, A., Chen, J.Y. 2011. Regenerated cellulose fibers from waste bagasse using ionic liquid. *Textile Research Journal*, **81**(18), 1949-1958.

Joshi, S., Drzal, L., Mohanty, A., Arora, S. 2004. Are natural fiber composites environmentally superior to glass fiber reinforced composites? . *Composites Part A: Applied Science and Manufacturing*, **35**(3), 371-376.

Kador, A.F., Karlgren, C., Verwest, H.K. 1990. A Fast Growing Fiber Source for Papermaking. *Tappi Journal*, **73**(11), 205-209.

Karnani, R., Krishnan, M., Narayan, R. 1997. Biofiber-reinforced polypropylene composites. *Polymer Engineering & Science*, **37**(2), 476-483.

Keller, A. 2003. Compounding and mechanical properties of biodegradable hemp fibre composites. *Composites Science and Technology*, **63**(9), 1307-1316.

Kozlowski, R., Mieleniak, B., Helwig, M., Przepiera, A. 1999. Flame resistant lignocellulosic-mineral composite particleboards. *Polymer Degradation and Stability*, **64**(3), 523-528.

Kozłowski, R., Władyka-Przybylak, M. 2008. Flammability and fire resistance of composites reinforced by natural fibers. *Polymers for Advanced Technologies*, **19**(6), 446-453.

Lewin, M. 2006. *Handbook of fiber chemistry*. CRC, Boca Raton, FL

Maldas, D., Kokta, B.V., Raj, R.G., Daneault, C. 1988. Improvement of the mechanical properties of sawdust wood fibre--polystyrene composites by chemical treatment. *Polymer*, **29**(7), 1255-1265.

Mohanty, A., Misra, M., Drzal, L. 2002. Sustainable bio-composites from renewable resources: opportunities and challenges in the green materials world. *Journal of Polymers and the Environment*, **10**(1), 19-26.

Mohanty, A.K., Misra, M., Hinrichsen, G. 2000. Biofibres, biodegradable polymers and biocomposites: An overview. *Macromolecular Materials and Engineering*, **276-277**(1), 1-24.

Nair, K.C.M., Diwan, S.M., Thomas, S. 1996. Tensile properties of short sisal fiber reinforced polystyrene composites. *Journal of Applied Polymer Science*, **60**(9), 1483-1497.

Pervaiz, M., Sain, M.M. 2003. Carbon storage potential in natural fiber composites. *Resources, Conservation and Recycling*, **39**(4), 325-340.

Rouison, D., Sain, M., Couturier, M. 2006. Resin transfer molding of hemp fiber composites: optimization of the process and mechanical properties of the materials. *Composites Science and Technology*, **66**(7–8), 895-906.

Sellers Jr, T., Miller, G.D., Fuller, M.J. 1993. Kenaf core as a board raw material. *Forest products journal*, **43**(7-8), 69-71.

Sherman, L. 1999. Natural fibers: the new fashion in automotive plastics. in: *Plastics Technology*, Vol. 45, Gardner Publications, Inc., pp. 62-68.

Shibata, S., Cao, Y., Fukumoto, I. 2008. Flexural modulus of the unidirectional and random composites made from biodegradable resin and bamboo and kenaf fibres. *Composites Part A: Applied Science and Manufacturing*, **39**(4), 640-646.

Shinji, O. 2008. Mechanical properties of kenaf fibers and kenaf/PLA composites. *Mechanics of Materials*, **40**(4–5), 446-452.

Singh, B., Gupta, M. 2005. Natural fiber composites for building applications. in: *Natural Fibers, Biopolymers, and Biocomposites*, CRC Press.

Song, F., Zhao, H., Hu, G. 2012. Explicit cross-link relations between effective elastic modulus and thermal conductivity for fiber composites. *Computational Materials Science*, **51**(1), 353-359.

Sydenstricker, T.H.D., Mochnaz, S., Amico, S.C. 2003. Pull-out and other evaluations in sisal-reinforced polyester biocomposites. *Polymer Testing*, **22**(4), 375-380.

Toriz, G., Denes, F., Young, R.A. 2002. Lignin-polypropylene composites. Part 1: Composites from unmodified lignin and polypropylene. *Polymer Composites*, **23**(5), 806-813.

Wambua, P., Ivens, J., Verpoest, I. 2003. Natural fibres: can they replace glass in fibre reinforced plastics? *Composites Science and Technology*, **63**(9), 1259-1264.

Wang, Y. 1999. Effect of Consolidation Method on the Mechanical Properties of Nonwoven Fabric Reinforced Composites. *Applied Composite Materials*, **6**(1), 19-34.

Wang, Y., Li, J. 1995. Properties of Composites Reinforced With E-Glass Nonwoven Fabrics. *Journal of Advanced Materials*, **26**(3), 28-34.

Xie, X.L., Fung, K.L., Li, R.K.Y., Tjong, S.C., Mai, Y.W. 2002. Structural and mechanical behavior of polypropylene/ maleated styrene-(ethylene-co-butylene)-styrene/sisal fiber composites prepared by injection molding. *Journal of Polymer Science Part B: Polymer Physics*, **40**(12), 1214-1222.

Xue, Y., Du, Y., Elder, S., Wang, K., Zhang, J. 2009. Temperature and loading rate effects on tensile properties of kenaf bast fiber bundles and composites. *Composites Part B: Engineering*, **40**(3), 189-196.

Yussuf, A.A., Massoumi, I., Hassan, A. 2010. Comparison of polylactic acid/kenaf and polylactic acid/rise husk composites: the influence of the natural fibers on the mechanical, thermal and biodegradability properties. *Journal of Polymers and the Environment*, **18**(3), 422-429.

Zampaloni, M., Pourboghrat, F., Yankovich, S.A., Rodgers, B.N., Moore, J., Drzal, L.T., Mohanty, A.K., Misra, M. 2007. Kenaf natural fiber reinforced polypropylene composites: A discussion on manufacturing problems and solutions. *Composites Part A: Applied Science and Manufacturing*, **38**(6), 1569-1580.

Chapter 2: Preliminary Analysis of Candidate Natural Fibers

2.1 INTRODUCTION

This chapter focused on comparing kenaf, jute, sunn hemp and treated sunn hemp fibers in terms of the physical and thermal properties. Comparison was also conducted on the mechanical properties by literature review. Jute and kenaf fibers were selected as candidates because a lot of previous work has been done on these two fibers in our research group. Sunn hemp fiber was selected because the United States Department of Agriculture (USDA) supplied the material and was interested in the potential applications of sunn hemp fiber. Sunn hemp fiber was treated with sodium hydroxide (NaOH) agent in order to see the effects of fiber surface chemical treatment, because there was limited literature on the surface modification on sunn hemp fiber. In contrast, such literature was well established on kenaf and jute fibers (Gassan & Bledzki, 1999a; Mazumder et al., 2000; Sgriccia et al., 2008). The potential of enhancing fiber quality and expanding fiber uses by surface modification on the physical and thermal properties of sunn hemp fibers was analyzed. By examining the physical, thermal and mechanical properties of three fibers, the most suitable fiber was chosen to use in this research.

The changes introduced by the alkali treatment on the chemical structure of sunn hemp fiber were analyzed by infrared spectroscopy (FTIR). The thermal behavior of four fibers was studied by thermogravimetric analysis (TGA) and differential scanning calorimetry (DSC). The biological structure of natural fiber was examined by optical microscopy (OM) and scanning electron microscopy (SEM). The data indicated that kenaf fiber had higher thermal stability than sunn hemp and jute fibers. After alkaline treatment, the moisture content, glass-transition temperature and decomposition temperature of sunn hemp fiber increased but not significantly.

The interface modification was proven to be an effective way to improve the mechanical properties of natural fiber and natural fiber reinforced composites (Bledzki et al., 1996; Herrera-Franco & Valadez-González, 2004; Herrera-Franco & Valadez-González, 2005; Jacob et al., 2004). Current interface modification methods include plasma treatment (Yuan et al., 2004), graft copolymerization (Heikal & El-Kalyoubi, 1982), and fiber surface chemical treatment (Gassan & Bledzki, 1997; Valadez-Gonzalez et al., 1999). Because the interface modification methods can improve the fiber–matrix adhesion, composite strength is ultimately increased. However, the interface modification process will cost extra time, energy and money. Therefore, by comparing the fiber properties before and after surface modification, it could be determined whether or not a chemical treatment is needed on natural fibers.

2.2 EXPERIMENTAL DETAILS

2.2.1 Materials

Kenaf fiber with grade KHB/WF/320 and jute/tossa fiber with grade KHB/TF/42 were provided by the Golden Fiber Trade Center Ltd. (Dhaka, Bangladesh). Sun hemp fiber was supplied by USDA ARS (Florence, South Carolina) in the form of the original dried plant. Figure 2.1 shows a picture of sunn hemp plants in the field. Chemical fiber extraction was processed by the following steps after the sunn hemp was received:

- The skin layer of sunn hemp stem was peeled off and immersed in 500 ml solution containing 1g/L H_2SO_4 at 50 °C for 1 h with a material to liquid volume ratio of 1:10.
- The sample was boiled in 750 ml of NaOH solution with a concentration of 14 g/L at 100 °C for 140 min with a material to liquid volume ratio of 1:15.

- The fibers were washed in 500 ml of solution containing 1 g/L H_2SO_4 at room temperature to neutralize the excess NaOH, and then thoroughly rinsed with tap water.
- The sample was soaked in 500 ml sodium hypochlorite (NaClO) solution containing 1 g/L active Cl^- at room temperature for 5 min with a material to liquid volume ratio of 1:10.
- The sample was immersed in 500 ml of solution containing 0.5 g/L Na_2SO_3 and NaOH at room temperature for 5 min with a material to liquid volume ratio of 1:10.
- The fibers were thoroughly rinsed with tap water and thereafter dried in an oven at 105 °C for 24 h.
- After the above chemical treatments, fibers are called “raw sunn hemp” in the following context.

Figure 2.1 Sunn hemp plants in field (photo provided by USDA ARS, Florence, South Carolina, USA)

2.2.2 Surface Modification

For modification, the sunn hemp fiber was soaked in a solution containing 15 wt% NaOH at room temperature for 1 h. Then, the fiber was washed with tap water containing a few drops of dilute sulfuric acid to neutralize the excess NaOH, and then thoroughly rinsed with tap water. The fiber was then dried in an oven at 105 °C for 24 h. After modification, fiber was called “treated sunn hemp” in the following context. This method is comparable to that employed by other authors for jute fiber (Gassan & Bledzki, 1999b). Figure 2.2 shows a picture of four fiber samples.

Figure 2.2 Pictures of four fibers: (A) kenaf (B) jute (C) raw sunn hemp (D) treated sunn hemp

2.2.3 Fiber Characterization

Sunn hemp stem cross-sections were observed in bright field on a Leica compound microscope (model DM IRBE) equipped with a DFC350 FX fluorescence camera (Leica Microsystems Inc., Wetzlar, Germany).

Scanning electron microscopy (SEM) micrographs of fiber surfaces and cross sections of the four fiber samples were taken using a LEO 1530 FE-SEM (Carl Zeiss Microscopy, LLC, Thornwood, NY). Prior to the SEM evaluation, the samples were coated with silver by means of a plasma sputtering apparatus to increase fiber conduction.

Fourier transform infrared spectroscopy (FTIR) was employed to determine the chemical changes that occur in the sunn hemp fiber during the treatments. A Thermo Nicolet AVATAR 370 FTIR (Thermo Electron Scientific Instruments LLC., Madison, WI) was used. The fiber samples were mixed with KBr and pressed into small discs with 1-mm thickness. The spectra were recorded over the range 4000–400 cm^{-1}, with a resolution of 4 cm^{-1} and averaged over 32 scans.

Thermogravimetry (TG) and differential thermogravimetry (DTG) techniques were employed to analyze the thermal stability of fibers. Scans were carried out at a heating rate of 10 °C/min in nitrogen atmosphere with a gas flow of 20 ml/min from 30 to 600 °C. The measurements were performed using a SHIMADZU TGA-50 thermoanalyzer (SHIMAZDU Inc., Tokyo, Japan). All samples are pre-conditioned at 22±1 °C and a relative humidity of 49±3% for 24 h. Each material was run in triplicate and the average weight loss and peak temperatures were obtained.

The Differential scanning calorimetric (DSC) measurements were performed on a SHIMADZU DSC-60 (SHIMAZDU Inc., Tokyo, Japan) at a heating rate of 5 °C/min in nitrogen atmosphere with a gas flow of 40 ml/min. Each thermogram was recorded from 25 to 400 °C. Each material was run in triplicate.

2.3 RESULTS AND DISCUSSION

2.3.1 Sunn Hemp Stem and Fiber Anatomy

It can be observed from Figure 2.3 (A) and Figure 2.3 (B) that the sunn hemp fiber is formed of separate bundles just outside the cortex. It has been found that the fiber bundles consist of 20 to 50 fiber cells which are very closely attached to each other.

The SEM photographs of each fiber sample illustrated that individual cellulosic fibers were bound together by lignin (Figure 2.4). It could be observed that the lignin was located between the individual fibers to provide the cohesion for bonding the fiber together. Figures 2.4 C and D show a smoother surface appearance of sunn hemp fiber upon treatment. These changes in fiber surface appearance may be due to the leaching out of alkali-soluble fractions like the waxy layer, as well as the removal of some lignin and hemi-cellulose during the alkaline treatment.

Figure 2.5 (A)–(D) show the cross-section morphology of the four fibers. The fiber cross-sections are irregular oval shapes with diameters ranging from 30 to 100 μm. The porous nature of kenaf and jute fibers may result in higher moisture contents and energy absorption than sunn hemp fiber.

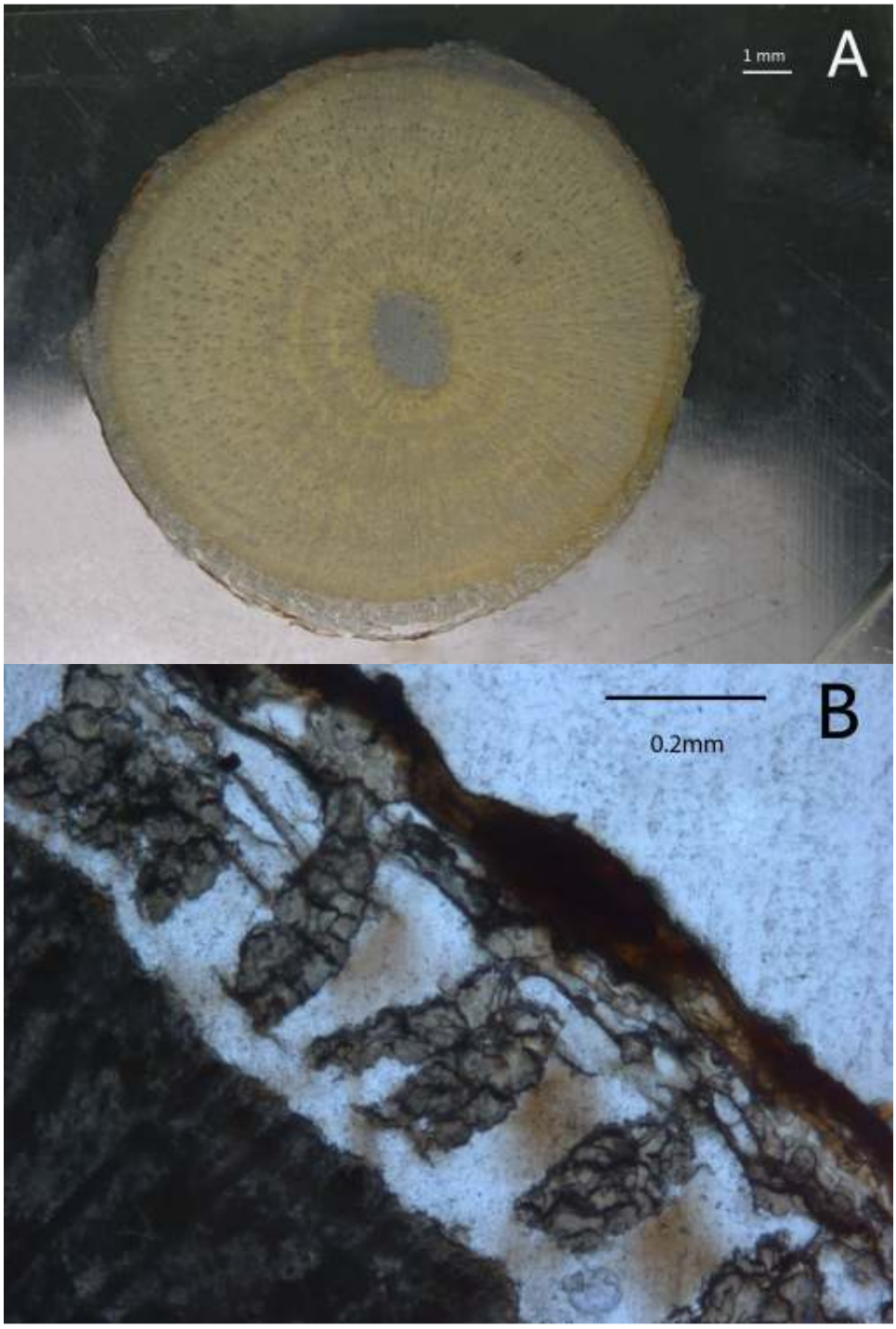

Figure 2.3 Sunn hemp stem cross-sections: (A) mature sunn hemp stem photograph under white light; (B) sunn hemp stem photographed with an optical microscope

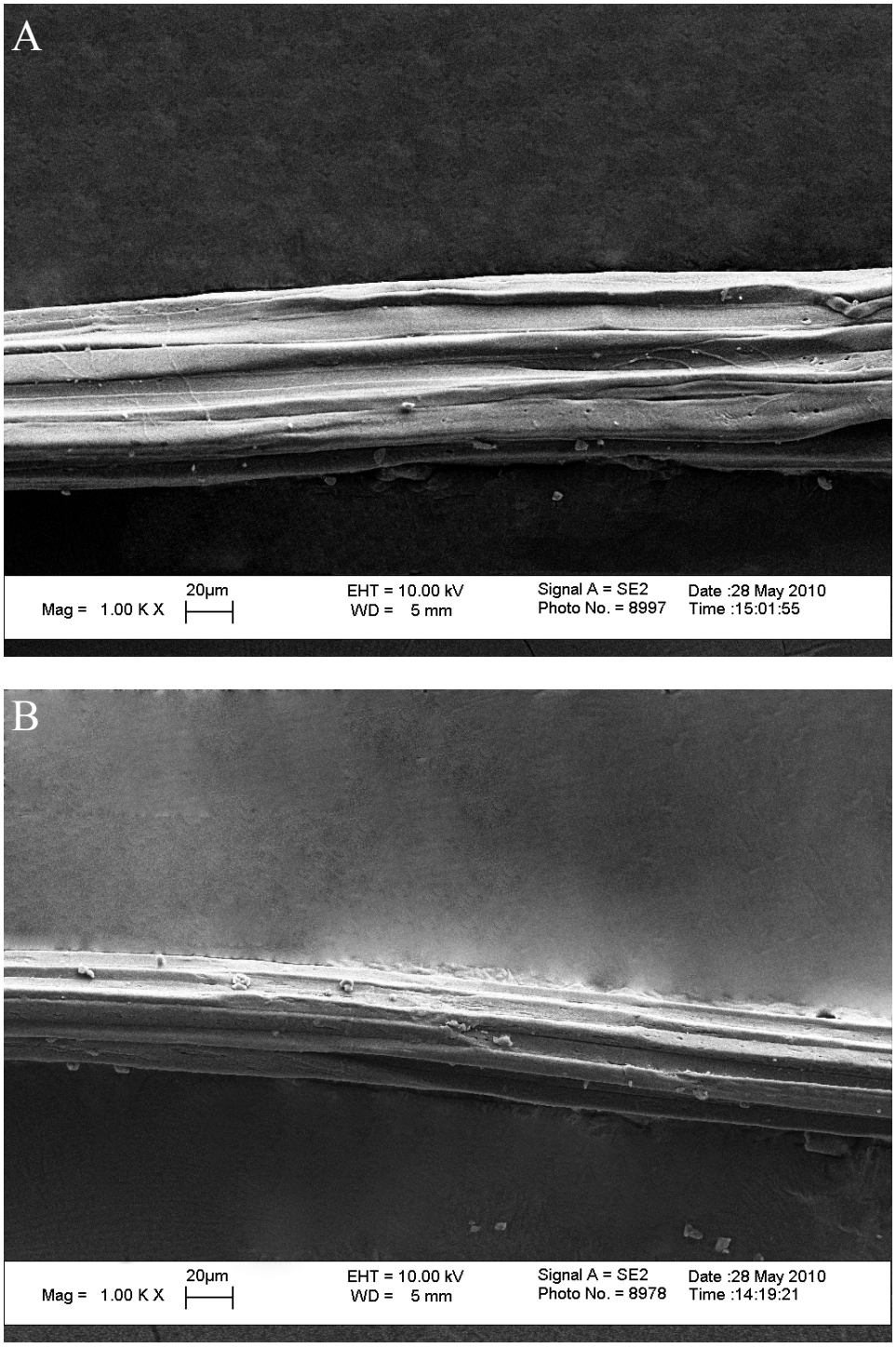

Figure 2.4 SEM micrographs of fiber surface of (A) kenaf (B) jute (C) raw sunn hemp (D) treated sunn hemp (magnification 1000×)

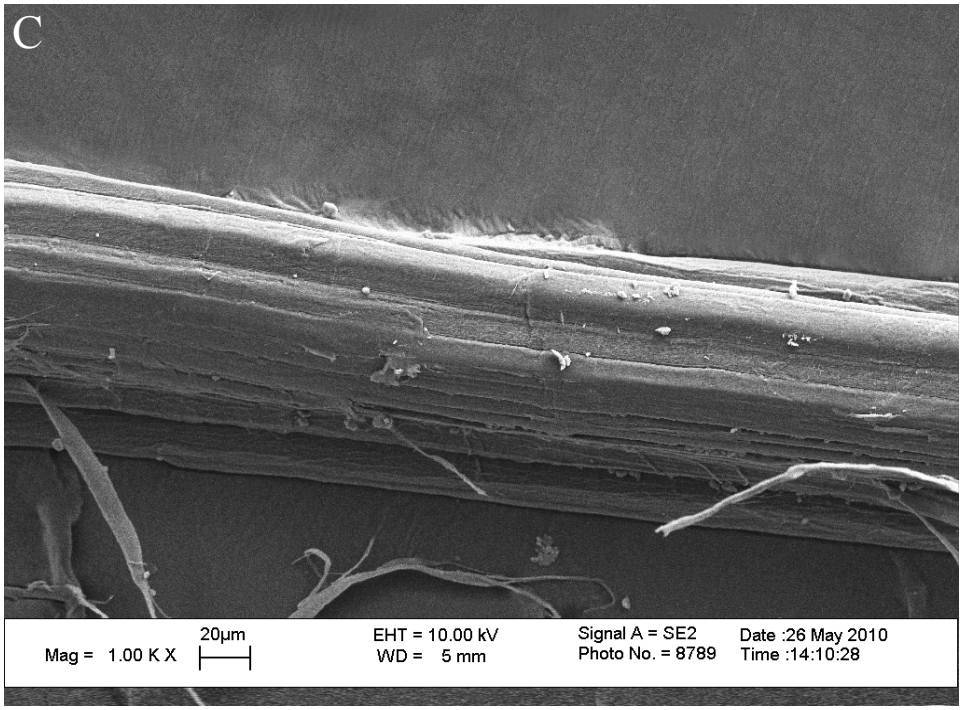

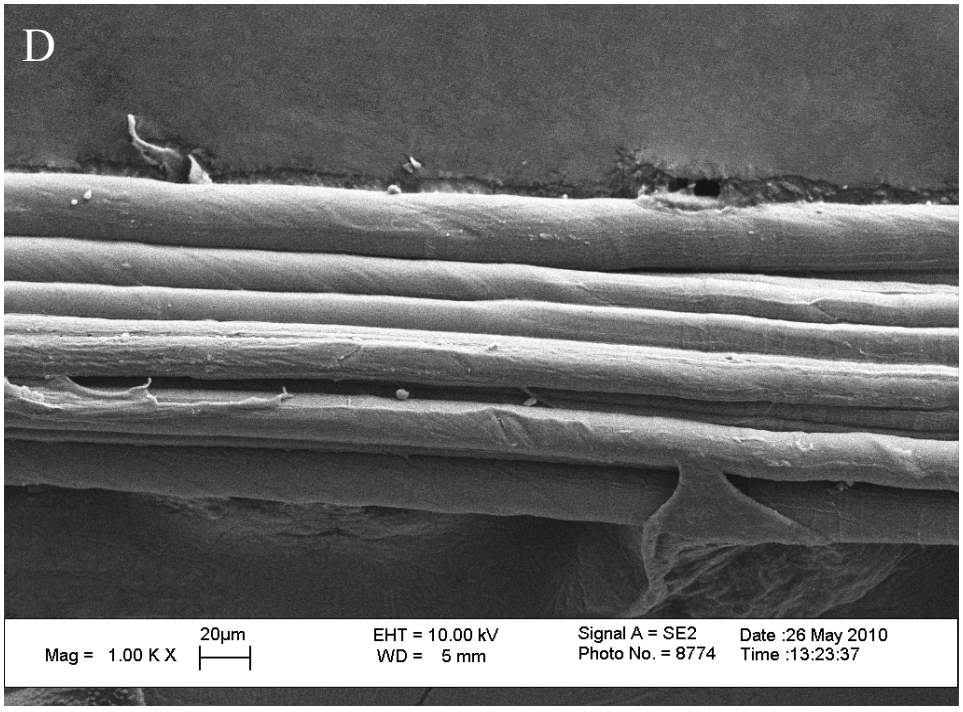

Figure 2.4 Cont.

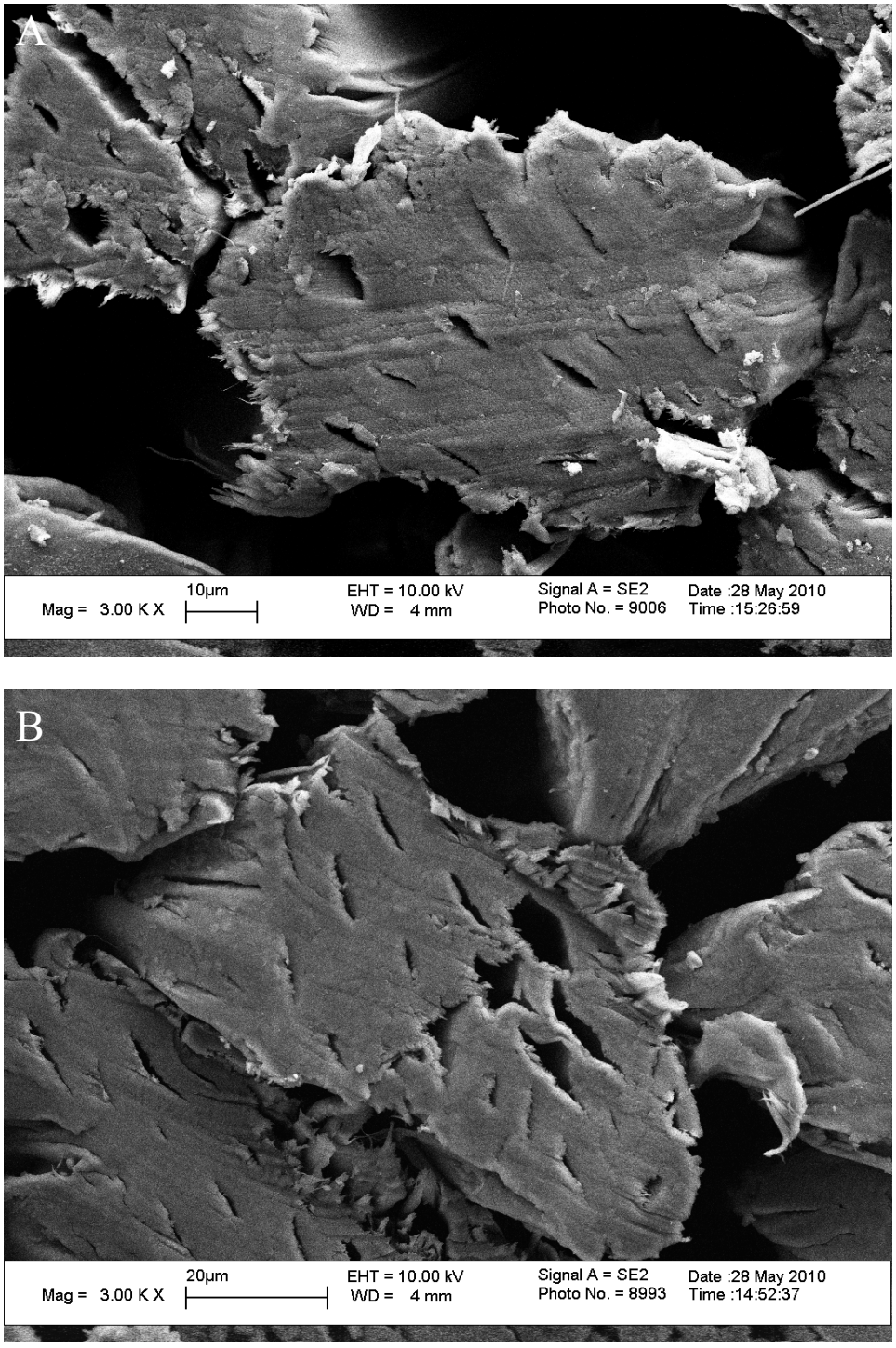

Figure 2.5 SEM micrographs of cross-sections of (A) kenaf (B) jute (C) raw sunn hemp (D) treated sunn hemp (magnification 3000×)

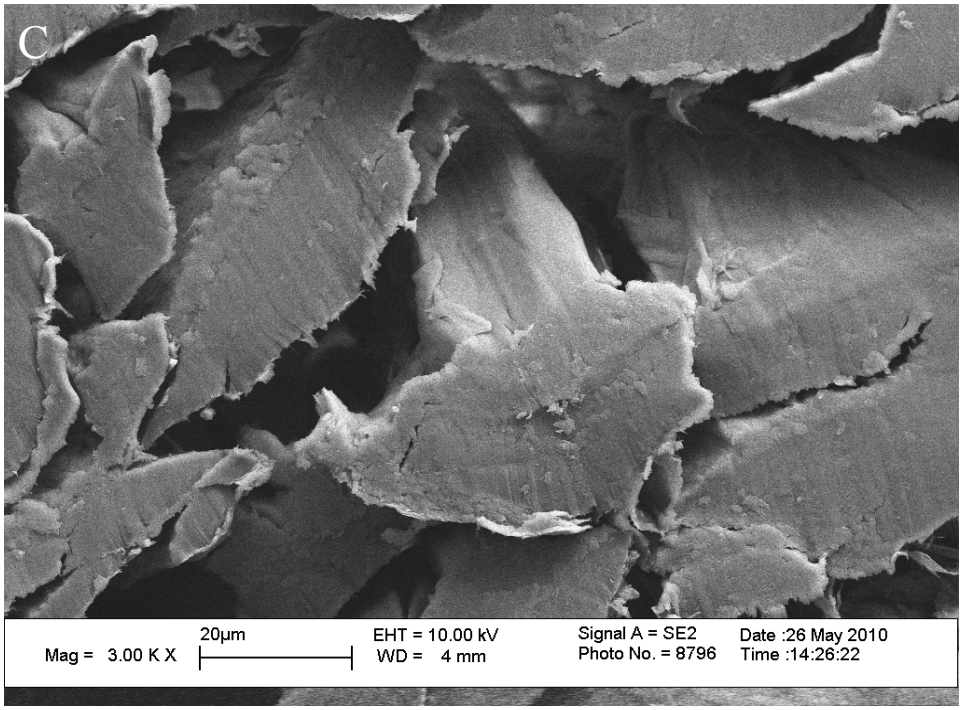

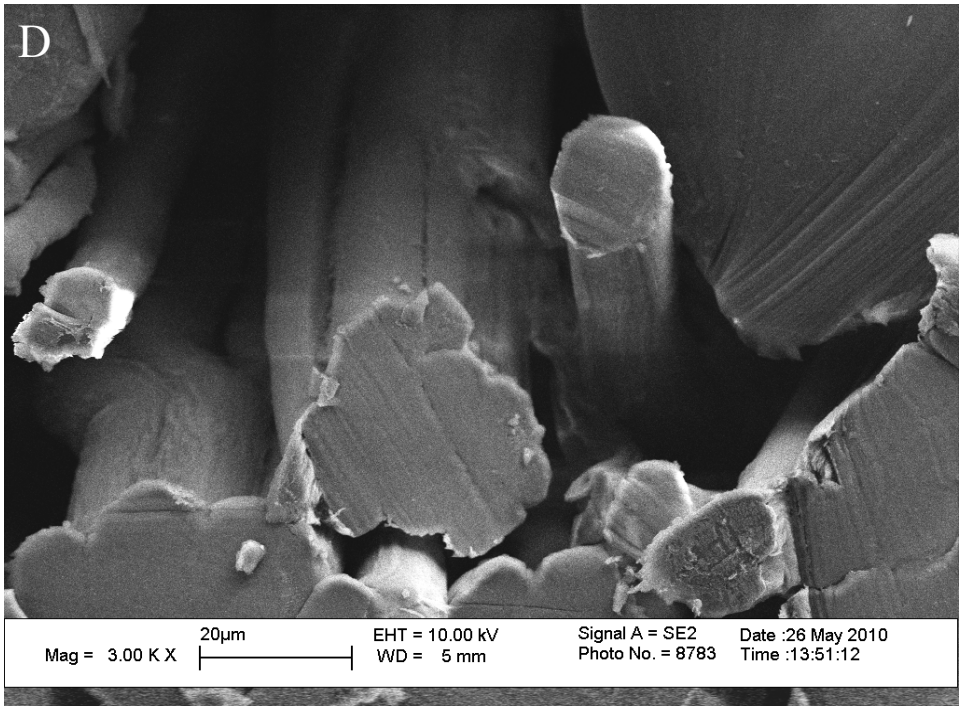

Figure 2.5 Cont.

2.3.2 FTIR Analysis

Physical and chemical treatments can produce important modifications to the chemical composition of sunn hemp fibers. The analysis by FTIR spectroscopy allows a quantitative evaluation for some of these changes. Figure 2.6 shows the FTIR spectra for the raw and treated sunn hemp fibers. After the NaOH treatment, there were reductions in certain vibrations for the raw sunn hemp fiber. For example, the band located at 1245 cm^{-1} associated with the C-O ring of lignin diminishes, and the peak intensities at 1735 and 1715 cm^{-1} were considerably reduced in the treated fibers as some C=O groups disappeared after the removal of pectin and hemi-cellulose. Other important changes are related with the increase of peaks at around 2900 cm^{-1} that correspond to the increase of some hydroxyl groups which may improve the hydrophilic property of sunn hemp fiber. In addition, the bands located at 1155 cm^{-1} and 1105 cm^{-1} associated with the C-C ring breathing band and the C-O-C band respectively were observed from both spectra, which resulted from the cellulose component. These results are consistent with the observations of other authors for different natural fibers (George et al., 2004; Mwaikambo & Ansell, 2002; Ouajai & Shanks, 2005).

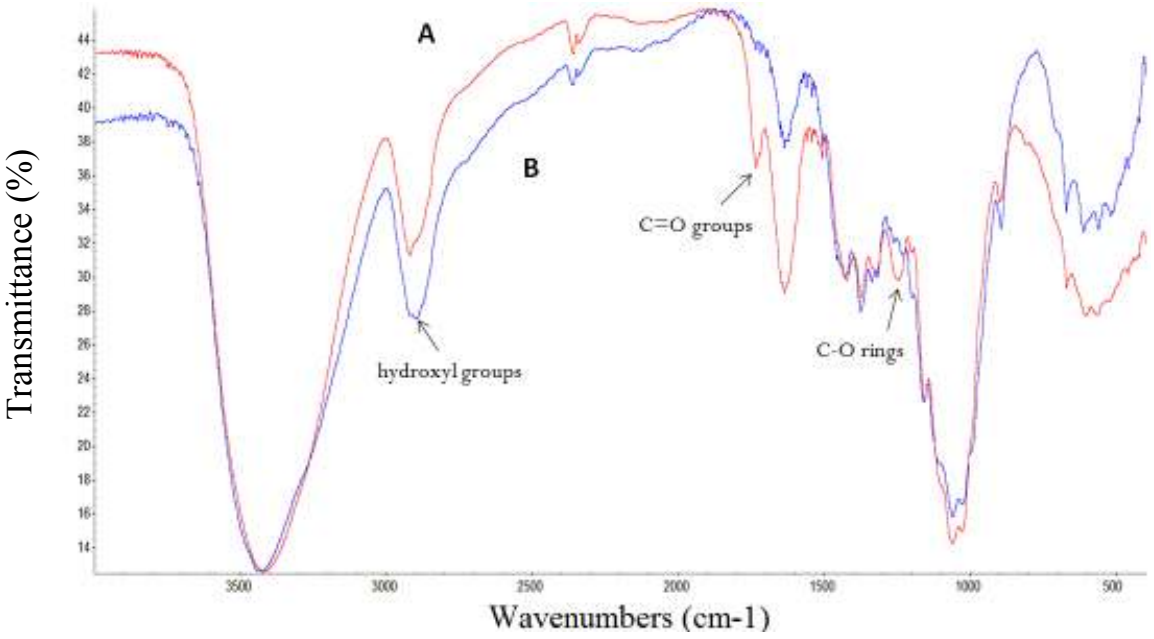

Figure 2.6 FTIR spectra of (A) raw sunn hemp and (B) treated sunn hemp

2.3.3 TG Analysis

TG analysis offers a precise control of weight loss with temperature. Figure 2.7 and Figure 2.8 show the thermal degradation patterns of the four fibers. From the results obtained on other fibers (Singh et al., 1996), three weight loss regions can be observed:

(1) In the first region below 140 °C, the weight loss is assigned to release of moisture present in these fibers.

(2) The second and third regions, between 220 and 450 °C, are associated with the decomposition of the fiber constituents such as hemi-cellulose, lignin, and cellulose (Van de Velde & Baetens, 2000).

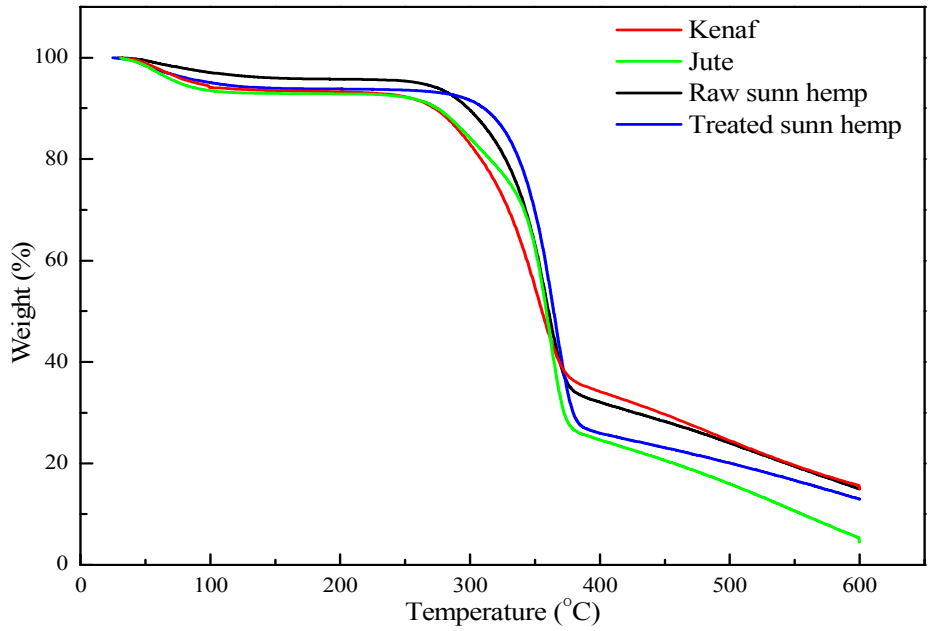

Figure 2.7 TG curves for the four fibers

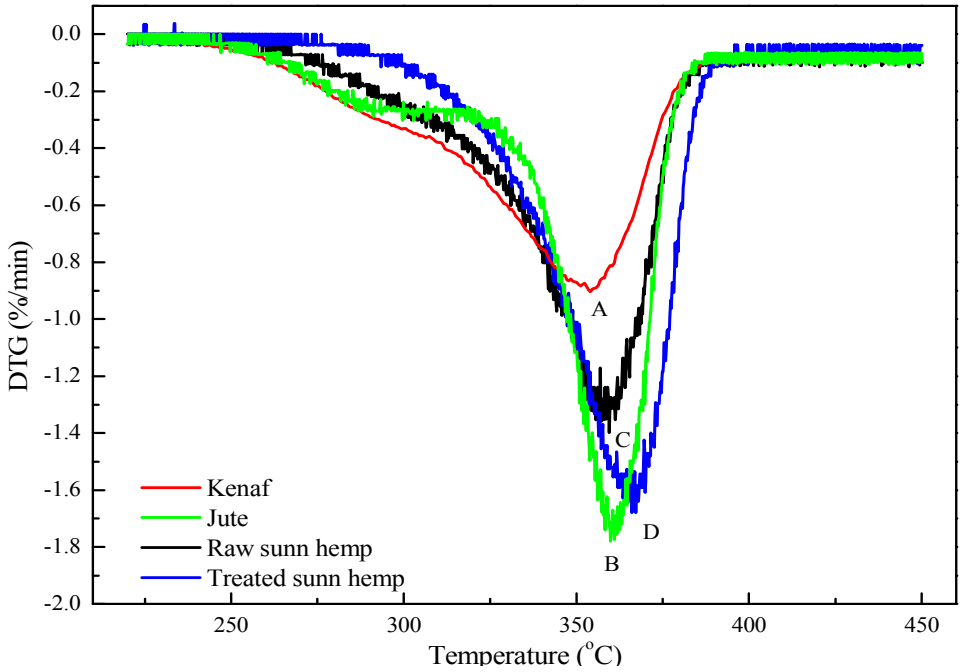

Figure 2.8 DTG curves for the four fibers: (A) kenaf (B) jute (C) raw sunn hemp (D) treated sunn hemp

Table 2.1 shows the weight losses and the peak temperatures for the four bast fibers in the different regions. By comparing the weight loss in the first decomposition region for raw and treated sunn hemp fibers, an increase of 34% in the moisture uptake was observed, thus indicating a hydrophilic tendency increase of sunn hemp fibers due to the NaOH treatment. This is also consistent with the observed tendency from FTIR spectra. For raw sunn hemp fiber, the maximum peak of decomposition occurred at 357 °C, while for treated sunn hemp fiber, it occurred at 367 °C. This is an indication that the thermal stability of sunn hemp fiber was enhanced by NaOH treatment. It also showed that jute had the highest moisture content and sunn hemp had the least. One reason for this difference in moisture content can be seen from the fiber cross-sectional SEM images in Figure 2.5 where the porous structure that helps retain water was found only in jute and kenaf, not in sunn hemp.

Table 2.1 Weight losses and decomposition peak temperatures of kenaf, jute, raw and treated sunn hemp fibers

Fiber	Weight Loss (%)		Maximum Peak Temperature (°C)
	20–140 °C	220–450 °C	
Kenaf	6.3	77.4	354
Jute	7.1	73.3	360
Raw sunn hemp	4.4	67.7	357
Treated sunn hemp	5.9	69.2	367

2.3.4 DSC Analysis

The DSC curves for the four fibers in the temperature range from 100 to 400 °C are shown in Figure 2.9, and the corresponding thermal characteristics are given in Table 2.2. The endothermic peaks for all fibers around 100 °C, which were the result of moisture loss, are not shown in Figure 2.9. The treated sunn hemp fiber exhibited a

relatively higher affinity for holding moisture compared to the untreated fiber. This may be attributed to the increasing crystallinity of the cellulose chain structure with the alkali solution, as observed from X-ray diffraction study (Das & Chakraborty, 2004). Ray et al (Ray et al., 2002) observed an increased enthalpy value for moisture desorption with increased crystallinity of the sample during the thermal study of alkali-treated jute fiber. In the DSC curves for all samples, the region of 140–160 °C shows a remarkable endothermic change, which suggests that the fibers experienced the glass transition stage at the peak temperatures. Similar to its TGA curve, sunn hemp fiber showed a jute-like behavior, i.e., the glass-transition temperature of sunn hemp was very close to jute fiber. However, the glass-transition temperature of treated sunn hemp fiber increased but not to a great extent (only 10 °C).

Additionally, all fibers show exotherms in the DSC curves in the region of 350-370 °C. Similar research has shown that many natural fibers mainly decomposed into hemi-cellulose, α-cellulose, and lignin in the region of 260 °C, 350 °C, and 410 °C, respectively (Basak et al., 1993). In this study, the α-cellulose component decomposed at 350–370 °C. And small peaks were observed at 270 °C for kenaf and jute, which is an indication of hemi-cellulose decomposition. The hemi-cellulose and lignin presented in sunn hemp fiber possibly form a stable structural network with α–cellulose through extensive intermolecular and intramolecular hydrogen bonding. Thus, the stable composite structure exhibited a single exothermic peak. Similar results were observed by Ray et al. (Ray et al., 2002) during an alkali treatment of jute fiber.

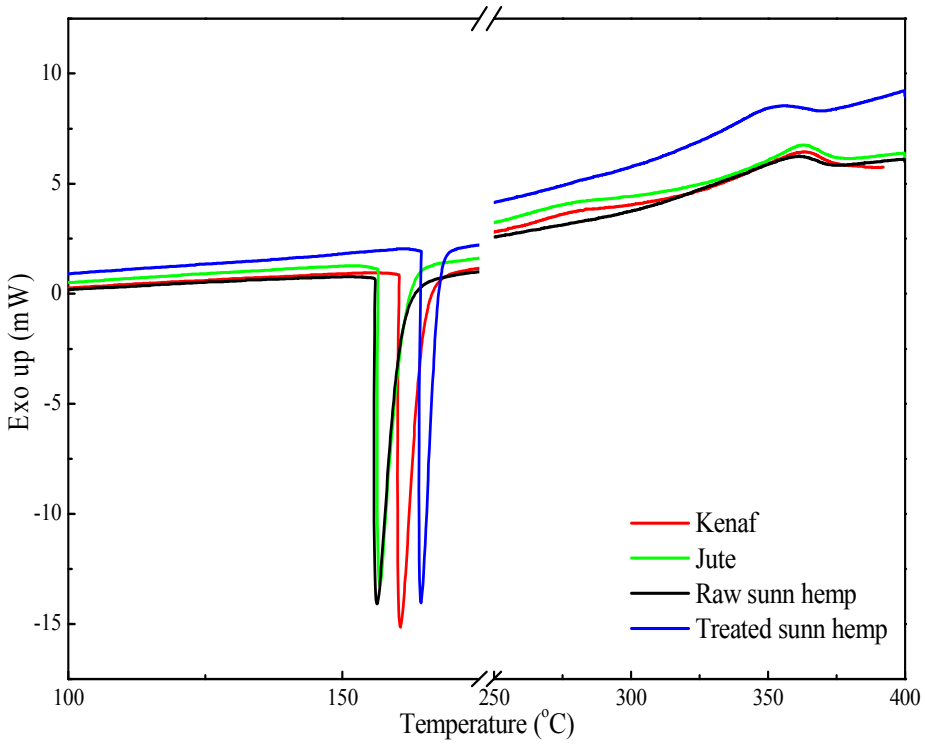

Figure 2.9 DSC curves for the four fibers

Table 2.2 Results for DSC analysis of kenaf, jute, raw and treated sunn hemp fibers

Fiber	Designation Peak Temperature (°C)	Nature of Peak
Kenaf	160.56	Endo
	363.18	Exo
Jute	156.80	Endo
	362.63	Exo
Raw sunn hemp	156.29	Endo
	361.48	Exo
Treated sunn hemp	164.34	Endo
	355.78	Exo

*Endo: endothermic; Exo: exothermic.

2.3.5 Mechanical Properties from Literature

The mechanical properties of three fibers are listed in Table 2.3. Kenaf fiber has higher specific modulus. Jute and kenaf fibers are cheaper than sunn-hemp due to the lower worldwide production of sunn hemp fiber.

2.4 CONCLUSIONS

Sunn hemp fiber was not selected for the subsequent research, although USDA was interested in this fiber, because sun hemp fiber did not show higher thermal stability or better mechanical properties than jute or kenaf fibers. Besides, the price of sunn hemp fiber is much higher than the other candidates. Kenaf fiber was used in the following research. The reasons to select kenaf are: (1) kenaf fiber has a porous structure that can result in higher energy absorption of kenaf fiber reinforced composites; and (2) kenaf fiber has a higher specific modulus, a moderate price, and available kenaf crop within the US.

Based on the study of surface modification on sunn hemp fiber, chemical surface modification on kenaf fiber was not applied for the subsequent research. After the alkaline treatment, the sunn hemp fiber surface appearance improved. The sunn hemp moisture content, glass-transition temperature, and decomposition temperature also increased, indicating that the thermal stability was enhanced by the fiber modification. However, these improvements were not very significant. Considering the time, energy and money spent for modification, it was not cost-effective or practical for industrial mass production. Therefore, kenaf fiber without surface modification was selected for subsequent research.

Table 2.3 Mechanical properties of kenaf, jute and sunn hemp fibers

Fiber	Density (kg/m^3)	Tensile strength (MPa)	Young's modulus (GPa)	Specific Modulus ($10^6 m^2 s^{-2}$)	Elongation at break (%)	Moisture absorption (%)	Price ($/Kg)	Reference
Kenaf	1.40	350-600	21-60	22-40	1.6-3.5	10	0.6-0.7	(Kozłowski & Władyka-Przybylak, 2008), (KEFI), (Davoodi et al., 2010)
Jute	1.30-1.46	400–800	10–30	7–21	1.5-1.8	12	0.5-0.6	(Kozłowski & Władyka-Przybylak, 2008), (IJSG, 2013; Lewin, 2006)(IJSG, 2013; Lewin,
Sunn hemp	1.07	389	35	32	5.5	8	3.4-6.1	(Lewin, 2006), (Saheb & Jog, 1999), (Treadwell & Alligood, 2008)

2.5 ACKNOWLEDGEMENTS

I would like to thank Gregory L Thompson, Department of Geological Sciences, Jackson School of Geosciences at University of Texas, Austin for the preparation of sunn hemp stem cross-section slides; Dwight K Romanovicz, Institute for Cellular and Molecular Biology, College of Natural Sciences at University of Texas, Austin for the use of optical microscope; and Dr. Philip J. Bauer, Research Agronomist, USDA, ARS for providing the raw sunn hemp plant.

2.6 REFERENCES

Basak, R.K., Saha, S.G., Sarkar, A.K., Saha, M., Das, N.N., Mukherjee, A.K. 1993. Thermal Properties of Jute Constituents and Flame Retardant Jute Fabrics. Textile Research Journal, 63(11), 658-666.

Bledzki, A.K., Reihmane, S., Gassan, J. 1996. Properties and modification methods for vegetable fibers for natural fiber composites. Journal of Applied Polymer Science, 59(8), 1329-1336.

Das, M., Chakraborty, D. 2004. Reinforcing action of mercerization on bamboo fibers. International Conference on Polymers for Advanced Technologies, December 15-16, 2004, Thiruvananthapuram, India.

Davoodi, M.M., Sapuan, S.M., Ahmad, D., Ali, A., Khalina, A., Jonoobi, M. 2010. Mechanical properties of hybrid kenaf/glass reinforced epoxy composite for passenger car bumper beam. Materials & Design, 31(10), 4927-4932.

Gassan, J., Bledzki, A.K. 1999a. Alkali treatment of jute fibers: relationship between structure and mechanical properties. Journal of Applied Polymer Science, 71(4), 623-629.

Gassan, J., Bledzki, A.K. 1997. The influence of fiber-surface treatment on the mechanical properties of jute-polypropylene composites. Composites Part A: Applied Science and Manufacturing, 28(12), 1001-1005.

Gassan, J., Bledzki, A.K. 1999b. Possibilities for improving the mechanical properties of jute/epoxy composites by alkali treatment of fibres. Composites Science and Technology, 59(9), 1303-1309.

George, J., Sreekala, M., Thomas, S. 2004. A review on interface modification and characterization of natural fiber reinforced plastic composites. Polymer Engineering & Science, 41(9), 1471-1485.

Heikal, S.O., El‐Kalyoubi, S.F. 1982. Graft copolymerization of acrylonitrile onto bagasse and wood pulps. Journal of Applied Polymer Science, 27(8), 3027-3041.

Herrera-Franco, P.J., Valadez-González, A. 2004. Mechanical properties of continuous natural fibre-reinforced polymer composites. Composites Part A: Applied Science and Manufacturing, 35(3), 339-345.

Herrera-Franco, P.J., Valadez-González, A. 2005. A study of the mechanical properties of short natural-fiber reinforced composites. Composites Part B: Engineering, 36(8), 597-608.

IJSG. 2013. International Jute Study Group. Available from: http://www.jute.org/index.php Access on January 27, 2013.

Jacob, M., Thomas, S., Varughese, K.T. 2004. Mechanical properties of sisal/oil palm hybrid fiber reinforced natural rubber composites. Composites Science and Technology, 64(7–8), 955-965.

KEFI. Properties of principal fibers, Available from: http://www.kenaf-fiber.com/en/infotec-tabella10.asp Access on January 13, 2013.

Kozłowski, R., Władyka-Przybylak, M. 2008. Flammability and fire resistance of composites reinforced by natural fibers. Polymers for Advanced Technologies, 19(6), 446-453.

Lewin, M. 2006. Handbook of fiber chemistry. CRC, Boca Raton, FL

Li, X., Tabil, L., Panigrahi, S. 2007. Chemical Treatments of Natural Fiber for Use in Natural Fiber-Reinforced Composites: A Review. Journal of Polymers and the Environment, 15(1), 25-33.

Mazumder, B.B., Ohtani, Y., Cheng, Z., Sameshima, K. 2000. Combination treatment of kenaf bast fiber for high viscosity pulp. Journal of wood science, 46(5), 364-370.

Mwaikambo, L.Y., Ansell, M.P. 2002. Chemical modification of hemp, sisal, jute, and kapok fibers by alkalization. Journal of Applied Polymer Science, 84(12), 2222-2234.

Ouajai, S., Shanks, R.A. 2005. Composition, structure and thermal degradation of hemp cellulose after chemical treatments. Polymer Degradation and Stability, 89(2), 327-335.

Ray, D., Sarkar, B.K., Basak, R.K., Rana, A.K. 2002. Study of the thermal behavior of alkali-treated jute fibers. Journal of Applied Polymer Science, 85(12), 2594-2599.

Saheb, D.N., Jog, J. 1999. Natural fiber polymer composites: a review. Advances in Polymer Technology, 18(4), 351-363.

Sgriccia, N., Hawley, M., Misra, M. 2008. Characterization of natural fiber surfaces and natural fiber composites. Composites Part A: Applied Science and Manufacturing, 39(10), 1632-1637.

Singh, B., Gupta, M., Verma, A. 1996. Influence of fiber surface treatment on the properties of sisal-polyester composites. Polymer Composites, 17(6), 910-918.

Treadwell, D.D., Alligood, M. 2008. Sunn hemp (Crotalaria juncea L.): A summer cover crop for Florida vegetable producers, HS 1126, Horticultural Sciences Department, University of Florida, Gainesville, FL.

Valadez-Gonzalez, A., Cervantes-Uc, J., Olayo, R., Herrera-Franco, P. 1999. Effect of fiber surface treatment on the fiber–matrix bond strength of natural fiber reinforced composites. Composites Part B: Engineering, 30(3), 309-320.

Van de Velde, K., Baetens, E. 2000. Thermal and mechanical properties of flax fibers for composites reinforcement. in: 3rd International Wood and Natural Fiber Composites Symposium. Kassel, Germany.

Yuan, X., Jayaraman, K., Bhattacharyya, D. 2004. Effects of plasma treatment in enhancing the performance of woodfibre-polypropylene composites. Composites Part A: Applied Science and Manufacturing, 35(12), 1363-1374.

Chapter 3: The Influence of Manufacturing Conditions on Mechanical and Thermal Performance of Kenaf/Polypropylene Nonwoven Composites

3.1 INTRODUCTION

The objective of this chapter is to explore the manufacturing conditions that affect end-use performance of KPNCs in terms of mechanical properties and thermal stability. The KPNCs with 50/50 blend ratio by weight, were produced by carding and needle-punching techniques, followed by a compression molding with 3.175-mm (1/8 in) and 6.35-mm (1/4 inch) thick gauges. The uniaxial tensile, three-point bending, in-plane shearing, and Izod impact tests were performed to evaluate the composite mechanical properties. The thermal properties were evaluated using TGA, DSC, and dynamic mechanical analysis (DMA). An adhesive-free sandwich structure was found to have excellent impact resistance performance. Based on the evaluation of end-use performance, the best processing condition combination was determined.

Characterization of tensile, flexural, shear and impact properties of KPNC is needed for accurate prediction of composites behavior during the formation of 2D- or 3D-shaped composite parts for many automotive applications. Therefore, the mechanical behavior of these structures is of fundamental importance to achieve good end-use performance. The fabrication techniques of natural fiber nonwovens and composites established in our previous work were used in this study (Chen et al., 2005a; Chen et al., 2007; Chen et al., 2005b), so that a consistent material production method can be applied to our in-depth studies. In this chapter, the focus was on investigating the influence of manufacturing conditions on the end-use performance of KPNCs. These findings could be useful information for industrial practice in nonwoven composite production.

3.2 EXPERIMENTAL DETAILS

3.2.1 Materials

The kenaf fiber was supplied by Engage Resources (Thailand), Ltd Co. PP staple fiber, which was supplied by Fiber Science, Inc. (Palm Bay, FL) with an average length of 50.8 mm and fineness of 7 denier was used for nonwoven formation and bonding. Fiber images are shown in Figure 3.1. Kenaf and PP fibers were conditioned at 22±1 °C and a relative humidity of 49±3% for 24 h before processing. No chemical treatment on kenaf and PP fibers was applied. Major mechanical properties of kenaf and PP fibers in comparison with E-glass fiber are listed in Table 3.1. This data was provided by the manufacturer or was from literature.

Figure 3.1 Kenaf (left) and PP (right) fiber bundles

Table 3.1 Mechanical properties of kenaf and PP fibers compared to glass fiber

Fiber	Density (kg/m^3)	Tensile strength (MPa)	Young's modulus (GPa)	Specific Modulus ($10^6 m^2 s^{-2}$)	Elongation at break (%)	Moisture absorption (%)	Price ($/Kg)	Reference
Kenaf	1.40	350-600	21-60	22-40	1.6-3.5	~ 9	0.6-0.7	(Davoodi et al., 2010), (KEFI) (Sherman, 1999)
PP	0.90	34	1.8	2	600.0	~ 0	1.8-2.4	-
E-glass	2.55	2400	73.0	29	2.5-3.0	~ 0	~ 3	(Kozłowski & Władyka-Przybylak, 2008)

3.2.2 Nonwoven Composite Fabrication

The manufacture of KPNCs involves three steps: carding, needle-punching, and compression molding as illustrated in Figure 3.2. The kenaf fiber, which acts as the reinforcement, was manually opened and mixed with PP fiber in 50/50 weight ratio. The mixture was then fed into a Universal Laboratory Carding Machine (Model F015D, SDL Atlas, Inc., Rock Hill, SC) to produce a fiber web. During carding, the mixture was further opened and individual fibers were combed to be parallel. The fiber web was carded once again in the perpendicular direction to improve web isotropy.

Subsequently, these fibrous felts were transferred to a Laboratory Needle Loom (Model 237, Morisson Benkshire Inc., North Adams, MA) in order to produce nonwoven felts. The feeding speed is 1.6 m/min and the punching rate is 228 strokes/min. By applying the mechanical needling technology, the fiber blends were greatly entangled and interacted in the out-of-plane direction. After needle-punching the nonwoven felts were much denser and stronger than the fiber web.

Next, the felts were cut into 0.3 m × 0.3 m size of segments and machine gauge lengths were set to 3.175 mm (1/8 in) and 6.35 mm (1/4 inch) for composite thickness control. The nonwoven composite samples were compression-molded in a MEYER® Transfer Printing and Laboratory Press System-Type APV 3530/16 (Meyer LLC., Roetz, Germany).

The pressing conditions are listed in Table 3.2. After compression molding, the samples were transferred to a pair of cold plates and cold pressed at 5×10^5 Pa for 30 s to obtain a sleek surface. The KPNC panels were then cut into specific sizes for quantitative characterization.

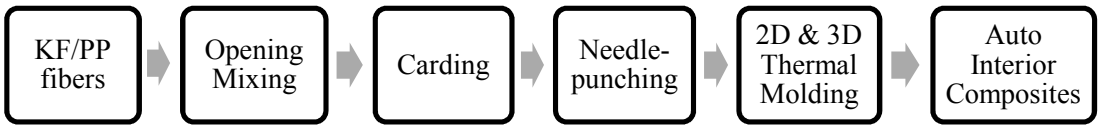

Figure 3.2 Nonwoven composite production

Table 3.2 Composite panel compression molding conditions and design of experiment table

	Temperature (°C)	Pressure (10^5 Pa)	Time (s)
High (+)	230	7	120
Low (-)	200	5	60

Test #	Temperature (T)	Time (t)	Pressure (P)
1	-	-	-
2	-	-	+
3	-	+	-
4	-	+	+
5	+	-	-
6	+	-	+
7	+	+	-
8	+	+	+

3.2.3 Morphology

Optical microscope (OM) photographs of microporous structures of nonwovens were taken using a LEICA compound microscope equipped with a DMLB camera. Prior to the OM evaluation, the samples were immersed in epoxy and sliced to a thickness of 150 μm. The fiber orientations in the nonwovens were observed.

3.2.4 Thermal Analysis

The thermogravimetry (TG) technique was employed to analyze the thermal stability of fibers. Scans were carried out at a heating rate of 10 °C/min in nitrogen atmosphere with a gas flow of 20 ml/min from 30 to 800 °C. The measurements were performed using the SHIMADZU TGA-50 thermo analyzer. Sample weights were maintained within 8–10 mg.

The heat resistant properties of kenaf and PP fibers were also characterized by TG technique in air with a gas flow of 20 ml/min from 30 to 600 °C. Four heating rates of 5, 10, 20 and 40 °C/min were used.

The DSC measurements were performed on the SHIMADZU DSC-60 at a heating rate of 5 °C/min in nitrogen with a gas flow of 40 ml/min. Each thermogram was recorded from 20 °C to 200 °C. In order to erase the previous thermal history of PP fiber and to study the recrystallization of kenaf and PP fibers, temperature was then cooled from 200 °C to 20 °C at 10 °C/min. For PP fiber, samples were subsequently heated to 200 °C at 5 °C/min in the second scan. The glass transition point (T_g) of kenaf and PP fibers and the melting point (T_m) of PP fiber were evaluated from the maxima in the endothermic peaks from the DSC curves. The crystallization temperatures (T_c) of kenaf and PP fibers were evaluated from the maxima in the exothermic peaks. The enthalpy of crystallization (ΔH_c) and enthalpy of melting (ΔH_m) were also calculated from the DSC curves.

A dynamic mechanical analyzer (DMA) (Model Q800, TA Instrument Inc., New Castle, DE) was conducted in accordance with ASTM D 7028 in a temperature range from 40 to 230 °C in dual-cantilever mode. A loading frequency of 1.0 Hz was used. The heating rate of all measurements was 5 °C/min and strain was 0.05%. Each thermal test

was run in triplicate and the average values were obtained. All thermal tests were conducted at 22±1 °C and a relative humidity of 49±3%.

3.2.5 Mechanical Properties

The tensile strength and modulus of the nonwoven composites were evaluated using a MTS universal tester (Model QT/5, MTS Systems Corporation, Research Triangle Park, NC) in accordance with the ASTM D 3039 for polymer matrix composite materials. Material flexibility was measured according to ASTM D 790 for reinforced plastics (three-point bending method). The in-plane shear properties of composite panels were tested using ASTM D 4255 (two-rail shear method). The in-plane shear deformation could be treated as a simple shear, because the in-plane shear strain for KPNC is usually very small ($\theta < 2°$). Because of this, we also assumed that $\tan\theta$ equals to θ. Composite impact strength was evaluated by a Tinius Olsen Model 92T impact tester (Tinius Olsen, Inc. Horsham, PA) in accordance with ASTM D 256 method A for determining the Izod pendulum impact resistance. The energy required to fracture a notched specimen at relatively high rate bending conditions is measured. Five specimens were tested for each condition and average values were reported for the evaluation of tensile, flexural, shear and impact properties. All tests were conducted at 22±1 °C and a relative humidity of 49±3%.

3.3 RESULTS AND DISCUSSION

3.3.1 Morphology

Figure 3.3 (A) shows the nonwoven felts made after carding and needle-punching. They are bulky and flexible with a porous fiber structure. KPNCs after thermal pressing are shown in Figure 3.3 (B). These composite panels are high in stiffness.

Fiber orientations in KPNC can be seen in Figure 3.4. A random kenaf fiber orientation was observed. Because the fibers in this typical nonwoven are oriented in all the directions in the composite plane rather than in just a few directions, we assumed that the in-plane properties of KPNCs are isotropic (Song et al., 2012).

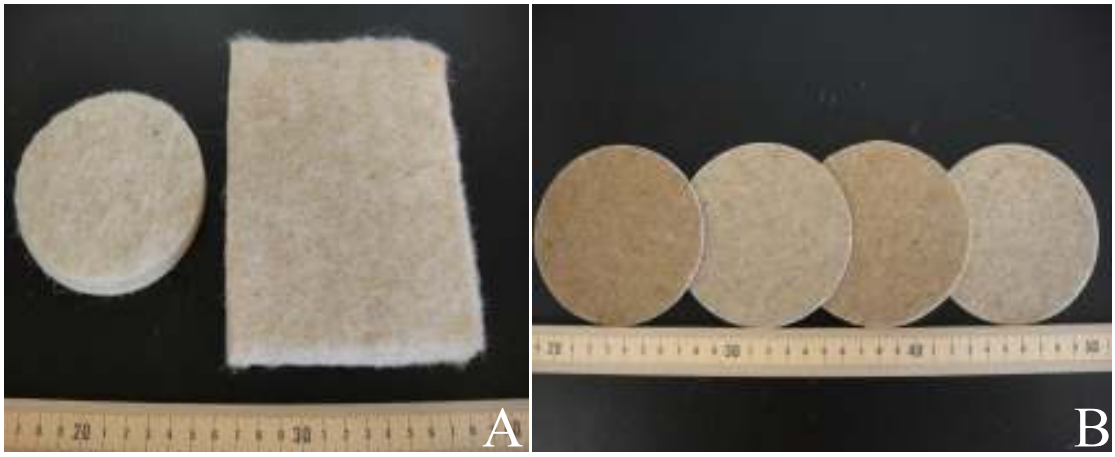

Figure 3.3 Nonwoven composite products: (A) nonwoven felts; (B) nonwoven composite panels

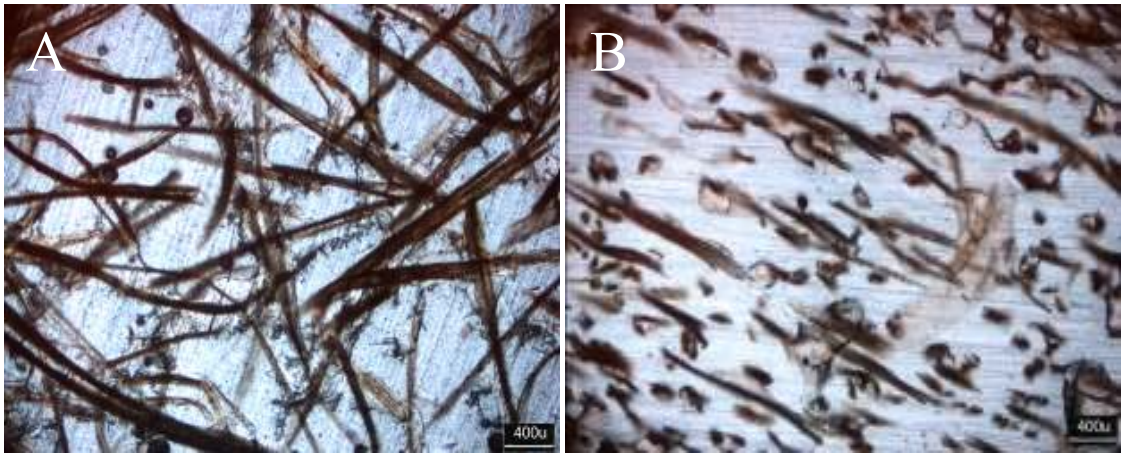

Figure 3.4 OM images of kenaf fiber orientations in nonwoven composites: (A) plane view; (B) cross-sectional view

3.3.2 Thermal Properties

The TGA and DSC tests were conducted on kenaf and PP fibers respectively. DMA test was conducted on KPNCs. Table 3.3 shows a summary of their thermal behavior. The evaluated thermal properties were used to determine the molding temperature range. As shown in Table 3.3, T_m of PP fiber is 160.9 °C. Figure 3.5 shows that kenaf fiber only lost 2.2 % of weight from 100 to 250 °C of thermal decomposition in air. Therefore, the KPNCs molding temperature should be within 160–250 °C. Two temperature levels of 200 and 230 °C were selected to ensure that PP fiber was able to melt for bonding and kenaf fiber mass loss was not significant during the compression molding.

Table 3.3 Summary of TGA, DSC and DMA test results

Sample	Glass Transition	Crystallization		Melting		Decomposition
	T_g (°C)	T_c (°C)	ΔH_c (J/g)	T_m (°C)	ΔH_m (J/g)	$T_{10\%}$ (°C)*
Kenaf	161.9	185.0	336.7	-	-	681.7
PP	41.4	112.6	89.44	160.9	78.0	440.0
KPNC	45.0	-	-	159.1	-	-

*$T_{10\%}$: temperature at 10% mass

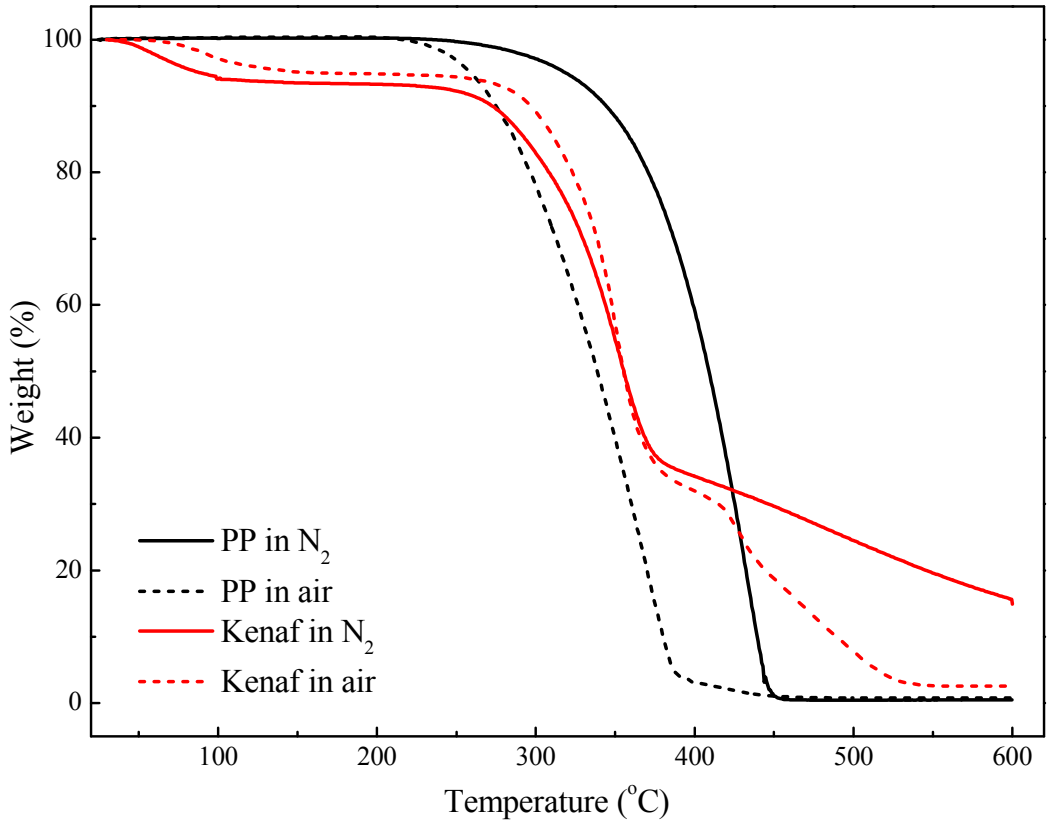

Figure 3.5 TG curves for kenaf and PP fibers in air and N_2

Figure 3.5 illustrates the overall thermogravimetric decomposition process of kenaf and PP fibers at a heating rate of 10 °C/min in air and N_2 atmosphere. The characteristics of kenaf fiber showed that the main thermal decomposition in N_2 (60% mass fraction) occurred within 272.6–446.5 °C. This is due to the decomposition of cellulose (Yang et al., 2007), which is the major component of kenaf fiber (44–57%). The decomposition of PP fiber happened within 344.4–425.3 °C, indicating that PP fiber can retain 90% of weight when kenaf fiber started the dramatic thermal decomposition. However, in the air atmosphere, the decomposition temperature $T_{90\%}$ was almost the same for both kenaf and PP fibers, until at $T_{30\%}$ (399.7 °C) where the kenaf weight loss

rate began slowing down, most probably because of the need of high temperature to decompose lignin (Pearl, 1967). Overall, for both kenaf and PP fibers, $T_{30\%}$ was higher in N_2 than in air (Table 3.4), indicating that the thermal decomposition was more efficient with the presence of oxygen.

Table 3.4 Temperatures 90 and 30% of weight of kenaf and PP fibers in air and N_2

Fiber	N_2		Air		
	$T_{90\%}$ (°C)*	$T_{30\%}$ (°C)*	$T_{90\%}$ (°C)	$T_{30\%}$ (°C)	Ea (kJ/mol)
Kenaf	272.6	446.5	275.2	399.7	200.54
PP	344.4	425.3	275.0	360.2	74.90

*$T_{90\%}$: temperature at 90% mass; $T_{30\%}$: temperature at 30% mass

The activation energy (Ea) was calculated based on the data obtained from the TG test at four heating rates in air. The value of Ea was used to evaluate the thermal stability of KPNCs (Flynn & Wall, 1966). The decomposition rate can be expressed by Equation 3.1 (Jiang et al., 2012):

$$\frac{d\alpha}{dt} = K(T) \times f(\alpha) \quad 3.1$$

In Equation 3.1, dα/dt is the decomposition rate; k(T) is the rate constant and depends on the temperature T; α is the degree of decomposition; $f(\alpha)$ is a function of α. k(T) can be expressed by the Arrhenius Equation 3.2:

$$K(T) = A\, e^{-E_a/RT} \quad 3.2$$

In Equation 3.2, A is the pre-exponential factor; R is the gas constant and T is the absolute temperature. The following equation 3.3 was obtained to calculate the activation energy for kenaf and PP fibers:

$$\ln\left(\frac{dT}{dt}\right) = \ln A - \ln\left(\frac{d\alpha}{dT}\right) + \ln\left[\alpha^m(1 - \alpha^n) + \left(-\frac{E_a}{R}\right)\frac{1}{T}\right] \quad 3.3$$

The average of A at the different heating rate was used since A varies with the heating rate. Because the derivative of decomposition rate with respect to temperature is zero at the peak temperature, the derivative of degree of decomposition with respect to temperature (dα/dt) at the peak temperature should be a constant and independent to the heating rate. Considering the fact that the variable term $\ln[\alpha^m(1-\alpha^n)]$ is very small compared to lnA, a linear relationship between heating rate and the reciprocal of the peak temperature can be simplified as Equation 3.4:

$$\ln\left(\frac{dT}{dt}\right) = \left(-\frac{E_a}{R}\right)\frac{1}{T_p} + c \quad 3.4$$

In this equation, [-(Ea/R)] is the slope of line and c is the intercept, as shown in Figure 3.6. For this decomposition reaction R is 8.314. So the activation energy can be calculated according to the slope and R value. As shown in Table 3.4, the Ea value of kenaf fiber was almost three times higher than PP fiber. The activation energy results were also consistent with the TG analysis in Table 3.4, indicating that KPNCs were more thermally stable than pure PP plastics by adding kenaf fiber as reinforcement.

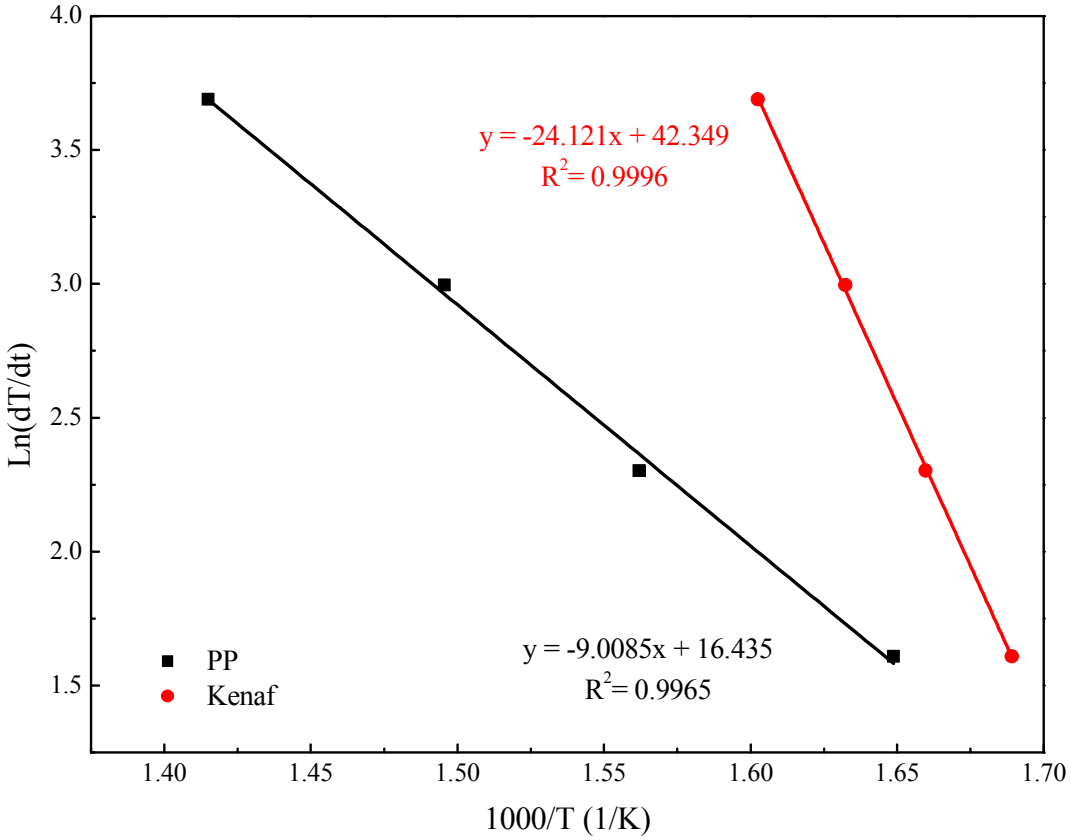

Figure 3.6 Linear plot of ln(dT/dt) versus 1000/T for Kenaf and PP fibers

3.3.3 Mechanical Properties

The mechanical test data is listed in the decreasing order of modulus in Table 3.5. Data in table is the mean value of ten specimens, with standard deviation shown in parenthesis. Means with the same letters are not statistically different according to Duncan's new multiple range test. Means with different letters are significantly different at the 95% confidence level. The sample ID is in the format of thermal press pressure ($\times 10^5$ Pa)/temperature (°C)/time (s). The Poisson's ratio is calculated based on the Young's modulus (E) and shear modulus (G), using equation $\nu = E/ [(2\times G) - 1]$, which

assures in-plane isotropy. The 3 mm thick KPNCs have twice the density compared to that of 6 mm thick samples.

As seen in Table 3.5, sample moduli decreased in the order of X/230/120, X/230/60, X/200/120, and X/200/60 for the 6 mm thick KPNCs (X represents the press pressure 5 or 7 $\times 10^5$ Pa). Table 3.6 shows the 2^3 factorial design of experiment results for the Young's modulus of 6 mm thick KPNCs. As can be seen from Table 3.7, temperature and time are the most significant factors affecting sample moduli.

The interaction plots are shown in Figure 3.7. Samples processed at 230 °C had a higher modulus than those at 200 °C. One possible explanation can be that the higher temperature increased the mobility of melt PP fiber, so that more fiber-fiber bonding points were formed. Samples processed for 120 s had a higher modulus than those for 60 s, as can be seen in Figure 3.7. Because 6-mm samples were too thick, the duration of 60 s was not long enough to allow heat transfer from the sample surface to inside. The processing time became a significant factor. Thus, it was concluded that the 6 mm thick samples X/230/120, which were processed at higher temperature for longer time, had the best mechanical performance among eight samples studied in this chapter. Although the overall effect of pressure was not found significant (Table 3.6), post-hoc comparison of individual means (Table 3.5) shows significant differences attributable to pressure. For instance, modulus of sample 5/230/120 was significantly higher than that of sample 7/230/120. Therefore, the effect of pressure needs to be further investigated in the future research.

It was also noted that because samples X/200/60 were processed at a low temperature (200 °C) for a short time (60 s), only the outer layers in contact with heating plates were melted and the inner part of the sample remained as non-melted nonwoven felts. Again, because the thickness of 6 mm was too thick to allow a thorough heat

transfer, these two samples formed a panel-felt-panel sandwich structure (Figure 3.8). This sandwich structure has a low strength but a high breaking strain (12–15%).

Table 3.5 Tensile, three-point bending, in-plane shearing, and impact test results for 6 mm thick KPNCs

Sample ID	Tensile Modulus (MPa)	Flexural Modulus (MPa)	In-plane Shear Modulus (MPa)	Impact Strength (kJ/m^2)	Poisson's Ratio
5/230/120	424 (25) a	306 (11) b	172 (10) a	2.94 (0.45) f	0.23
5/230/60	347 (21) d	183 (5) d	139 (8) c	3.33(0.69) d e f	0.25
5/200/120	323 (8) e	177 (6) d	130 (4) c d	3.98 (0.63) c	0.25
5/200/60	300 (15) f	158 (14) e	124 (5) d	9.70 (0.85) a	0.21
7/230/120	395 (13) b	356 (28) a	165 (6) a	3.16 (0.28) e f	0.20
7/230/60	366 (19) c	273 (22) c	150 (10) b	3.78 (0.64) c d	0.22
7/200/120	340 (6) d e	150 (16) e	135 (10) c	3.64 (0.36) c d e	0.26
7/200/60	262 (6) g	108 (13) f	101 (8) e	9.00 (1.70) b	0.30

Table 3.6 2^3 factorial design of experiment results for the Young's modulus of 6 mm thick KPNCs

	T	t	T × t	P	T × P	t × P	error	E (MPa)
Test (i)	1	2	3	4	5	6	7	
1	-	-	-	-	-	-	-	300
2	-	-	-	+	+	+	+	262
3	-	+	+	-	-	+	+	323
4	-	+	+	+	+	-	-	340
5	+	-	+	-	+	-	+	347
6	+	-	+	+	-	+	-	366
7	+	+	-	-	+	+	-	424
8	+	+	-	+	-	-	+	395
I(i,-)	1225	1275	1381	1394	1384	1382	1430	
II(i,+)	1532	1482	1376	1363	1373	1375	1327	
I-II	-307	-207	5	31	11	7	103	
$(I-II)^2$	94249	42849	25	961	121	49	10609	
$Q=(I-II)^2/N$	11781	5356	3	120	15	6	1326	
f	1	1	1	1	1	1	1	

T: temperature, t: time, P: pressure, E: Young's modulus, N=8, (+) high level and (-) low level

Table 3.7 Significance test results for the Young's modulus of 6 mm thick KPNCs

Factor	Q(i)	f	Mean square	F value	$F_{0.05}(1,5)$	$F_{0.01}(1,5)$	significance
T	11781	1	11781	40.05	7.71	21.20	**
t	5356	1	5356	18.21	7.71	21.20	*
e	1326	5	1326	5.00	7.71	21.20	no
sum	18463	7	18463				

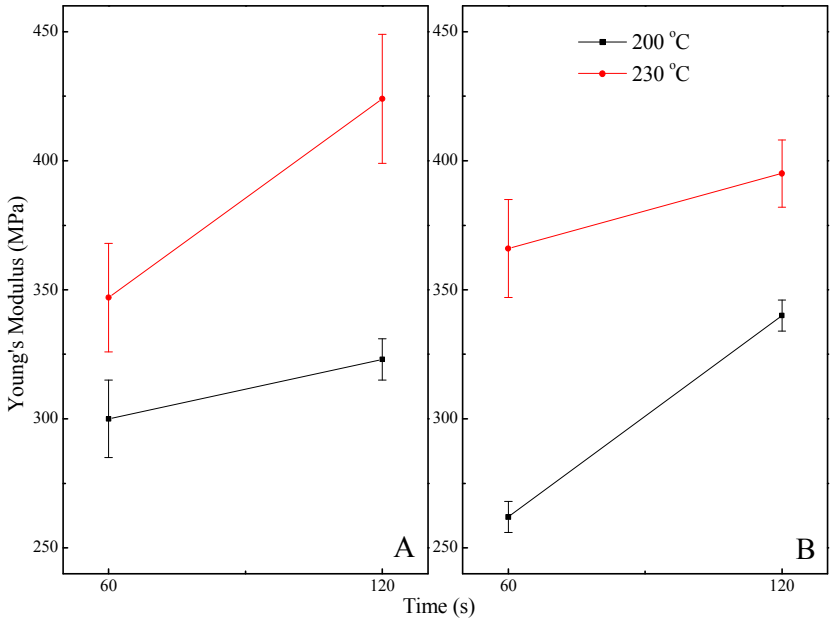

Figure 3.7 Interaction plots showing the influence of manufacture conditions (A) 0.5 MPa and (B) 0.7 MPa on the Young's modulus of 6 mm thick KPNCs

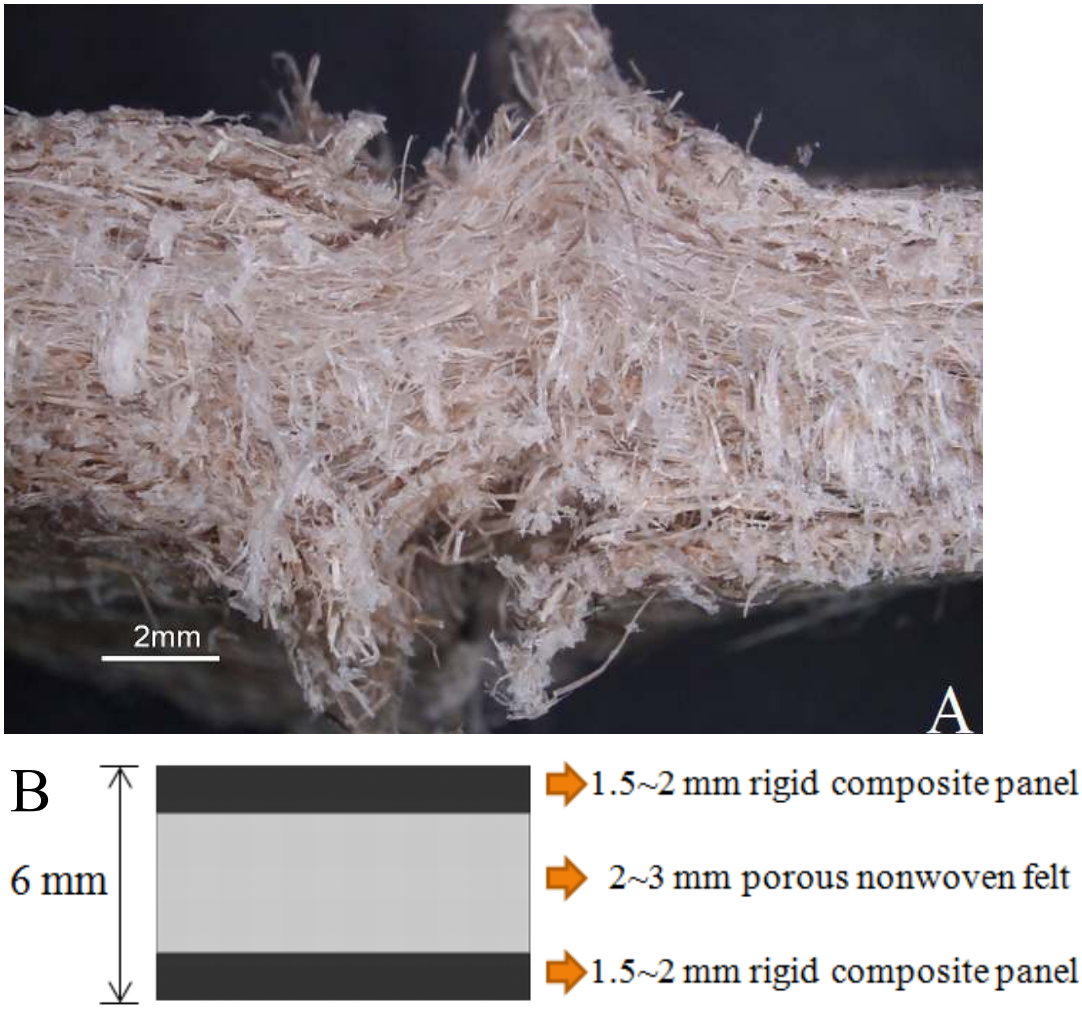

Figure 3.8 (A) A picture of failed sample 5/200/60 after Izod impact test; (B) An illustration of this adhesive-free sandwich structure

Figure 3.9 shows the interaction plots on the Izod impact strength of 6 mm thick KPNCs. Samples processed at 200 °C had higher impact strength than those at 230 °C. Samples X/200/60, which were processed at 200 °C for 60 s, had the highest Izod impact strength. Because a middle layer of porous nonwoven felt within the sandwich structure makes samples X/200/60 can absorb more energy when subjected to impact force, even though it exhibited lower panel stiffness.

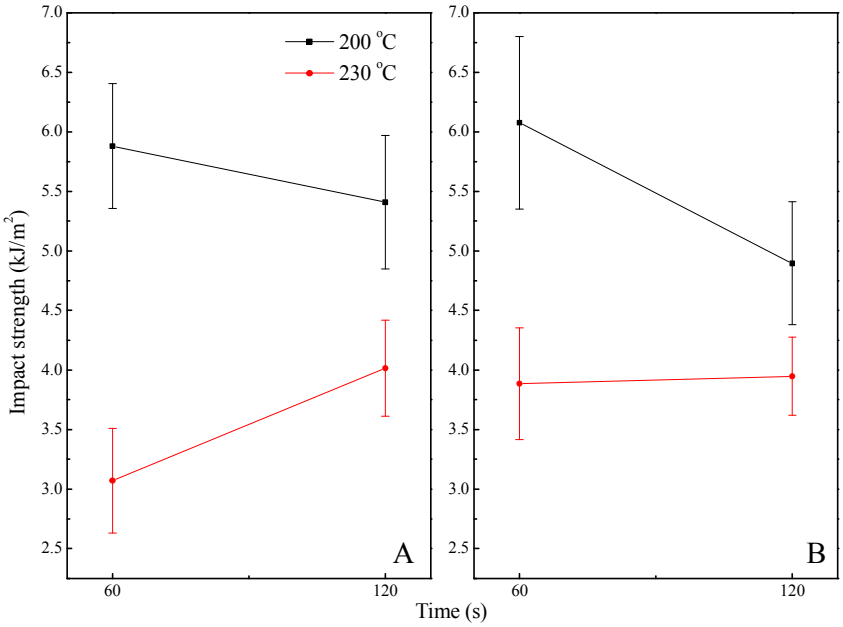

Figure 3.9 Interaction plots showing the influence of manufacture conditions (A) 0.5 MPa and (B) 0.7 MPa on the Izod impact strength of 6 mm thick KPNCs

As seen in Table 3.8, sample moduli decreased in the order of X/230/60, X/200/120, X/230/120, and X/200/60 for 3 mm thick KPNCs. Table 3.9 shows the 2^3 factorial design of experiment results for the Young's modulus of 3 mm thick KPNCs. As can be seen from Table 3.10, temperature, time and the interaction between them are the most significant factors affecting sample moduli. Figure 3.10 shows this interaction between temperature and time. It demonstrated that the effects of time on Young's modulus are dependent on the temperature levels. At the lower temperature level (200 °C), the Young's modulus increased with processing time, while at 230 °C, the Young's modulus decreased with processing time. This interaction suggested a possible thermal decomposition occurring when the samples were processed for prolonged time at high temperature. Similar to the case of 6 mm thick samples, significant influence of pressure can also be seen based on the post-hoc comparison (Table 3.8), although the overall

effect of pressure was not found significant (Table 3.9). In the case of the 3 mm thick samples, however, higher pressure (0.7 MPa) tended to yield better Young's moduli. One possible explanation was that samples processed at 0.7 MPa had a more compact structure than that at 0.5 MPa. More fiber-fiber bondings were formed in a compact structure, thus increased the Young's moduli.

Samples processed at 230 °C for 60 s had higher modulus than those at 200 °C for 120 s. One possible reason is that higher temperature increased the mobility of the melt PP fiber, so that more fiber-fiber bonding points were formed. Samples X/230/120 had lower moduli than X/200/120 samples. Because decomposition may occur at higher temperature (230 °C) for excessive time (120 s) (Hao et al., 2010), resulting in a kenaf fiber strength loss. Therefore, it was concluded that samples X/230/60 which were processed at higher temperature (230 °C) and shorter time (60 s) had the best mechanical performance among eight samples studied in this chapter, with highest tensile modulus (1630 MPa) for sample 7/230/60 and highest tensile failure strain (1.5%) for sample 5/230/60.

Table 3.8 Tensile, three-point bending, in-plane shearing, and impact test results of 3 mm thick KPNCs

Sample ID	Tensile Modulus (MPa)	Flexural Modulus (MPa)	In-plane Shear Modulus (MPa)	Impact Strength (kJ/m^2)	Poisson's Ratio
5/230/60	1521 (11) c	1022 (39) b	584 (11) c	3.07 (0.44) e	0.30
5/200/120	1486 (15) d	934 (34) c	570 (10) d	5.41 (0.56) b	0.30
5/230/120	1445 (25) e	834 (45) d	556 (9) e	4.00 (0.39) d	0.30
5/200/60	1357 (39) g	433 (49) e	543 (8) e	5.88 (0.53) a	0.25
7/230/60	1630 (15) a	1363 (28) a	631 (11) a	3.88 (0.47) d	0.29
7/200/120	1590 (23) b	990 (49) b	619 (9) a	4.90 (0.52) c	0.28
7/230/120	1519 (35) c	840 (39) d	598 (15) b	3.95 (0.33) d	0.27
7/200/60	1392 (39) f	451 (32) e	547 (16) e	6.08 (0.72) a	0.27

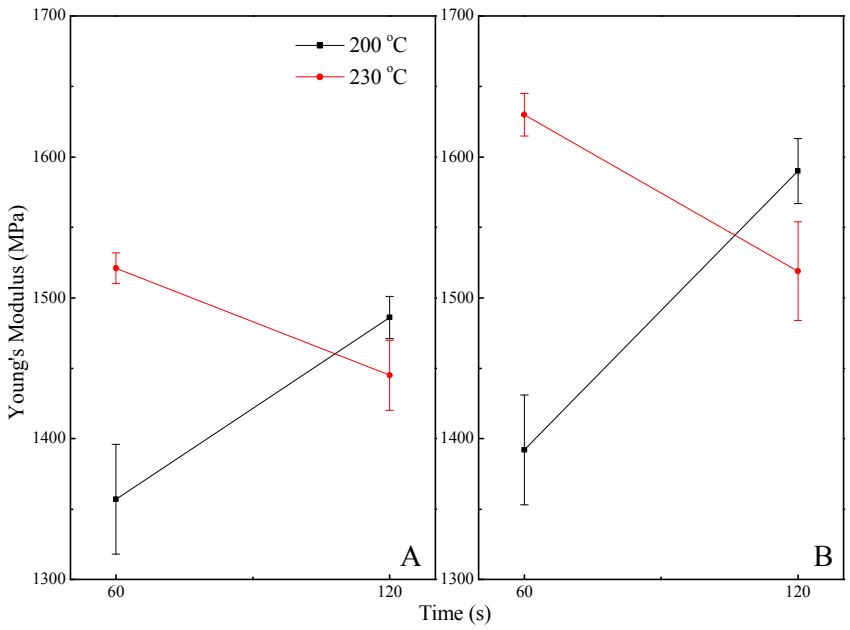

Figure 3.10 Interaction plots showing the influence of manufacture conditions (A) 0.5 MPa and (B) 0.7 MPa on the Young's modulus of 3 mm thick KPNCs

Table 3.9 2^3 factorial design of experiment results for the Young's modulus of 3 mm thick KPNCs

	T	t	T × t	P	T × P	t × P	error	E (MPa)
Test (i)	1	2	3	4	5	6	7	
1	-	-	-	-	-	-	-	1357
2	-	-	-	+	+	+	+	1392
3	-	+	+	-	-	+	+	1486
4	-	+	+	+	+	-	-	1590
5	+	-	+	-	+	-	+	1521
6	+	-	+	+	-	+	-	1630
7	+	+	-	-	+	+	-	1445
8	+	+	-	+	-	-	+	1519
I(i,-)	5825	5809	5713	5900	5992	5987	6022	
II(i,+)	6115	6131	6227	6040	5948	5953	5918	
I-II	-290	-322	-514	-140	44	34	104	
$(I-II)^2$	84100	103684	264196	19600	1936	1156	10816	
$Q=(I-II)^2/N$	10513	12961	33025	2450	242	145	1352	
f	1	1	1	1	1	1	1	

T: temperature, t: time, P: pressure, E: Young's modulus, N=8, (+) high level and (-) low level

Table 3.10 Significance test results for the Young's modulus of 3 mm thick KPNCs

Factor	Q(i)	f	Mean square	F value	$F_{0.05}(1, 3)$	$F_{0.01}(1, 3)$	Significance
T	10513	1	10513	18.14	10.13	34.12	*
t	12961	1	12961	22.36	10.13	34.12	*
T × t	33025	1	33025	56.99	10.13	34.12	**
P	2450	1	2450	4.23	10.13	34.12	no
e	1352	3	1352	2.33	10.13	34.12	no
sum	60301	7	60301				

Typical stress–strain curves for 3 mm thick KPNC are shown in Figure 3.11, from which the nonlinearity in stress–strain response can be seen. The nonlinearity was a combination of the nonlinear behavior of PP materials and progressive failure of kenaf fiber due to various interacting micro-failure modes, such as matrix cracking, interfacial debonding, fiber pull-out and fiber breakage (Rösler et al., 2007). Figure 3.12 shows some typical 3 mm thick specimens after tensile testing. The nonwoven composite failed in a brittle manner. The failure surfaces were non-planar, with some fiber pull-out. By visual inspection, the color of the fracture region appeared to be white under normal daylight, indicating when the sample failure occurred.

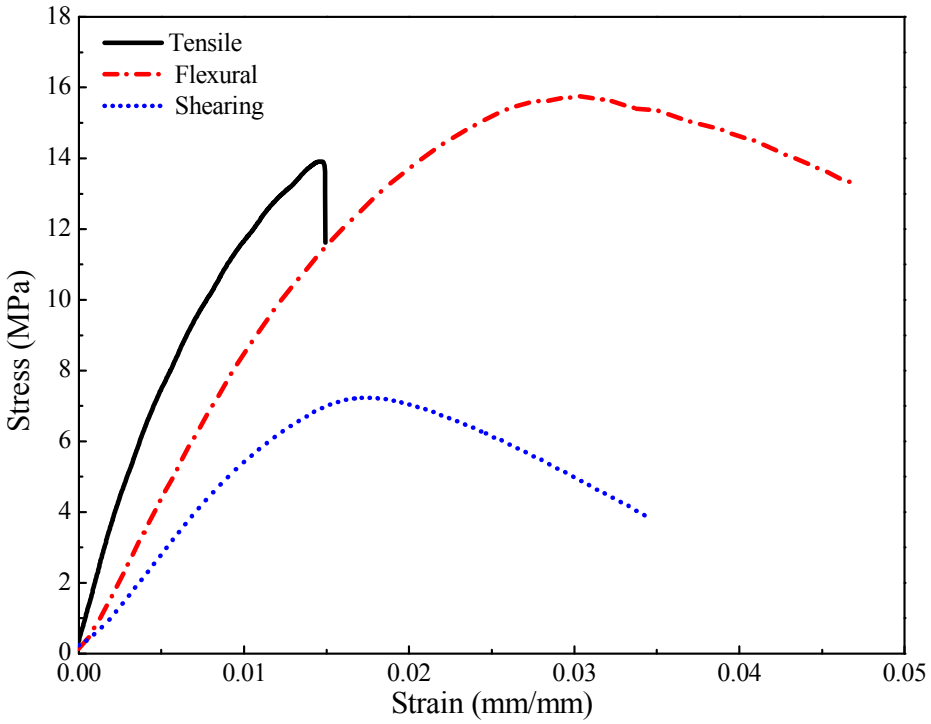

Figure 3.11 Typical stress–stain curves for 3 mm thick sample 5/230/60

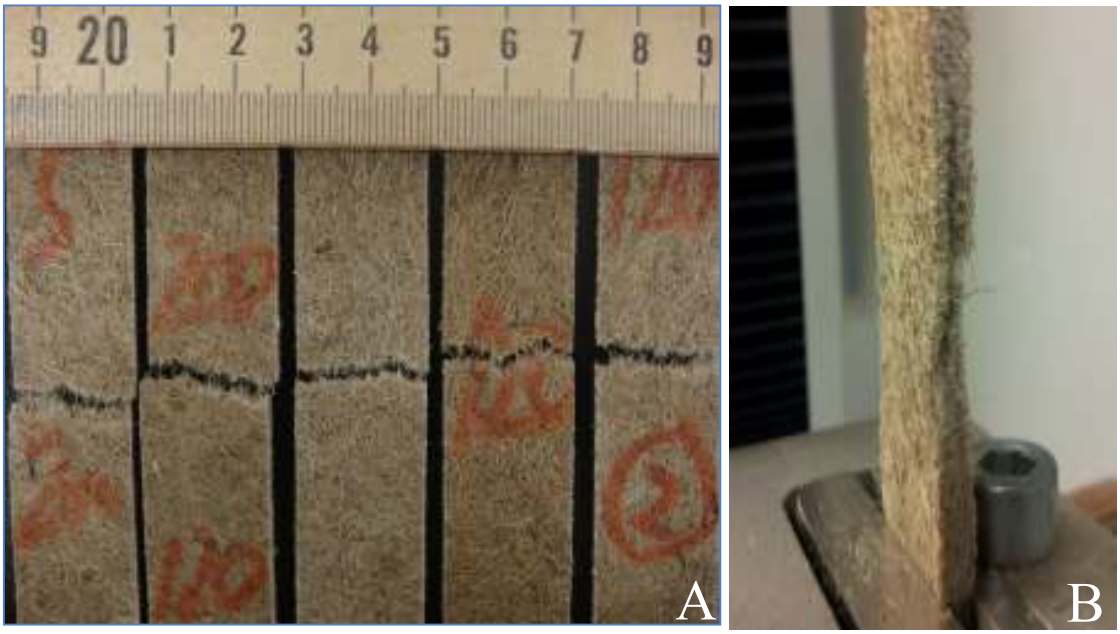

Figure 3.12 Photographs of tested tensile specimens: (A) Plane view; (B) Lateral view

3.3.4 Thermo-mechanical Properties

To perform the DMA tests, 3 mm thick samples 7/230/60 and 5/200/60 that had the highest and lowest modulus were examined respectively. The derivatives of storage moduli in Figure 3.13 show T_g and T_m. These curves illustrate that the composite experienced the glass transition at the peak T_g and the complete strength loss of composite at T_m. For sample 7/200/60, T_g is 46.3 °C and T_m is 158.1 °C; for sample 7/230/60, T_g is 43.7 °C and T_m is 160.1 °C. Two samples showed no significant differences between the T_g and T_m values (t test, $p<0.05$), indicating that the thermo-mechanical properties of the samples processed under different manufacturing conditions were similar. The T_g and T_m values of two KNPC samples were very close to that of virgin PP fiber, as shown in Table 3.3. This can be rationalized by considering that the PP fiber, being thermoplastic, showed viscoelastic properties and the kenaf fiber, being non-thermoplastic, exhibited elastic properties in this composite structure (Fisher & Brinson,

2001; Yancey & Pindera, 1990). As a result, the KPNC dynamic mechanical behavior was dominated by the viscoelastic PP bonding fiber rather than the cellulose kenaf fiber. This explains why various processing conditions had limited influence on the thermo-mechanical properties of KPNCs.

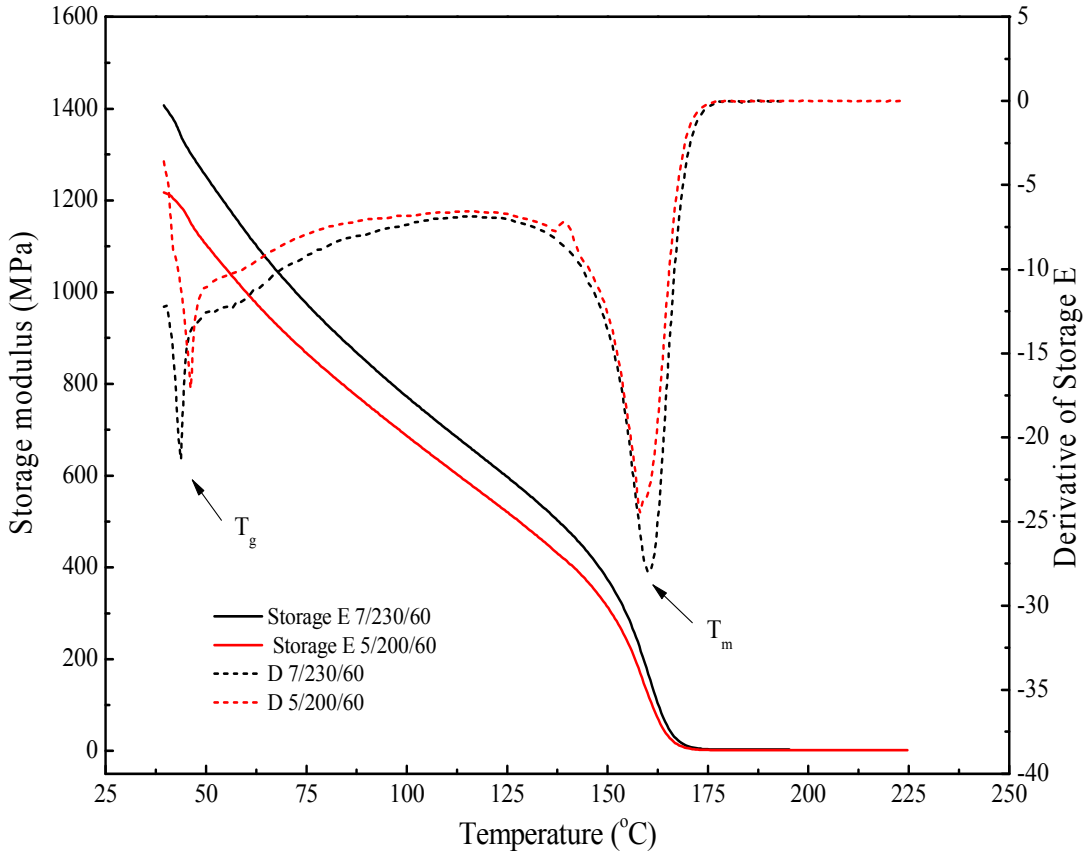

Figure 3.13 Storage moduli and derivatives of 3 mm thick samples 7/230/60 and 5/200/60

3.4 CONCLUSIONS

The influence of manufacturing conditions was investigated by evaluating the mechanical and thermal performance of KPNCs. It was found that temperature and time were the most significant processing factors for 6 mm thick KPNCs and the interaction

between temperature and time was also a significant factor for 3 mm thick KPNCs. Although the overall effect of pressure was not found significant, post-hoc comparisons showed significant differences in moduli attributable to pressure within the same levels of temperature and time.

For the 3 mm thick KPNCs, sample 7/230/60 had the highest tensile modulus. Because more fiber bondings are formed at higher temperature; the degradation of kenaf fiber is less at shorter time; and samples are more compact at higher pressing pressure. The manufacturing conditions at higher temperature (230 °C) and shorter time (60 s) are recommended in order to achieve best mechanical performance among eight samples studied in this chapter.

For the 6 mm thick KPNCs, longer processing time was needed since the sample thickness was doubled comparing to the 3 mm thick samples. Processing at 230 °C for 120 s (sample 5/230/120 or 7/230/120) gave the best mechanical properties among eight samples studied in this chapter. In contrast, samples 5/200/60 and 7/200/60, having the lowest moduli, were the best impact energy absorbers due to their panel-felt-panel sandwich structure.

The manufacturing conditions did not significantly affect the composite thermo-mechanical properties. KPNCs were more thermally stable than virgin PP plastics by adding kenaf fiber as reinforcement.

3.5 ACKNOWLEDGEMENTS

I would like to thank Mr. Gregory L. Thompson, Department of Geological Sciences, Jackson School of Geosciences at University of Texas, Austin for the preparation of 150 μm KPNC slides. Thanks are also extended to Mr. Yizhuo Chen, Department of Textile and Apparel, School of Human Ecology at University of Texas,

Austin for the help with nonwoven fabrication. I would also like to thank Dr. Qinglin Wu, School of Renewable Natural Resources at Louisiana State University, for the use of the impact tester.

3.6 REFERENCES

Chen, Y., Chiparus, O., Sun, L., Negulescu, I., Parikh, D.V., Calamari, T.A. 2005a. Natural fibers for automotive nonwoven composites. *Journal of Industrial Textiles*, **35**(Compendex), 47-62.

Chen, Y., Sun, L., Negulescu, I., Wu, Q., Henderson, G. 2007. Comparative Study of Hemp Fiber for Nonwoven Composites. *Journal of Industrial Hemp*, **12**(1), 27 - 45.

Chen, Y., Sun, L.F., Chiparus, O., Negulescu, I., Yachmenev, V., Warnock, M. 2005b. Kenaf/ramie composite for automotive headliner. *Journal of Polymers and the Environment*, **13**(2), 107-114.

Davoodi, M.M., Sapuan, S.M., Ahmad, D., Ali, A., Khalina, A., Jonoobi, M. 2010. Mechanical properties of hybrid kenaf/glass reinforced epoxy composite for passenger car bumper beam. *Materials & Design*, **31**(10), 4927-4932.

Fisher, F.T., Brinson, L.C. 2001. Viscoelastic interphases in polymer–matrix composites: theoretical models and finite-element analysis. *Composites Science and Technology*, **61**(5), 731-748.

Flynn, J.H., Wall, L.A. 1966. A quick, direct method for the determination of activation energy from thermogravimetric data. *Journal of Polymer Science Part B: Polymer Letters*, **4**(5), 323-328.

Hao, A., Jiang, W., Chen, J. 2010. Sunn hemp fiber physical and thermal properties in comparison with kenaf and jute fibers. in: *Plant Fibers as Renewable Feedstocks for Biofuel and Bio-based Products*, (Ed.) F. Liu, CCG International Inc., pp. 2-15.

Jiang, W., Sun, L., Hao, A., Lynch, V., Chen, J.Y. 2012. Nano-particles modified cellulose films regenerated from ionic liquid solutions. *Journal of Nanostructured Polymers and Nanocomposites*, **8**(3), 71-77.

KEFI. Properties of principal fibers, Available from: http://www.kenaf-fiber.com/en/infotec-tabella10.asp Access on January 13, 2013.

Kozłowski, R., Władyka-Przybylak, M. 2008. Flammability and fire resistance of composites reinforced by natural fibers. *Polymers for Advanced Technologies*, **19**(6), 446-453.

Pearl, I.A. 1967. *The chemistry of lignin*. Marcel Dekker, New York.

Rösler, J., Harders, H., Bäker, M. 2007. *Mechanical behaviour of engineering materials: metals, ceramics, polymers, and composites*. Springer.

Sherman, L. 1999. Natural fibers: the new fashion in automotive plastics. in: *Plastics Technology*, Vol. 45, Gardner Publications, Inc., pp. 62-68.

Song, F., Zhao, H., Hu, G. 2012. Explicit cross-link relations between effective elastic modulus and thermal conductivity for fiber composites. *Computational Materials Science*, **51**(1), 353-359.

Yancey, R.N., Pindera, M.-J. 1990. Micromechanical analysis of the creep response of unidirectional composites. *Journal of Engineering Materials and Technology*, **112**(2), 157-163.

Yang, H., Yan, R., Chen, H., Lee, D.H., Zheng, C. 2007. Characteristics of hemicellulose, cellulose and lignin pyrolysis. *Fuel*, **86**(12–13), 1781-1788.

Chapter 4: Notch Effects and Crack Propagation Analysis on Kenaf/Polypropylene Nonwoven Composites

4.1 INTRODUCTION

In this chapter, the open-hole (OH) and pin filled-hole (FH) effects on the tensile properties of KPNCs in production of automotive interior parts were investigated. The influence of specimen width-to-hole diameter (W/D) ratios of 6, 3 and 2 on failure load was studied. Two sample thicknesses of 3 mm and 6 mm were evaluated. Mechanical properties of the KPNCs in terms of uniaxial tensile, open-hole tensile (OHT), and pin filled-hole tensile (FHT) were measured experimentally. A preliminary model by extended finite element method (XFEM) was established to predict the failure load and simulate crack propagation of 3 mm thick OH and FH specimens. Good agreement was found between experimental and simulation results. By calculating the stress concentration factor Kt for brittle materials, the net section stress factor Kn for ductile materials, and the strength reduction factor Kr, it was found that KPNC was relatively ductile and insensitive to the notch.

The tensile strength of notched composites is one of the important factors for composite structural design. The strength data can be used for selections of geometric parameters and materials and for determination of structural reliability. There are generally two types of joints in composite structures: mechanically fastened joints and adhesively bonded joints. Mechanical joining by fasteners are more commonly used in complex structures because of their low cost, simplicity, and easy to disassembly for repair and recycle (Vodicka, 2006). However, mechanically fastened joints also create large stress concentrations, act as a damage initiation point, and ultimately lead to composite failure. In addition, the failure mechanics of the notched and pinned composite is not governed by either perfectly elastic or perfectly plastic theories. Therefore, it is

important to appropriately predict the failure strength and failure modes of these notched and pinned connections in order to achieve the structural integrity and reliability in composite structures. Adhesive joining does not require making notches and it distributes the load over a larger area than mechanical joining. However, adhesive joining is more sensitive to environmental conditions such as service temperature, moisture condition and UV-degradation (Brockmann et al., 2008; Gledhill & Kinloch, 1974; Loh et al., 2002).

Three typical joint failure modes of composite failure under in-plane loading are shown in Figure 4.1. They are net-tension, shear out and bearing modes. According to Hart-Smith (Hart-Smith, 1980), net-tension failure occurs when the W/D ratio is small. The net-tension failure is catastrophic. Therefore, such failure should be avoided when selecting an optimal W/D ratio in composite structural design. Bearing failure occurs when the W/D ratio is large. This failure mode leads to an elongation of the hole. Bearing failure is progressive and less likely to cause serious problems than net-tension failure mode (Camanho & Lambert, 2006). Shear-out failure is a special case of bearing failure. It is regarded as a threshold where the failure mode changes from net-tension to bearing.

There have been a lot of studies on the strength of mechanically fastened joints in composite structures. Major factors such as joint geometry, fiber orientation, laminate stacking sequence, contact friction and material properties affect the strength of pin joints. The hole size effect is important on the notched and pinned strength analysis. A comprehensive study on the stress concentration factor of a pin-loaded plate was done by Crews (Crews et al., 1981). It was found that the stress concentration factor decreased with increasing hole diameters. Collings (Collings, 1982) and Kretsis (Kretsis & Matthews, 1985) demonstrated that the joining strength and failure mechanism for carbon or glass fiber-reinforced composites were strongly dependent on the ply orientation.

Rowlands (Rowlands et al., 1982) found that changes in contact friction and clearance had little effect on the radial stress at the hole boundary.

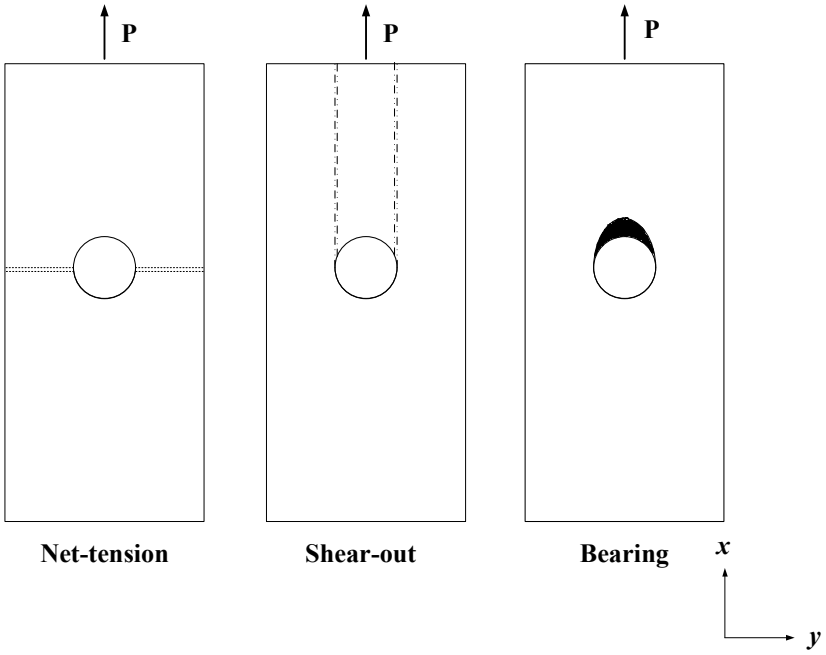

Figure 4.1 Typical pin filled-hole tensile failure modes

Several methods of failure strength prediction have been proposed to fit the experimental data. Kanninen (Kanninen et al., 1977) pointed out that linear elastic fracture mechanics could not generally cope with the complexity of composites. More innovative generalizations with various micro-mechanical failure processes were required. Hart-Smith (Hart-Smith, 1980) utilized a simple stress concentration factor for failure prediction. However, this method was very conservative for composites. Choi (Choi & Chun, 2003) proposed a failure area index method. This method is relatively simple without compromising accuracy, but had some failure criteria dependency. Whitney (Whitney & Nuismer, 1974) introduced characteristic distance approaches such as the point stress criterion and the average stress criterion. These criteria were frequently

used (Agarwal, 1979; Chang et al., 1984; Ueng & Zhang, 1985) but were dependent on the geometry of the specimen. The damage zone model (DZM) was proposed by Backlund (Backlund, 1981). This model simulated damage development in the region at intense stress at the edge of a notch using FEM. Excellent agreement between predicted and experimental strengths has been reported (Aronsson & Backlund, 1986). Hollmann (Hollmann, 1996) suggested an improved DZM to predict the failure of bolted graphite/epoxy composites. This model did not take into account the lamina interaction and fracture energy dissipation. Yan (Yan et al., 1998) used a non-linear FE technique for failure prediction. The predicted failure of strength is significantly influenced by the failure criteria and material property rule adopted (Thoppul et al., 2009). Tserpes (Tserpes et al., 2002) compared the 3D Hashin-type criterion (Hashin, 1980) and the maximum principle stress criterion (Jones, 1998) on graphite/epoxy composite laminates. It was found that the inclusion of the shear stress term in the fiber tensile Hashin-type criterion caused an over-estimation of damage but was overcome by the maximum principle stress criterion in the contact area where high shear stresses developed.

The FEM has been widely used in predicting the mechanical response of woven composites (Hao et al., 2008b; Shahkarami & Vaziri, 2007). Hou (Hou et al., 2009) established continuous and discontinuous models for predicting the failure of nonwoven composites. Bais-Singh (Bais-Singh et al., 1998) incorporated correct boundary conditions and force equilibrium conditions in the model and discussed the important effects of fiber buckling and material nonlinearity. Liao (Liao & Adanur, 1999) presented a new model, which is based on a fiber rupture criterion, to determine the damage progression and failure strength of nonwovens. Mueller (Mueller & Kochmann, 2004) designed the bond point geometry of thermo-bonded nonwovens. In this study, the FEM

was used to develop preliminary linear models for calculating the stress concentration factor.

XFEM was applied to develop preliminary models for calculating the response and for simulating the crack propagation of the OH and pin FH composite under axial loading. XFEM was developed by Belytschko (Belytschko & Black, 1999), Dolbow (Dolbow & Belytschko, 1999) and Sukumar (Sukumar et al., 2000) in 1999. Belytschko provided a classic comprehensive review of the cracking modeling using XFEM. The failure load prediction of joints can be achieved by conventional FEM. But when a crack is initiated near the notch, the crack tips need to be re-meshed. Thus, it increases the computation cost and may cause the simulation results to not converge. The convenience of adopting XFEM lies on the fact that cracks can be modeled independent of the mesh. Furthermore, the simulation of crack initiation and propagation is arbitrary and solution-independent without the need of remeshing (ABAQUS, 2009a). XFEM is an extension of conventional FEM based on the concept of partition of unity. It relies on traction-separation laws. It allows the existence and growth of discontinuities within bulk solids along an arbitrary path by enriching degrees of freedom with special displacement functions as expressed in Equation 4.1 (ABAQUS, 2009b):

$$u = \sum_{i=1}^{N} N_I(x)[u_I + H(x)a_I + \sum_{\alpha=1}^{4} F_\alpha(x)b_I^\alpha], \qquad 4.1$$

where u is the displacement vector; N_I is the shape functions; u_I is the nodal displacement vectors by conventional FEM that applies to all nodes in the model; H(x) is the jump function; $H(x)\cdot a_I$ applies to elements which cracks pass through; $F_\alpha(x)$ is the asymptotic crack-tip functions; a_I and b_I^α are the nodal enriched degree of freedom vector; and $\sum_{\alpha=1}^{4} F_\alpha(x)b_I^\alpha$ is the displacement of the crack tip elements. XFEM has a remarkable

advantage to deal with strong or weak discontinuities, such as cracks of the KNPC material studied in this work. Since the introduction of XFEM technique in ABAQUS v.6.9, it has become more mature. It has proven its capability by providing reliable solutions for cases which involve crack initiation and propagation.

As seen in Figure 4.2, the simulation procedure includes displacement analysis and failure criteria. At each displacement step, non-linear finite element analysis is conducted until a converged solution is obtained. A failure criterion is then checked. If not met, the next strain step is then applied and continued until failure occurs. The effect of material non-linearity on the failure criteria is also taken into account.

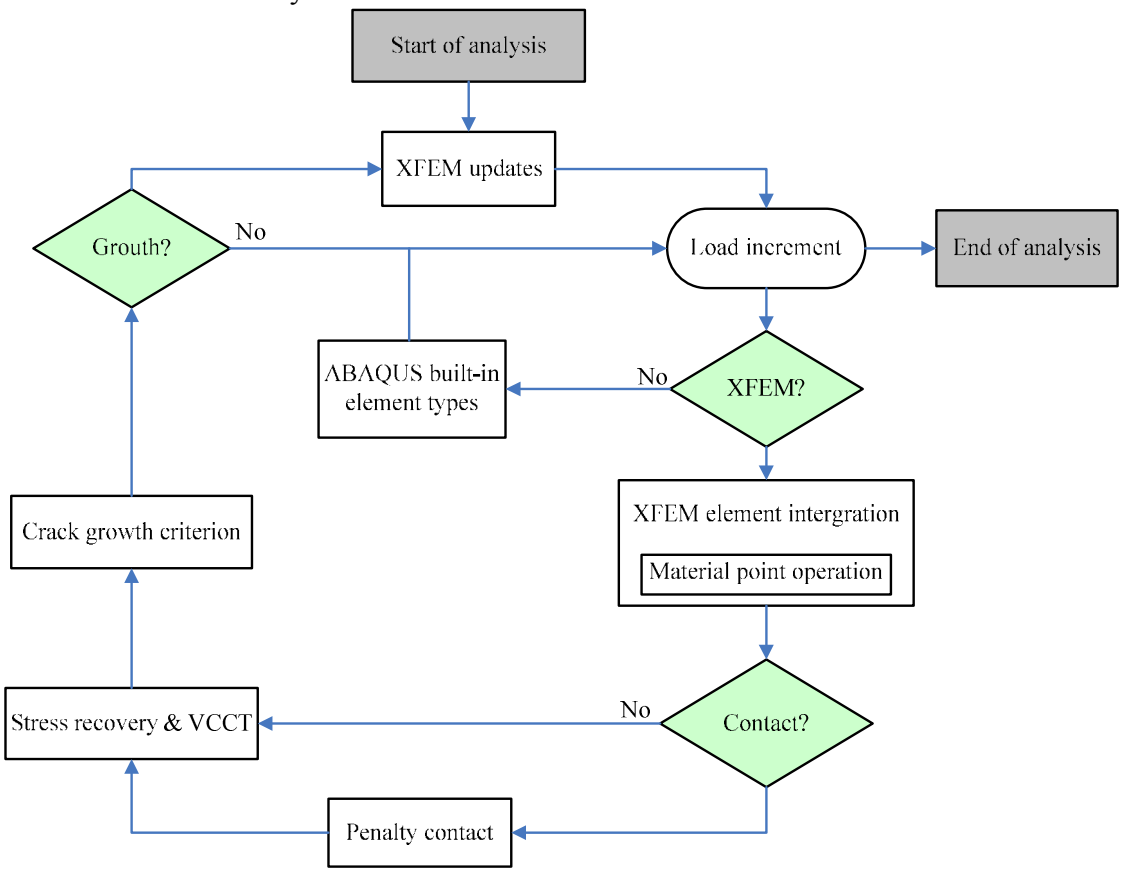

Figure 4.2 XFEM flowchart for ABAQUS/Standard, after (Ye et al., 2012; Yu et al., 2008)

4.2 EXPERIMENTAL DETAILS

4.2 1 Materials

The materials used in this chapter were the same as in Chapter 3. The 3 mm thick samples were processed at 5 or 7 MPa, 230 °C for 60 s; the 6 mm thick samples were processed at 5 or 7 MPa, 230 °C for 120 s. Unlike samples in Chapter 3, the 3 mm and 6 mm thick KPNC panels had the same density in this chapter.

4.2.2 Material Characterization

Uniaxial tensile test of KNPC was conducted using a MTS universal tester (Model QT/5, MTS Systems Corporation, Research Triangle Park, NC) with a load cell with a capacity of 5000 N at a crosshead speed of 2 mm/min and complied with the ASTM standard test method D 3039. OHT test was conducted in accordance with ASTM D 5766 to determine the OHT strength and the pin FHT test was conducted in accordance with ASTM D 6742 standard to determine the FHT strength of KPNCs. The FHT test method and its specimen configuration are similar to that used for OHT test but with a close-tolerance pin inserted in the hole.

The geometry of the composite plate is shown in Figure 4.3. A hole with diameter D is centrally located in the x-y plane. A uniform tensile load P is applied gradually to the rigid pin and this load is resisted by the composite plate for FHT test. The load is parallel to the plate and is symmetric with respect to the centerline. The OHT and FHT tests were used to find the load–displacement curves for each specimen, the ultimate failure load P_{max}, the corresponding modes of failure and the amount of crack propagation before failure. The pins are 3.175 mm (1/8 in), 6.35 mm (1/4 in) and 9.525 mm (3/8 in) in diameter, which are equivalent to W/D ratios of 6, 3 and 2 when the samples are 19±1 mm in width. The pins are made of stainless steel with a young's modulus of 180 GPa,

which is significantly greater than the composite. Thus deformation of the pins was neglected in this FHT test. Two composite nominal thicknesses were investigated: 3 and 6 mm. Five specimens were tested for each sample. All tests were conducted at 23±1 °C and a relative humidity of 43±5%.

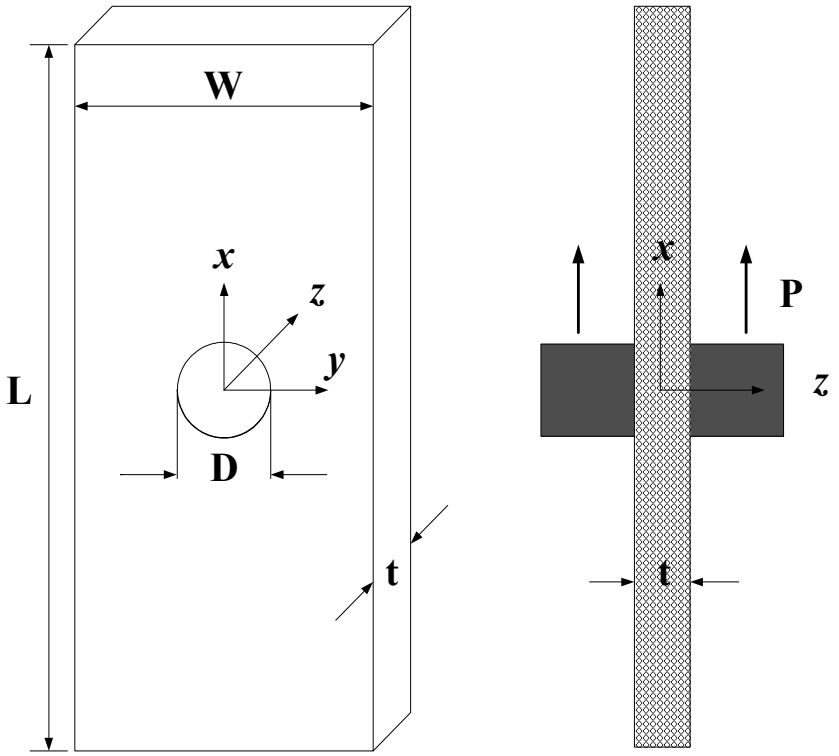

Figure 4.3 Sample geometry

The elastic stress concentration factors at holes were calculated using the theory proposed by Hart-Smith (Hart-Smith, 1986; Hart-Smith, 1980) . For ductile materials, the plastic yielding near the notch reduces the stress raising effect. The tensile stress can be then approximated using the first order strength analysis. For brittle materials, the stress concentration factor (K_t) is a measure of the strength-reducing effect of the stress concentration. Therefore, the net section stress factor K_n is suitable for ductile materials

and the stress concentration factor K_t is suitable for brittle materials. Here, the net section stress factor is defined as:

$$K_n = \frac{w}{w - d}, \tag{4.2}$$

where w is the width of the specimen and d is the diameter of the hole. The stress concentration factor K_t is defined as:

$$K_t = \frac{\sigma_0}{\sigma_\infty}, \tag{4.3}$$

where σ_0 is the highest stress near the hole, and σ_∞ is the nominal stress in the remote field, which was calculated using a FE model. In this study, a more practical measure, the strength reduction factor K_r is used. K_r is defined as:

$$K_r = \frac{\varepsilon_0}{\varepsilon_h}, \tag{4.4}$$

where ε_0 the nominal strain at rupture for a no-hole specimen, and ε_h is the nominal failure strain for the specimen with an open hole. K_r is not determined by the stress ratio here because strain gauges cannot be applied to the KPNC specimen with a high roughness surface.

4.2.3 Finite Element Modeling

A commercially available FEM code, ABAQUS version 6.12, was used for FE simulation. The computation was run at the Dell workstation at UT Austin (Dell Poweredge T610 running Ubuntu Linux server, 8×3.73 GHz Xeon processors, 24 GB memory). Four models, the 3 mm thick OH and FH models with two W/D ratios of 3 and 2 were computed. The axial response of specimen was simulated numerically using a FE model based on the XFEM. There was no need to re-mesh during the simulation of initiation and propagation of cracks using XFEM. KPNC was assumed to be a

homogenous and isotropic material in the OH and FH models; the pin was modeled as rigid body in the FH model. The plane stress element CPS4 was adopted for KPNC in the OH and FH models. Only one half of the specimen was modeled due to the in-plane symmetry of the specimen. After studying the mesh sensitivity, a mesh with 1275 elements in total was created. The mesh of the OH and PH models is depicted in Figure 4.4. The specimen was partitioned into five regions, and each region had different mesh densities. Considering the crack growth domain is limited to the part around the pin, the middle part has finest mesh with 13 elements over a height of 3 mm. At the region right above the hole, 6 elements were chosen. While for the part far away from the hole, 30 elements were found to be sufficient to provide good accuracy. A convergence study was done in order to validate the mesh.

The OH and PH models were fixed at the bottom while a constant displacement rate was applied. Symmetric boundary conditions were applied. Considering the local deformation around the hole of the specimen, a nonlinear geometry option was adopted. The top nodes of the OH model were restrained to remain horizontal during the loading. In the PH model, the pin was only allowed to move along the y direction. Finite sliding contact was also simulated during the analysis, with the outer surface of the pin as the master surface and the counterpart of specimen as the slave surface in the pin FH model. The friction coefficient was set to 0.26 (EngineeringToolBox, 2013). The cohesive segments approach of damage modeling was utilized. The maximum principal stress criterion was applied for the crack initiation, taking into account experimental data gathered during uniaxial testing of intact specimen. The OH and FH models used an energy-based criterion for the evolution of damage based on the Izod impact test results in Chapter 3. A damage evolution value of 3608 J/m^2 was used for 3 mm thick sample 5/230/60.

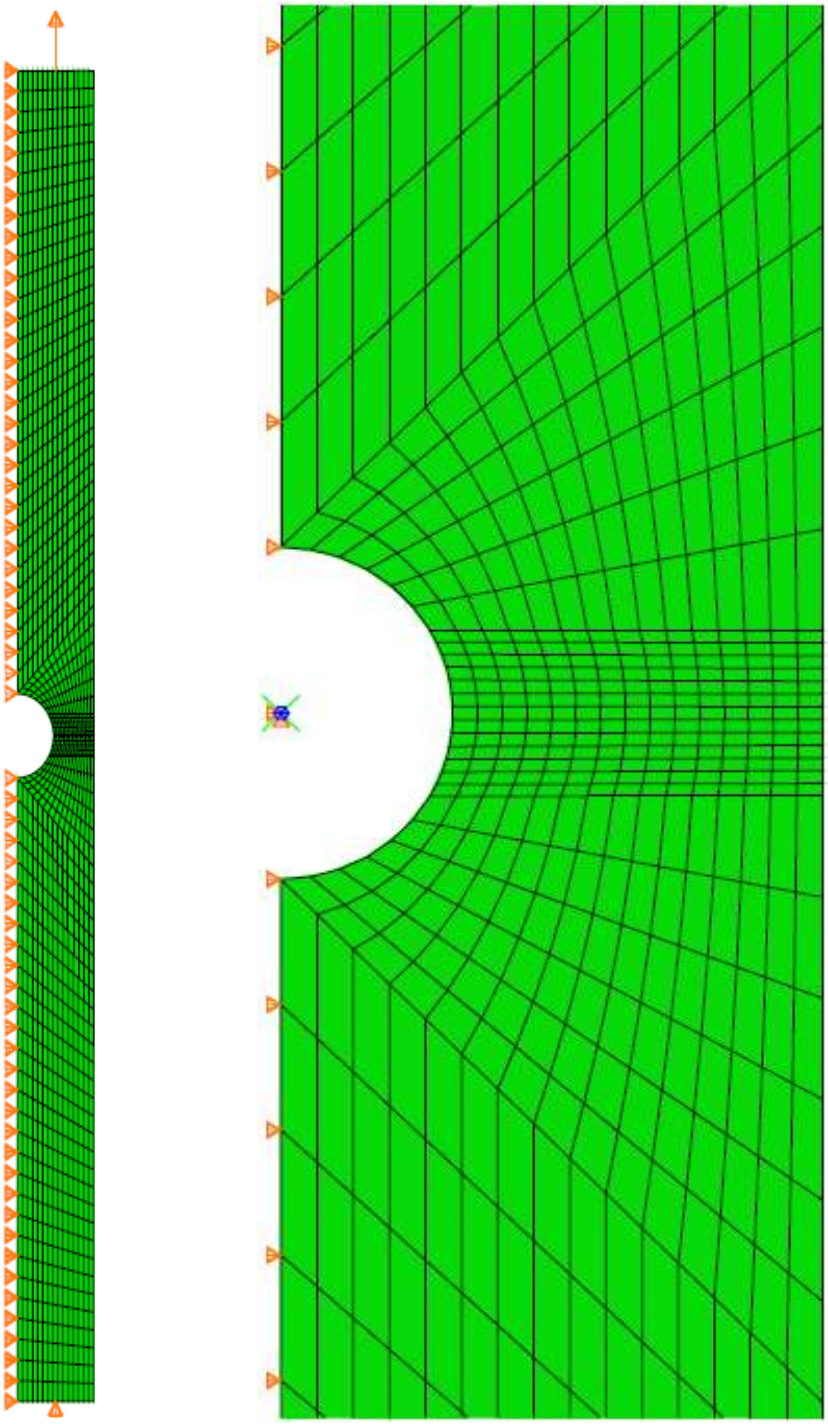

Figure 4.4 Mesh with boundary conditions: (left) an overall view of OH model; (right) Zoomed-in view at the hole of FH model

4.3 RESULTS AND DISCUSSION

4.3.1 Open-Hole Tensile (OHT) Tests

Figure 4.5 (A) shows the pictures of failed samples after the OHT test. As seen in Figure 4.6(A) and Figure 4.6(B), the failure load and displacement for 3 mm thick samples decreased as the hole diameter increased. For samples with W/D=6, only 5 out of 15 specimens broke at the hole. The samples with W/D ratio of 12 were further examined. Ten specimens were tested. However, none of them broke at the hole. Furthermore, the load-displacement curves for these samples with no hole and with W/D ratio of 12 were identical, i.e. no significant differences were observed between the no-hole sample and sample with W/D ratio of 12 (t-test, $p<0.05$). Therefore, it was concluded that the W/D ratio of 6 was close to the failure threshold value for the OHT properties of this composite.

As seen in Figure 4.7 (A) and Figure 4.7 (B), the failure load, displacement and stiffness of 6 mm thick sample also decreased as the hole diameter increased. Samples with W/D ratio of 3 lost almost half of the bearing load and the displacement also decreased by half. Comparing the load-displacement curves for 3 mm and 6 mm thick composites, it can be seen that the bearing load of the 6 mm thick KNPC was more than twice as large as that of the 3 mm thick sample, and the displacement of 6 mm thick KPNC was also larger than that of the 3 mm thick sample, indicating that the failure load and displacement was not linearly proportional to the sample thickness. By doubling the sample thickness, the 6 mm thick KPNC had more fibers to be stretched and thus helped redistribute the stress concentration near the hole, and therefore helped delay the onset of failure.

In a structural component, geometric irregularities such as rivet holes and re-entrant corners are typical stress raising factors. Materials vary greatly in the sensitivity

of these factors. For ductile materials, the plastic yielding near the notch reduces the stress raising effect to a level that this stress raising factor is often neglected. This allows the tensile stress to be approximated using the first order strength analysis. The net section stress factor K_n (Equation 4.1) is suitable for evaluating the strength reduction of ductile materials. On the other hand, the strength-reducing effects resulting from stress concentrations are quantized using the stress concentration factor K_t (Equation 4.2) that can be used for evaluating brittle materials as described in the previous section. In this study, the strength reduction factor K_r (Equation 4.3) was introduced. It is a more practical measure. As a general trend, for both 3 mm and 6 mm thick samples, the strength reduction factor K_r was closer to the net section stress factor K_n, as shown in Table 4.2 and Table 4.3. This shows that KPNC was relatively ductile and insensitive to the notch. The highest stress occurring near the hole was mitigated by the nonlinear yielding behavior of KPNC, especially for samples with W/D ratio of 6. It can be also observed that as the W/D ratio decreased from 6 to 2, the K_r values increased and became closer to K_t values, indicating that KPNC became more brittle. Thus the notch sensitivity increased when hole sizes increased.

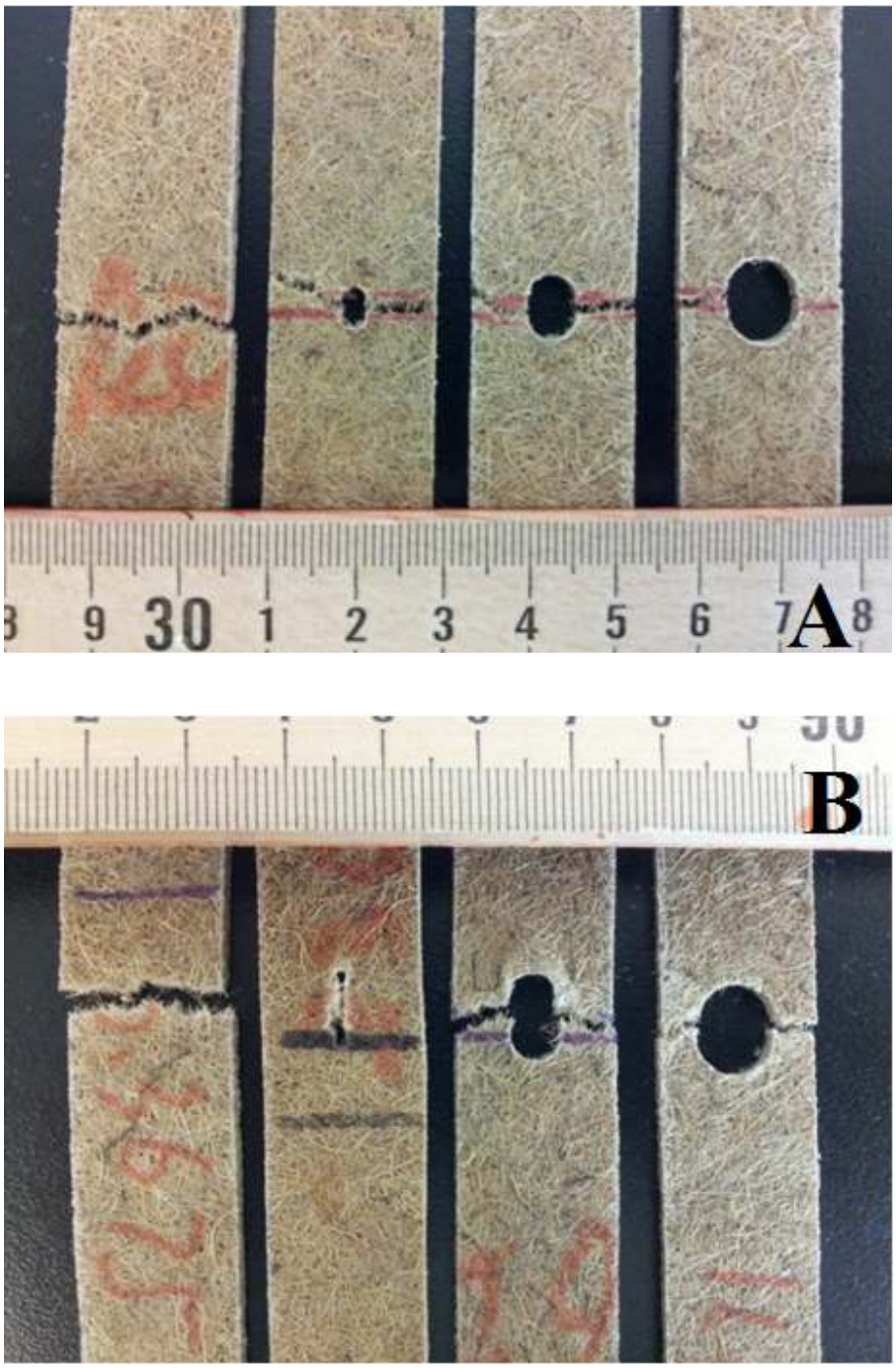

Figure 4.5 Pictures of 3 mm thick (A) OHT and (B) FHT samples (W/D ratios from left to right: no hole, 6, 3, and 2)

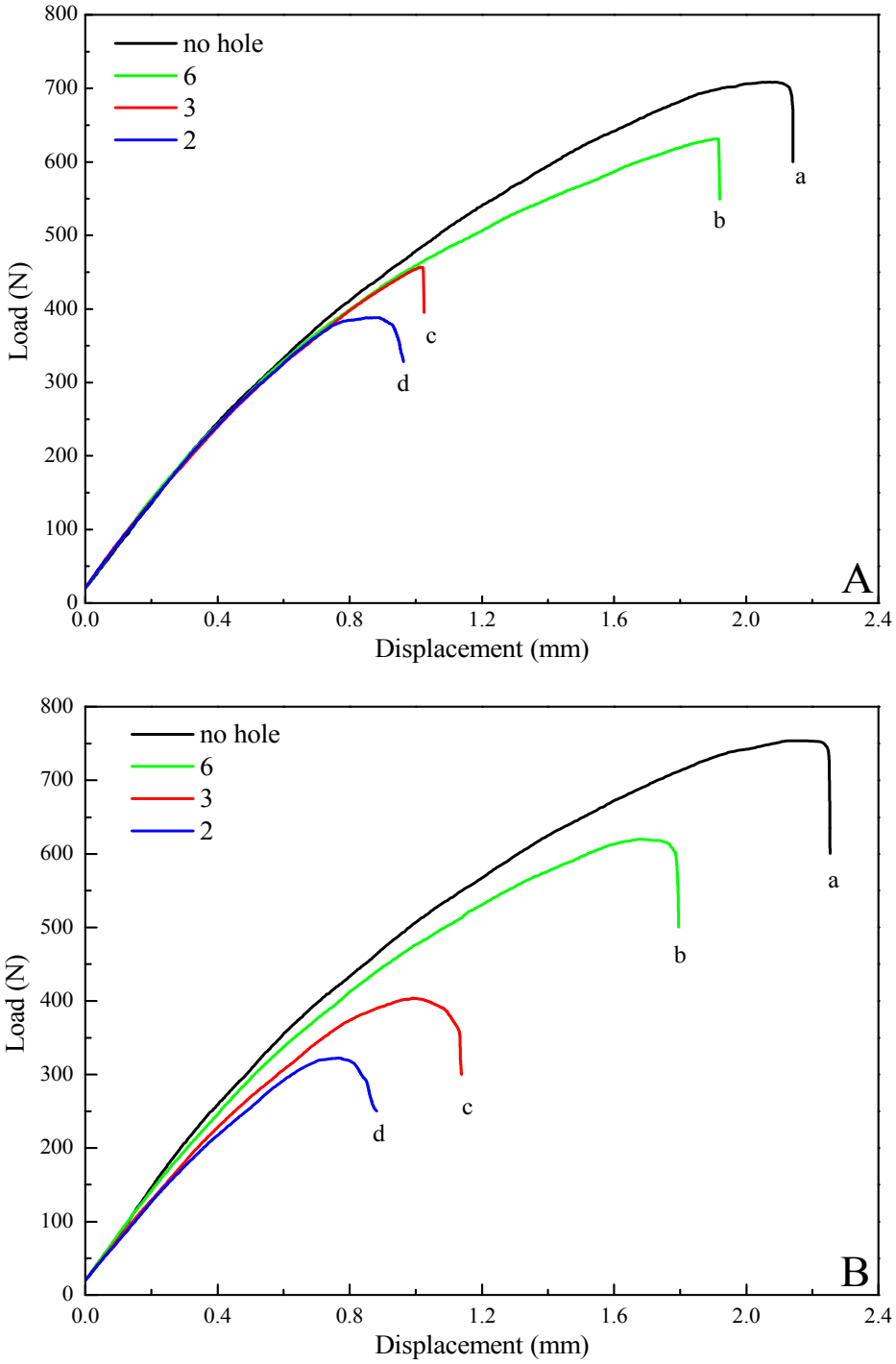

Figure 4.6 Load-displacement curves for 3 mm thick composite OHT tests of sample (A) 7/230/60 and (B) 5/230/60. W/D ratio: (a) no hole (b) 6 (c) 3 (d) 2

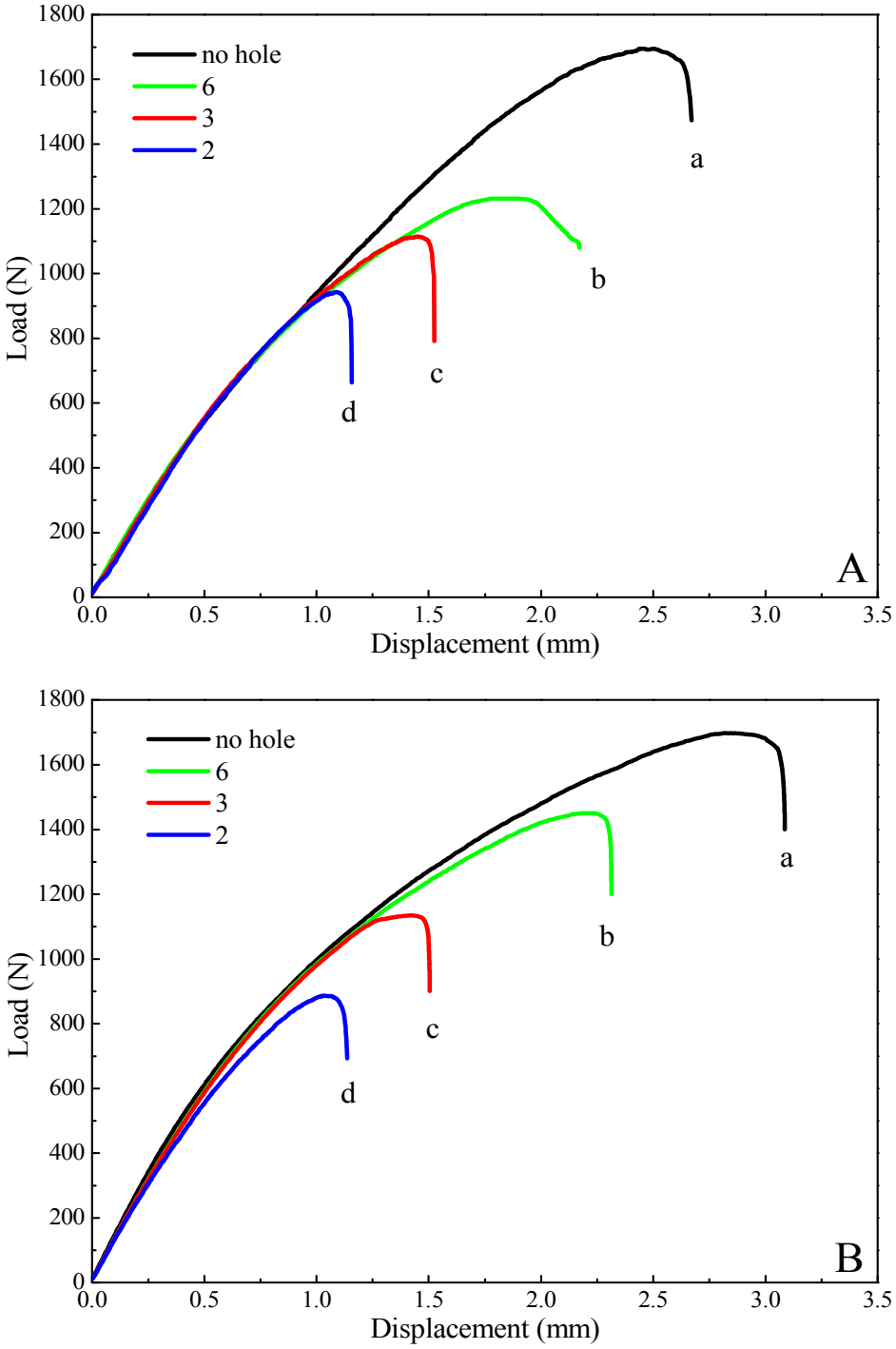

Figure 4.7 Load-displacement curves for 6 mm thick composite OHT tests of sample (A) 7/230/120 and (B) 5/230/120. W/D ratio: (a) no hole (b) 6 (c) 3 (d) 2

Table 4.1 KPNC OHT tests: nominal failure strains for various W/D ratios (standard deviation in parenthesis)

W/D Ratio	Nominal failure strain (%)			
	3 mm thickness		6 mm thickness	
	7/230/60	5/230/60	7/230/120	5/230/120
No hole	1.48 (0.1380)	1.50 (0.0730)	1.78 (0.0730)	2.04 (0.0936)
6	1.28 (0.154)	1.17 (0.0095)	1.42 (0.0193)	1.54 (0.0568)
3	0.82 (0.1040)	0.74 (0.0092)	1.02 (0.0164)	1.00 (0.0767)
2	0.64 (0.0770)	0.55 (0.0069)	0.77 (0.0852)	0.75 (0.0649)

Table 4.2 3 mm thick composite OHT tests: calculated factors for various W/D ratios

W/D Ratio	Net section stress factor (K_n)	Stress concentration factor (K_t)*	Strength reduction factor (K_r)	
			7/230/60	5/230/60
6	1.19	3.09	1.16	1.28
3	1.47	3.32	1.80	2.03
2	1.91	3.83	2.31	2.73

* Sample 7/230/60, E=1483 MPa, Poisson's ratio ν=0.29, density= 551 kg/m^3;
Sample 5/230/60, E=1521 MPa, Poisson's ratio ν=0.30, density=538 kg/m^3.

Table 4.3 6 mm thick composite OHT tests: calculated factors for various W/D ratios

W/D Ratio	Net section stress factor (K_n)	Stress concentration factor (K_t)*	Strength reduction factor (K_r)	
			7/230/120	5/230/120
6	1.18	2.92	1.25	1.32
3	1.46	3.32	1.75	2.04
2	1.87	3.70	2.31	2.72

* Sample 7/230/120, E=1447 MPa, Poisson's ratio ν=0.22, density= 554 kg/m^3;
Sample 5/230/120, E=1260 MPa, Poisson's ratio ν=0.25, density=533 kg/m^3.

4.3.2 Pin Filled-Hole Tensile (FHT) Tests

In order to analyze the effect of the pin on stiffness, strength and failure progression, FHT tests were carried out. Figure 4.5 (B) shows the pictures of failed samples after FHT tests. As can be seen in Figure 4.5 (B), samples with a W/D ratio of 6 had a shear-out failure mode using this FHT test method, indicating that the W/D ratio of 6 was close to the failure threshold value for the FHT properties of this composite.

As shown in Figure 4.8 (A) and Figure 4.8 (B), samples with the W/D ratio of 3 have a larger failure strain than that with the W/D ratio of 2. Unlike samples with the W/D ratio of 2, samples with the W/D ratio of 3 exhibited a bilinear deformation response. In the first stage, the load-displacement response was mainly governed by elastic behavior of the composite before damage. The second stage occurred when cracks near the hole initiated. The debonding and fracture of fiber, matrix cracking, and delamination were the causes of the lower slope. Comparing the first stage, the moduli of samples with and without pins were very close, which was similar to what was observed for the OHT test. This indicated that the pin had little effect on the initial stiffness of KPNC. By comparing failure loads between the FHT and OHT tests, the samples with the W/D ratio of 3 experienced a 20% increase after inserting the pin to the open hole, while the samples with the W/D ratio of 2 did not change significantly.

Comparing the FHT failure displacements, the specimens with W/D ratios of 3 and 2 also exhibited two types of responses: In the FHT test with a W/D ratio of 2, the inserted pin caused the samples to fail a little earlier compared to the OHT test. For samples with the W/D ratio of 3, the failure displacement was much larger than that measured in the OHT test. This resulted from the fact that during tensile loading the inserted pin compressed the sample hole wall to develop a region of compressive deformation before the tensile fracture occurred. A series of numerical models were

carried out using ABAQUS, where an elastic response was examined. In Table 4.5 and Table 4.6, the stress concentration factor K_t, which was extracted from the numerical model, showed the extent of stress concentration at the end of first linear stage.

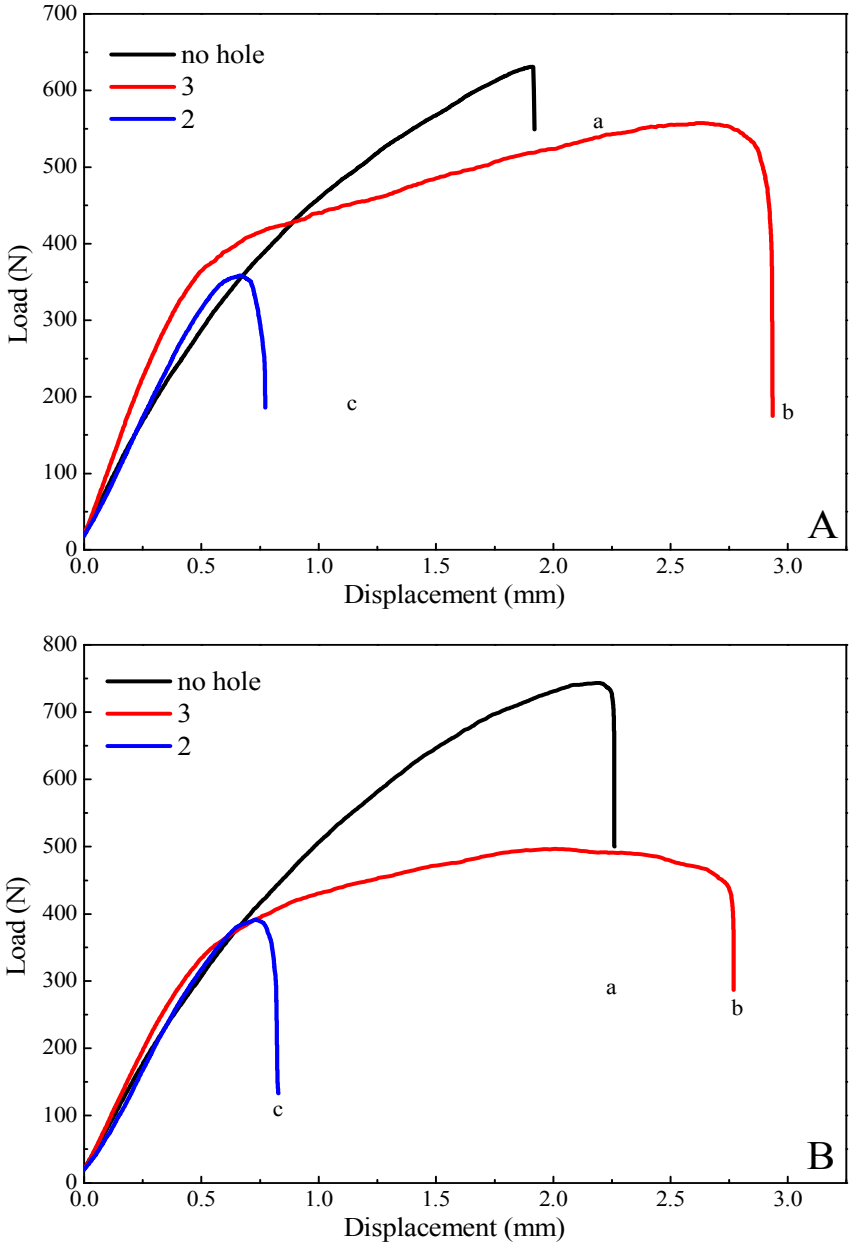

Figure 4.8 Load-displacement curves for 3 mm thick composite pin FHT tests of sample (A) 7/230/60 and (B) 5/230/60. W/D ratio: (a) no hole (b) 3 (c) 2

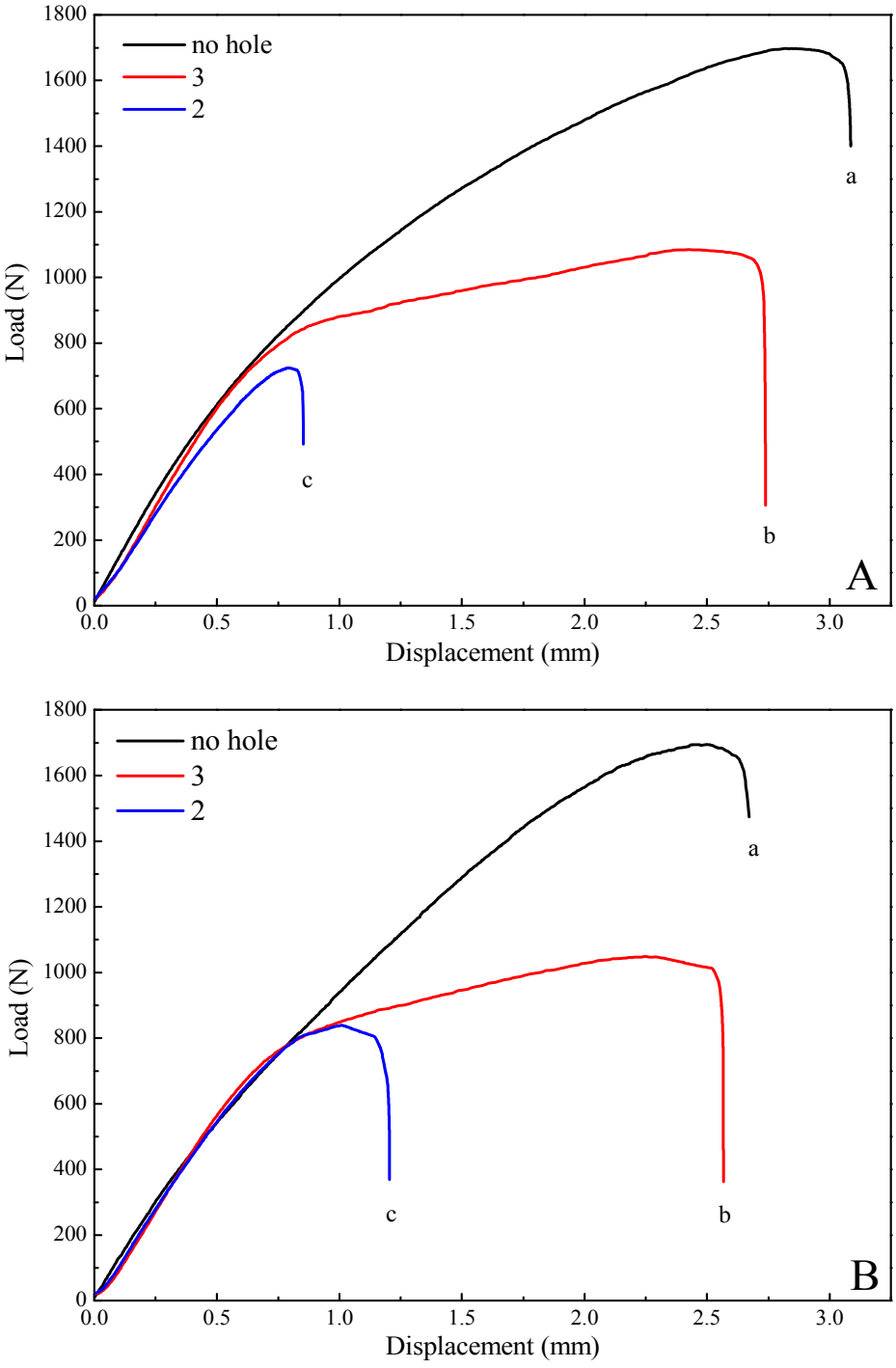

Figure 4.9 Load-displacement curves for 6 mm thick composite pin FHT tests of sample (A) 7/230/120 and (B) 5/230/120. W/D ratio: (a) no hole (b) 3 (c) 2

Table 4.4 KPNC FHT tests: nominal failure strains for various W/D ratios (standard deviation in parenthesis)

W/D Ratio	Nominal failure strain (%)			
	3 mm thickness		6 mm thickness	
	7/230/60	5/230/60	7/230/120	5/230/120
No hole	1.48 (0.1380)	1.50 (0.0730)	2.04(0.0936)	1.78 (0.0730)
3	1.93 (0.1425)	1.85 (0.1907)	3.65 (0.3001)	3.35 (0.2665)
2	0.49 (0.0294)	0.53 (0.0271)	1.14 (0.1004)	1.63 (0.3356)

Table 4.5 3 mm thick composite FHT tests: calculated factors for various W/D ratios

W/D Ratio	Net section stress factor (K_n)	Stress concentration factor (K_t)*	Strength reduction factor (K_r)	
			7/230/60	5/230/60
3	1.47	3.74	0.77	0.81
2	1.91	3.69	3.02	2.83

* Sample 7/230/60, E=1483 MPa, Poisson's ratio ν=0.29, density= 551 kg/m^3;
Sample 5/230/60, E=1521 MPa, Poisson's ratio ν=0.30, density=538 kg/m^3.

Table 4.6 6 mm thick composite FHT tests: calculated factors for various W/D ratios

W/D Ratio	Net section stress factor (K_n)	Stress concentration factor (K_t)*.	Strength reduction factor (K_r)	
			7/230/120	5/230/120
3	1.46	3.64	0.56	0.53
2	1.87	3.82	1.79	1.09

* Sample 7/230/120, E=1447 MPa, Poisson's ratio ν=0.22, density= 554 kg/m^3;
Sample 5/230/120, E=1260 MPa, Poisson's ratio ν=0.25, density=533 kg/m^3.

4.3.3 Failure Prediction and Crack Propagation Simulation by XFEM

The failure prediction for the OHT tests by XFEM was compared with experimental data. As seen in Figure 4.10, a good agreement was found. The difference between the experiment and XFEM simulation on the load-displacement was due to the homogeneous isotropic assumption on material properties. The failure load prediction of 3 mm thick KPNC with a W/D ratio of 3 was 9.6% higher than experiment; and the failure load prediction of 3 mm thick KPNC with a W/D ratio of 2 was 3.9% higher than experiment. The KPNC was assumed solid in the simulation, but in fact, the KPNC material has voids and gaps between individual fibers. These voids and gaps lead to a decrease in failure load in the experimental tensile testing. The predicted failure displacement of 3 mm thick KPNC with a W/D ratio of 3 was 17.0% smaller than the experimental data; the predicted failure displacement of 3 mm thick KPNC with a W/D ratio of 2 was 15.5% smaller than the experiment. Fiber pull-out was not taken into account in the simulation, but in fact, the fiber was straightened and pulled out when KPNC was subject to tension. Thus it delayed the final failure of the KPNC and resulted in larger displacement values. The larger experimental failure displacement than the XFEM simulated values resulted from the KPNC's ductile behavior as discussed in the previous section. Figure 4.11 shows the simulated Von Mises stress distribution after crack propagation using the OH model. It can be observed that the crack pattern matched the actual experimental crack path as seen in Figure 4.5 (A).

The failure prediction of the FHT test by XFEM was compared with the experimental data. As seen in Figure 4.12, XFEM successfully predicted the bilinear deformation path of sample with the W/D ratio of 3, but the XFEM simulation overestimated the failure load and underestimated the failure displacement. This was due to the homogeneous and isotropic assumption on material properties. Figure 4.13 shows

the simulated Von Mises stress distribution after crack propagation of the FH model. The crack pattern also matched the actual experimental crack path very well as shown in Figure 4.5 (B), indicating the validity of XFEM in simulating crack propagation of KPNCs with an open hole or pin filled hole.

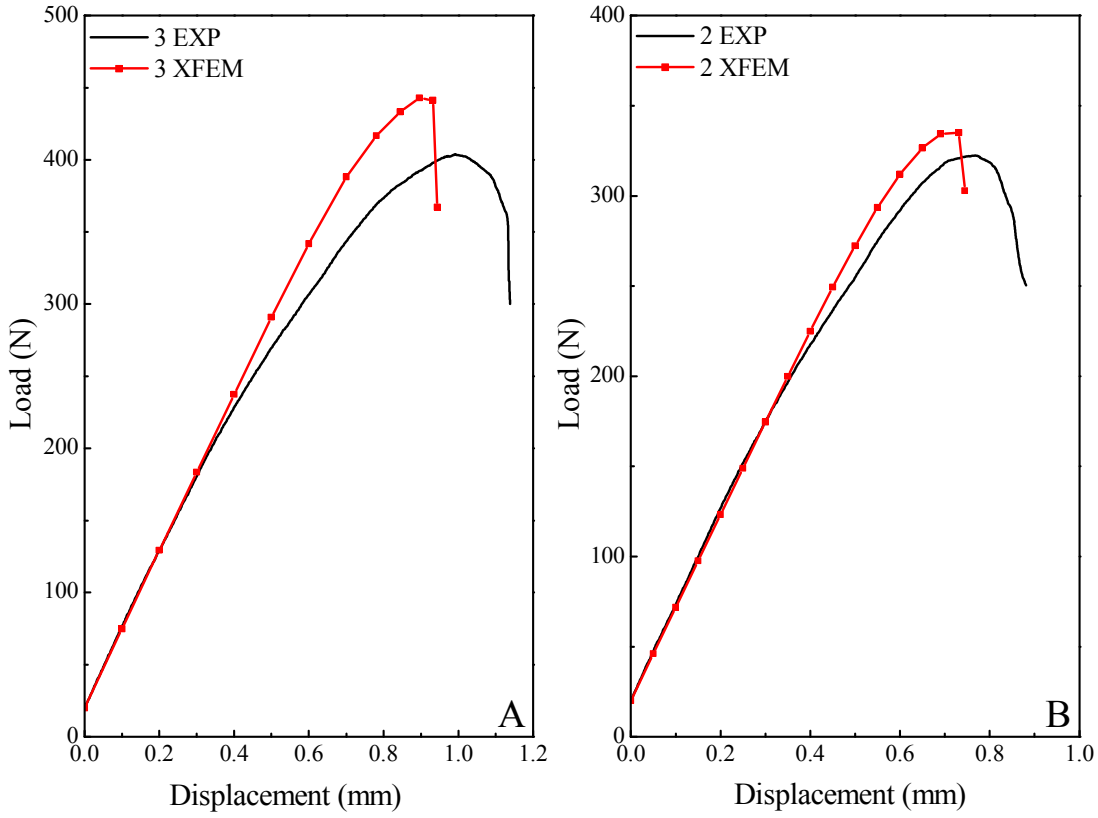

Figure 4.10 Load-displacement curves for 3 mm thick composite OHT tests of sample 5/230/60. W/D ratio: (A) 3 and (B) 2; symbol lines represent the simulation results by XFEM

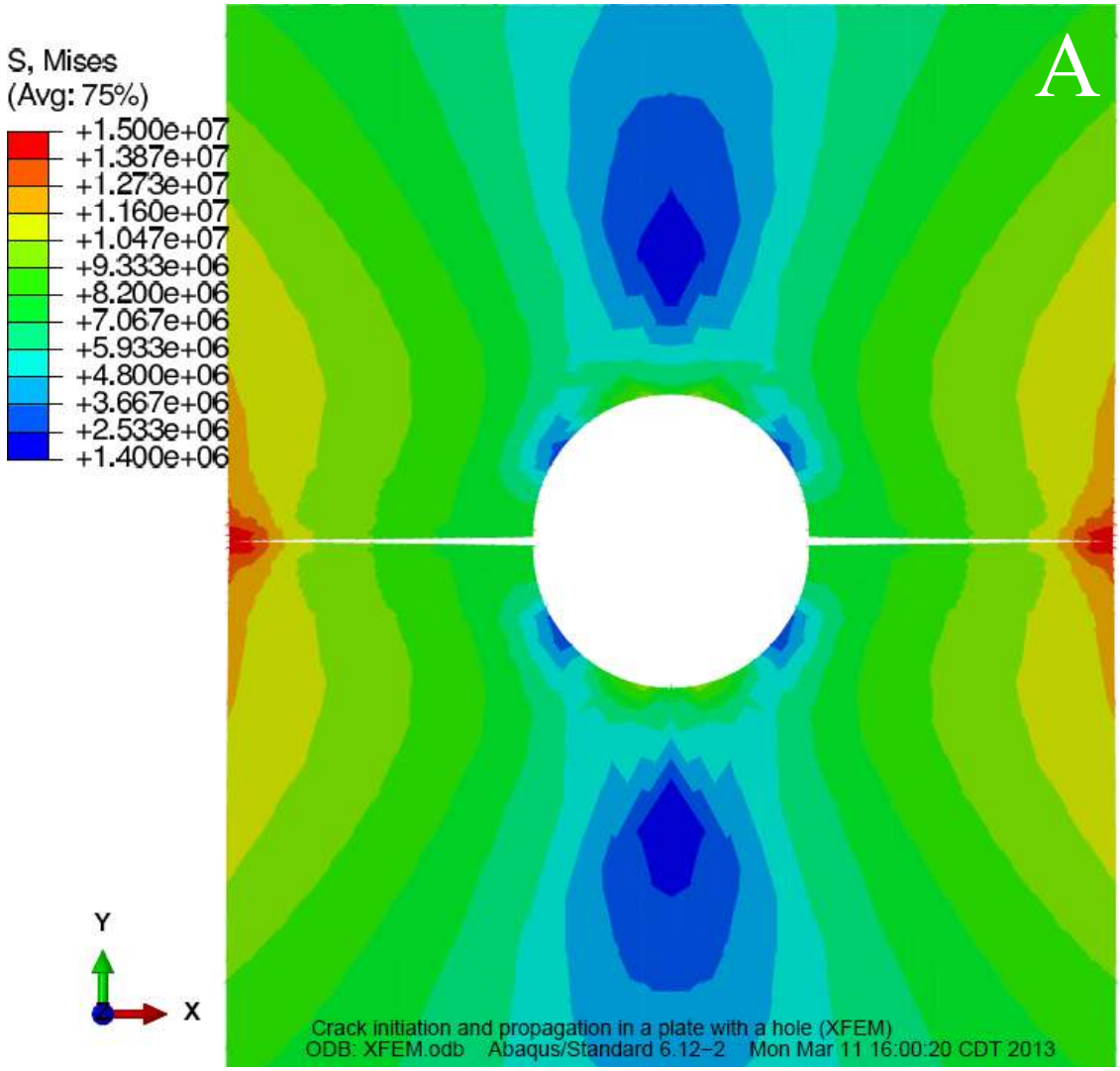

Figure 4.11 Failure images of 3 mm thick composite OHT tests of sample 5/230/60. W/D ratio: (A) 3 and (B) 2

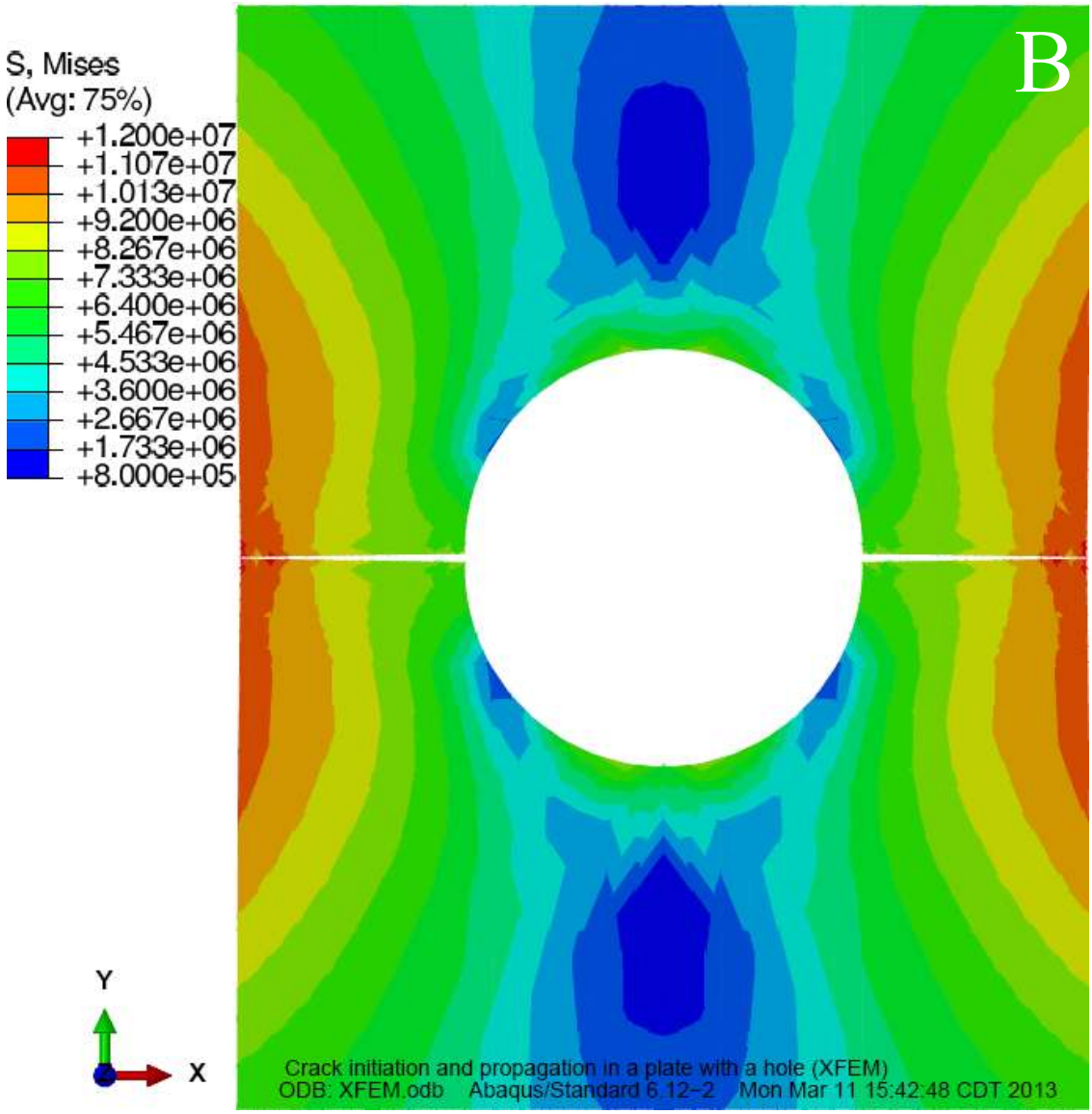

Figure 4.11 Cont.

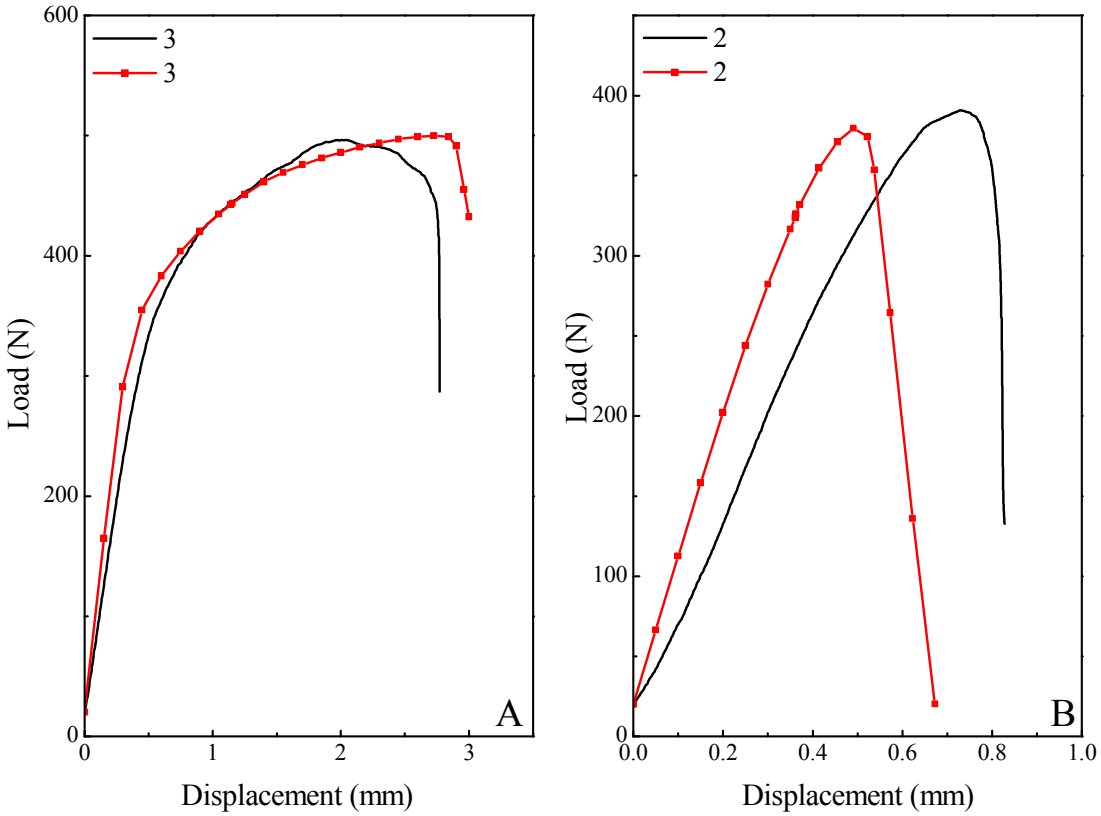

Figure 4.12 Load-displacement curves for 3 mm thick composite FHT tests of sample 5/230/60. W/D ratio: (A) 3 and (B) 2; symbol lines represent the simulation results by XFEM

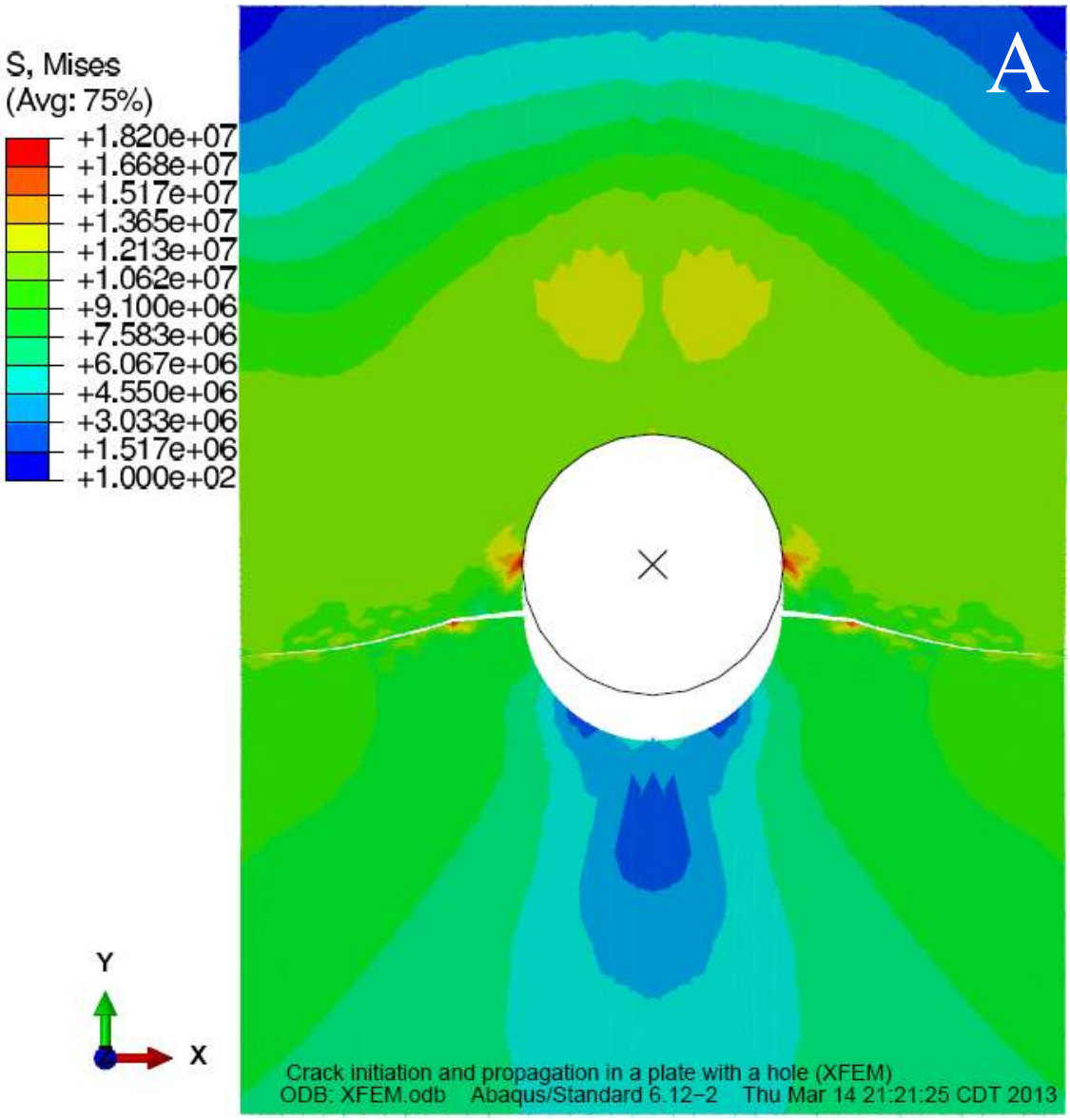

Figure 4.13 Failure images of 3 mm thick composite pin FHT tests of sample 5/230/60. W/D ratio: (A) 3 and (B) 2

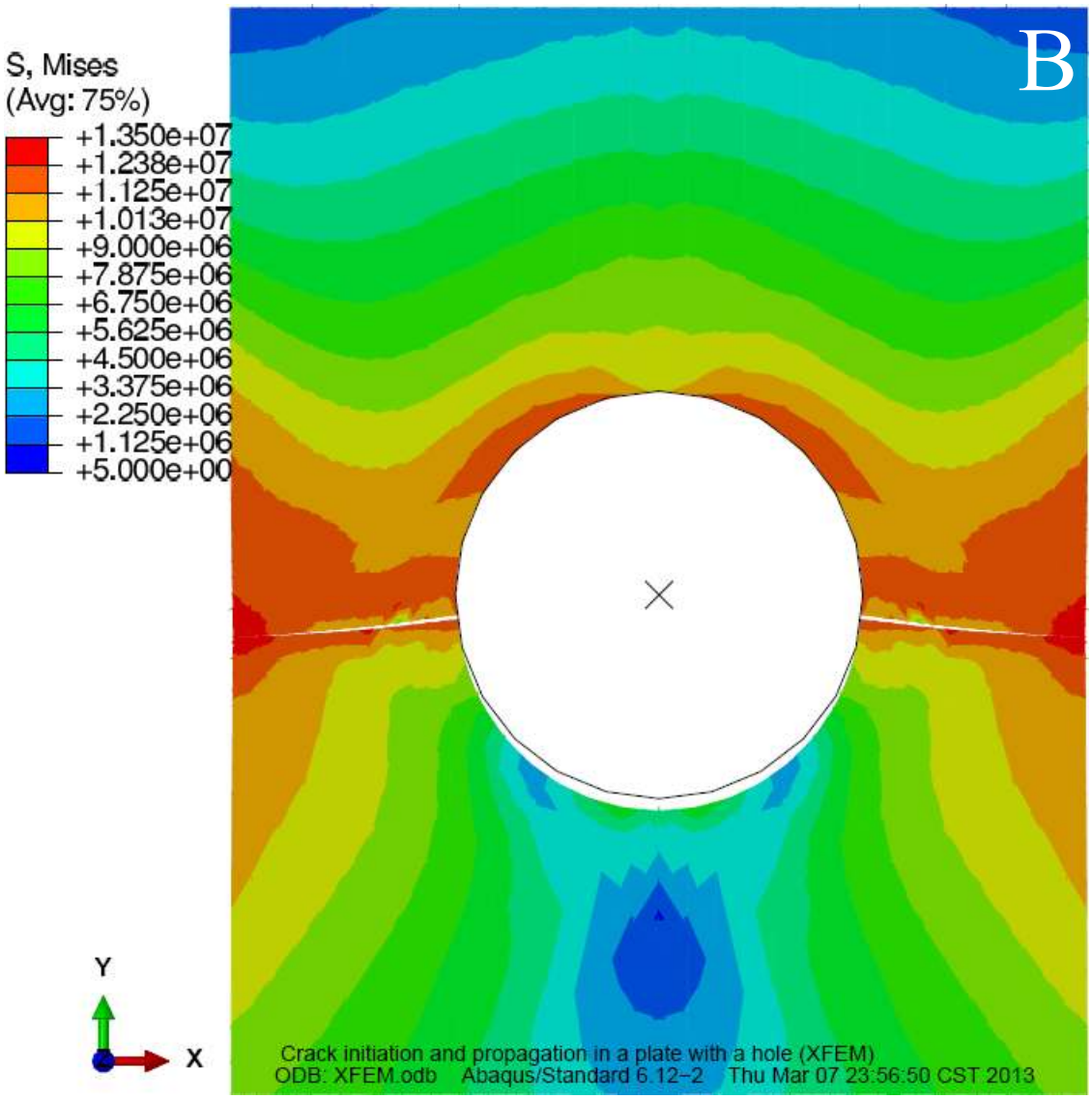

Figure 4.13 Cont.

4.4 CONCLUSIONS

In this chapter, the notch effects on the tensile properties of KPNCs were evaluated by performing OHT and pin FHT tests. Three W/D ratios of 6, 3 and 2 were compared. The OHT test showed that the strength-reducing effect of stress concentration was mitigated greatly by the ductile-like behavior of KPNCs. Therefore, KPNCs were relatively insensitive to notch effects. The FHT test showed that the pins had little effect on the initial stiffness of the specimen. As to the strength and failure, the effects of pin tended to be dependent on the W/D ratios. After inserting the pin, the specimen with W/D= 3 showed more ductile behavior, while the specimen with W/D= 2 exhibited the lowest breaking strength and strain. This may provide a basic understanding on the pin joint effects for KPNC materials used for automotive interior parts.

The predictions of the load-displacement curves by the XFE model showed good agreement with experimental data for the OHT and FHT tests with the two W/D ratios. The crack propagation pattern predicted by XFEM also matched the experimental crack path very well. It indicated the applicability of XFEM in predicting the failure strength and simulating crack propagation of natural fiber reinforced composites with an open hole or pin filled hole.

4.5 ACKNOWLEDGEMENTS

Appreciations are given to Dr. Haifeng Zhao and Mr. Lin Yuan, Department of Aerospace Engineering and Engineering Mechanics at University of Texas at Austin for valuable technical discussions about this chapter.

4.6 REFERENCES

ABAQUS. 2009a. ABAQUS/CAE User's Manual Daussalt Systemes, Inc., Vélizy-Villacoublay, France

ABAQUS. 2009b. Extended Finite Element Method (XFEM) in Abaqus http://www.simulia.com/download/rum11/UK/Advanced-XFEM-Analysis.pdf, Vol. 2013.

Agarwal, B. 1979. Static strength prediction of bolted joint in composite material. *Structures, Structural Dynamics, and Materials Conference, 20 th, St. Louis, Mo*. pp. 303-309.

Aronsson, C.-G., Backlund, J. 1986. Tensile fracture of laminates with cracks. *Journal of Composite Materials*, **20**(3), 287-307.

Backlund, J. 1981. Fracture analysis of notched composites. *Computers & Structures*, **13**(1), 145-154.

Bais-Singh, S., Biggers, S.B., Goswami, B.C. 1998. Finite Element Modeling of the Nonuniform Deformation of Spun-Bonded Nonwovens. *Textile Research Journal*, **68**(5), 327-342.

Belytschko, T., Black, T. 1999. Elastic crack growth in finite elements with minimal remeshing. *International journal for numerical methods in engineering*, **45**(5), 601-620.

Brockmann, W., Geiß, P.L., Klingen, J., Schröder, K.B. 2008. *Adhesive bonding: materials, applications and technology*. Wiley-VCH.

Camanho, P.P., Lambert, M. 2006. A design methodology for mechanically fastened joints in laminated composite materials. *Composites Science and Technology*, **66**(15), 3004-3020.

Chang, F.-K., Scott, R.A., Springer, G.S. 1984. Failure of composite laminates containing pin loaded holes—method of solution. *Journal of Composite Materials*, **18**(3), 255-278.

Choi, J.-H., Chun, Y.-J. 2003. Failure load prediction of mechanically fastened composite joints. *Journal of Composite Materials*, **37**(24), 2163-2177.

Collings, T. 1982. On the bearing strengths of CFRP laminates. *Composites*, **13**(3), 241-252.

Crews, J.H.J., Hong, C., Raju, I. 1981. Stress-Concentration Factors for Finite Orthotropic Laminates with a Pin-Loaded Hole. DTIC Document.

Dolbow, J., Belytschko, T. 1999. A finite element method for crack growth without remeshing. *International journal for numerical methods in engineering*, **46**(1), 131-150.

EngineeringToolBox. 2013. Frictional Coefficients for some Common Materials and Materials Combinations http://www.engineeringtoolbox.com/friction-coefficients-d_778.html.

Gledhill, R., Kinloch, A. 1974. Environmental failure of structural adhesive joints. *The Journal of Adhesion*, **6**(4), 315-330.

Hao, A., Sun, B., Qiu, Y., Gu, B. 2008. Dynamic properties of 3-D orthogonal woven composite T-beam under transverse impact. *Composites Part A: Applied Science and Manufacturing*, **39**(7), 1073-1082.

Hart-Smith, L.J. 1986. Design and analysis of bolted and riveted joints in fibrous composite structures. *Douglas Paper 7739*, 1-15.

Hart-Smith, L.J. 1980. Mechanically-fastened joints for advanced composites-phenomelogical considerations and simple analysis. in: *Fibrous composites in structural design*, (Ed.) O.D. Leneo EM, Burke JJ Plenum Press. New York.

Hashin, Z. 1980. Failure criteria for unidirectional fiber composites. *Journal of applied mechanics*, **47**, 329.

Hollmann, K. 1996. Failure analysis of bolted composite joints exhibiting in-plane failure modes. *Journal of Composite Materials*, **30**(3), 358-383.

Hou, X., Acar, M., Silberschmidt, V.V. 2009. 2D finite element analysis of thermally bonded nonwoven materials: Continuous and discontinuous models. *Computational Materials Science*, **46**(3), 700-707.

Jones, R. 1998. *Mechanics of composite materials*. CRC.

Kanninen, M., Rybicki, E., Brinson, H. 1977. A critical look at current applications of fracture mechanics to the failure of fibre-reinforced composites. *Composites*, **8**(1), 17-22.

Kretsis, G., Matthews, F. 1985. The strength of bolted joints in glass fibre/epoxy laminates. *Composites*, **16**(2), 92-102.

Liao, T., Adanur, S. 1999. Computerized Failure Analysis of Nonwoven Fabrics Based on Fiber Failure Criterion. *Textile Research Journal*, **69**(7), 489-496.

Loh, W., Crocombe, A., Abdel Wahab, M., Ashcroft, I. 2002. Environmental degradation of the interfacial fracture energy in an adhesively bonded joint. *Engineering fracture mechanics*, **69**(18), 2113-2128.

Mueller, D.H., Kochmann, M. 2004. Numerical Modelling of Thermobonded Nonwovens. *International Nonwovens Journal*, **13**(1), 56-62.

Rowlands, R., Rahman, M., Wilkinson, T., Chiang, Y. 1982. Single-and multiple-bolted joints in orthotropic materials. *Composites*, **13**(3), 273-279.

Shahkarami, A., Vaziri, R. 2007. A continuum shell finite element model for impact simulation of woven fabrics. *International Journal of Impact Engineering*, **34**(1), 104-119.

Sukumar, N., Moës, N., Moran, B., Belytschko, T. 2000. Extended finite element method for three‐dimensional crack modelling. *International journal for numerical methods in engineering*, **48**(11), 1549-1570.

Thoppul, S.D., Finegan, J., Gibson, R.F. 2009. Mechanics of mechanically fastened joints in polymer–matrix composite structures–a review. *Composites Science and Technology*, **69**(3), 301-329.

Tserpes, K., Labeas, G., Papanikos, P., Kermanidis, T. 2002. Strength prediction of bolted joints in graphite/epoxy composite laminates. *Composites Part B: Engineering*, **33**(7), 521-529.

Ueng, C., Zhang, K.-D. 1985. Strength prediction of a mechanically fastened joint in laminated composites. *AIAA journal*, **23**(11), 1832-1834.

Vodicka, R. 2006. Thermoplastics for Airframe Applications-A Review of the Properties and Repair Methods for Thermoplastic Composites. *Thermoplastics for Airframe Applications: A Review of the Properties and Repair Methods for Thermoplastic Composites*.

Whitney, J., Nuismer, R. 1974. Stress fracture criteria for laminated composites containing stress concentrations. *Journal of Composite Materials*, **8**(3), 253-265.

Yan, U., Sun, H., Wei, W., Chang, F. 1998. Response and Failure of Composite Plates With a Bolt-Filled Hole. DTIC Document.

Ye, C., Shi, J., Cheng, G.J. 2012. An eXtended Finite Element Method (XFEM) study on the effect of reinforcing particles on the crack propagation behavior in a metal–matrix composite. *International Journal of Fatigue*, **44**(0), 151-156.

Yu, L., Waisman, H., Shi, J., Liu, P., Jum, L. 2008. Pre-processing Toolkit for Three-dimensional X-FEM. *Aerospace and Electronics Conference, 2008. NAECON 2008. IEEE National*, 16-18 July 2008. pp. 265-272.

Chapter 5: Time and Temperature Dependent Behavior of Kenaf/Polypropylene Nonwoven Composites

5.1 INTRODUCTION

This chapter reports an exploratory study on the creep performance of KPNCs comparing to solid virgin PP plastics. Because PP is a standard plastic currently used in the automotive interior application (Holbery & Houston, 2006), this study intends to explore the application of KPNC as a bio-based substitution for PP plastics used in the automotive industry. Only one KPNC sample (5/230/60) was utilized but an extensive series of tests were conducted to characterize the creep behavior of KPNC. A direct comparison between KPNC and PP can not be applied in this study, because KPNC not only has a different microstructure from PP, but also has a high volume fraction of pores. It is not possible to prepare PP sample with a similar microstructure to KPNC, so that a direct comparison can not be made.

Lee (Lee et al., 2004) investigated the creep behavior of wood flour-filled PP composites. Tajvidi (Tajvidi et al., 2005) used the time-temperature superposition (TTS) method to predict the creep strains of kenaf reinforced high-density polyethylene (HDPE) composites. Xu (Xu et al., 2010) evaluated the creep behavior of bagasse reinforced polyvinyl chloride (PVC) composites. Rouison (Rouison et al., 2006) studied the creep deformation of hemp reinforced polyester composites. However, these materials are all injection-molded or resin-transfer-molded PMCs, which are greatly different from the nonwoven composites that have a porous structure. This porous structure results in higher creep strains and lower stiffness of KPNC. No previous literature can be found in the creep study of natural fiber nonwoven composites such as KPNC in this study.

The creep behavior of nonwoven felts (before compression molding) in geotextile applications has been studied by some researchers (Bueno et al., 2005; Das et al., 2005;

Liqing et al., 2001). Although the materials used in these studies also have a nonwoven structure, they are soft nonwoven fabrics largely different from nonwoven composites whose stiffness was greatly enhanced by compression molding. Thus the major contribution of this original work is to provide a comprehensive set of data and analyses of the creep behavior of a typical natural fiber nonwoven composite. This original work provides a reference for other researchers to compare their work on nonwoven composites in the future. The cyclic creep tests, recovery rate model and creep recoverability analysis discussed in Session 5.3.2.5 is also original. This creep recovery analysis contributes to the limited literature in this area.

In this chapter, the strain rate effects on the tensile properties of KPNC were studied first. The strain rate effects confirmed the time-dependence of KPNCs. Afterward, the creep behavior of KPNC and PP were performed by DMA which allowed it to be studied more extensively. A linear viscoelastic limit (LVL) was found. The long-term creep behavior of KPNC in comparison to virgin PP plastic was predicted using the time-temperature superposition (TTS) principle. A three-day creep test was also conducted to validate the effectiveness of the TTS prediction. The creep recovery, stress effects and cyclic creep performance were also evaluated. Two popular creep models, the four-element Burgers model and the Findley power law model, were used to model the creep behavior in this study.

5.1.1 Creep Tests

Polymers used in engineering applications are often subjected to stress for a long time and at high temperatures. In this case, polymers exhibit time- and temperature-dependent behavior. Therefore, understanding the viscoelastic properties of polymers is very important. Creep is the progressive deformation of a material at a constant stress.

Creep behavior is another very important end-use property for natural fiber-reinforced PMCs, because both the natural fiber reinforcement and polymer matrix exhibit time- and temperature-dependent properties.

When performing a creep test, a plastic material deforms continuously as shown in Figure 5.1. The initial strain is generally predicted by its elastic stress-strain curve. The material will continue to deform slowly with time until yielding or rupture. The primary stage is when the creep rate decreases rapidly with time. The creep deformation then reaches a steady state, which is called the secondary stage, followed by a tertiary stage with a rapid increase of strain rate before fracture. Figure 5.1 is an idealized curve, because some materials do not exhibit the secondary stage, while the tertiary creep only occurs at high stresses for some ductile materials (Krempl & Khan, 2003). All plastics creep to a certain extent due to their viscoelastic properties. The degree of creep depends on factors such as type of plastic, magnitude of load, temperature and time (Acha et al., 2007; Bledzki & Faruk, 2004; Sullivan, 1990).

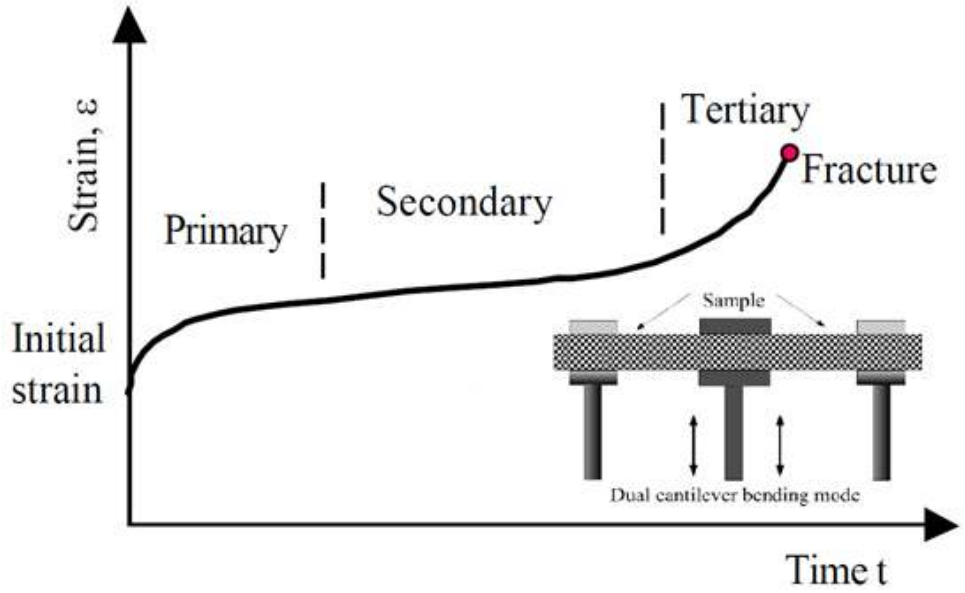

Figure 5.1 Creep curve for plastics; a constant load is applied isothermally

There have been considerable studies on the creep behavior of natural fiber reinforced PMCs. Park (Park & Balatinecz, 1998) investigated the flexural creep behavior of wood/PP composites and fitted the experimental data using a power law model. It was found that the creep resistance of this PMC has been greatly improved by adding wood fibers. Shi (Shi et al., 2012) performed creep frequency sweep tests and applied the TTS theory to starch-based PMCs. They were able to successfully predict the creep response in 20 days using this approach. Tajvidi (Tajvidi et al., 2005) studied kenaf fiber/HDPE composites and found that a single horizontal shift factor in the TTS theory was not adequate. The master curve generated by TTS deviated from the experimental data. A modified TTS principle was proposed by combining a horizontal and vertical shift. Xu (Xu et al., 2010) analyzed the creep recovery of bagasse fiber-reinforced PMCs and compared the modeling results of a 4-, 6-, and 8-element Burgers model. Xu et al. concluded that more elements resulted in a better curve fitting. Eight elements were necessary for their case. Pooler (Pooler & Smith, 2004) evaluated the stress effects on the non-linear viscoelastic properties of wood-based PMCs. The time-stress superposition (TSS) principle similar to TTS was applied in Pooler's research.

Although there are a great number of studies on the creep behavior of PMCs, there is no comprehensive study on the creep behavior of nonwoven composites. In this chapter, a variety of creep tests were conducted on KPNCs and virgin PP plastics, and some models suitable for evaluating the creep behavior of these materials are discussed.

5.1.2 Creep and Recovery Models

Many models have been proposed to describe the creep behavior of polymers. The creep behavior is represented by simple rheological models if the polymer is tested

under LVL. These models can be divided into physical models and empirical models based on the interpretation of parameters.

The four-element Burgers model has been widely used as a physical model to capture the creep behavior of natural fiber-reinforced PMCs (Alvarez et al., 2004; Cyras et al., 2002; Xu et al., 2011). This model has one Maxwell unit and one Kelvin unit connected in series as shown in Figure 5.2. The creep strain for PMC consists of three parts: instantaneous deformation resulting from the Maxwell spring; viscoelastic deformation resulting from Kelvin units; and viscous deformation resulting from the Maxwell dashpot. It can be expressed as (Lee et al., 2004):

$$\varepsilon(t) = \frac{\sigma}{E_M} + \frac{\sigma}{E_K}\left[1-\exp(-t/\tau)\right] + \frac{\sigma}{\eta_M}t \quad , \quad \tau = \frac{\eta_K}{E_K} \quad , \qquad 5.1$$

where ε (t) is the creep strain; σ is the applied stress; t is the time; τ is the retardation time for the Kelvin element to produce 63.21% (or 1–1/*e*) of its total deformation; E_M and E_K are the elastic moduli of the springs; and η_M and η_K are viscosities of the dashpots in this model. The parameters E_M, E_K, η_M, and η_K can be obtained by fitting experimental data with Equation 5.1 and be used for characterization of creep properties. In this equation, the first term is a constant and independent of time; the second term contributes to the early stage of creep, but reaches a maximum quickly; and the last term determines the long-term creep trend at a constant creep rate.

Based on the four-element Burgers model, the creep rate ε'(t) can be expressed as:

$$\varepsilon'(t) = \frac{d\varepsilon(t)}{dt} = \frac{\sigma}{\eta_K}\exp\left(-\frac{E_K}{\eta_K}t\right) + \frac{\sigma}{\eta_M} \qquad 5.2$$

The creep rate reaches to a constant value when the creep reaches a steady-state (t=∞), as shown below:

$$\varepsilon'(\infty) = \frac{\sigma}{\eta_M} \quad 5.3$$

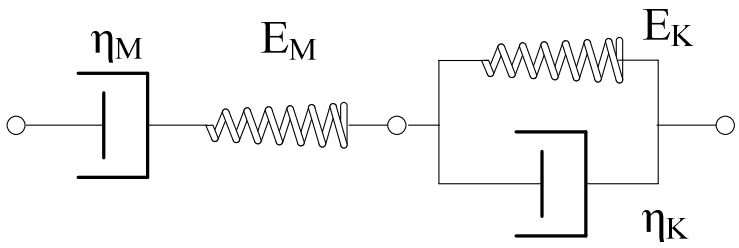

Maxwell Unit Kelvin Unit

Figure 5.2 Illustration of the four-element Burgers model

The Findley power law model is one of the most popular empirical models for analyzing creep behavior of polymers. It can be expressed as (Findley & Davis, 1989):

$$\varepsilon(t) = \varepsilon_0 + \varepsilon_c \times t^n, \quad 5.4$$

where ε(t) is the creep strain at time t; ε_0 is the time-independent initial strain; εc is the amplitude of creep strain which is a time-dependent coefficient; n is the time exponent that is independent of stress and is generally less than one; ε_0 and ε_c are functions of stress and environmental variables.

When the constant stress is removed at time t_0, the sample starts to recover, which is the reverse of creep. The maximum deformation is achieved at time t_0:

$$R(t) = \varepsilon(t_0) - \varepsilon(t_0 + t). \quad 5.5$$

The creep deformation in the recovery process can be divided into two parts: recoverable strain, R(t), at time t, and non-recoverable strain, NR(t), at time t, as expressed below:

$$\varepsilon(t) = R(t) + NR(t). \quad 5.6$$

The recoverable strain for the four-element Burgers model is:

$$R(t) = \frac{\sigma}{E_M} + \frac{\sigma}{E_K}\left[1 - \exp\left(-\frac{E_K}{\eta_K}t\right)\right]. \quad 5.7$$

The non-recoverable strain for the four-element Burgers model is:

$$NR(t) = \frac{\sigma}{\eta_M}t. \quad 5.8$$

The magnitude of the non-recoverable deformation depends on the time, temperature and amount of stress applied to the polymer. The recovery rate at time t is defined as:

$$RR(t)\% = \frac{R(t)}{\varepsilon(t)} \times 100\% = 100\% - \frac{NR(t)}{\varepsilon(t)} \times 100\%. \quad 5.9$$

In the cyclic creep and recovery analysis, the recovery rate of each cycle was calculated using Equation 5.9. The cyclic creep and recovery experimental data was fitted to an exponential decay model expressed by:

$$RR(N) = a \times \exp(-N/b) + RR(\infty), \quad 5.10$$

where RR(N) is defined as the recovery rate of the Nth cycle; RR(∞) is defined as the recovery rate after infinite numbers of creep cycles; a is an exponential decay amplitude; and b is a decay constant.

5.1.3 Time-Temperature Superposition (TTS)

Although long-term creep is very important for evaluating the end-use performance of natural fiber reinforced composites, it is usually not practical to perform a creep test for an extremely long period of time. TTS is one of the most useful extrapolation techniques to predict the long-term creep behavior using short-term testing (Nayak et al., 2009; Pothan et al., 2003; Scott et al., 1995). TTS assumes that the viscoelastic behavior of amorphous polymers at one temperature can be related to that at

another temperature by a change in the time scale only. The curves from tests at different temperatures horizontally are shifted along a logarithmic time axis until the curves overlap to form one continuous master curve. The TTS technique was originally developed for amorphous polymers. Ward (Ward, 1983) concluded TTS could not be applied to crystalline polymers because of their complicated thermal behavior. However, Nielsen (Nielsen & Landel, 1993) suggested that TTS could be applicable to semi-crystalline polymers if a vertical shifting factor was also introduced into the TTS method. Since the TTS method has limits to its application (Knauss, 2008), verification of the master curve with a three-day creep test is necessary to validate this model for KPNCs.

The shifting factor (a_T) is defined as the shifting distance in the logarithmic time axis. a_T can be also calculated from the Arrhenius equation (Equation 5.11) and Williams-Landel-Ferry (WLF) equation (Equation 5.12), as shown below (Nuñez et al., 2004):

$$\ln(a_T) = \frac{E_a}{R} \cdot \left(\frac{1}{T} - \frac{1}{T_0}\right) \tag{5.11}$$

$$\log(a_T) = \frac{-C_1 \cdot (T - T_0)}{C_2 + (T - T_0)}, \tag{5.12}$$

where E_a is the material activation energy; R is the universal gas constant; C_1 and C_2 are constants related to polymer properties; and T_0 is the reference temperature (40 °C in this study).

5.2 EXPERIMENTAL DETAILS

5.2.1 Tensile Tests at Various Strain Rates

The strain rate effects on the tensile properties of KPNC were studied to evaluate the time-dependency of KPNCs. Tensile tests were carried out at three crosshead speeds of 0.2 mm/min, 2 mm/min and 20 mm/min, using a MTS universal tester (Model QT/5, MTS Systems Corporation, Research Triangle Park, NC). These were equivalent to the strain rates of $2.22\times10^{-5}s^{-1}$, $2.22\times10^{-4}s^{-1}$ and $2.22\times10^{-3}s^{-1}$ when the nominal gauge length of the specimen was 150 mm. 3 mm thick samples 7/230/60 and 5/230/60 were evaluated in this test.

5.2.2 Creep Tests

Creep tests were performed using a dynamic mechanical analyzer (DMA) (Model Q800, TA Instrument Inc., New Castle, DE) in the dual-cantilever mode. The 3 mm thick sample 5/230/60 that had the largest failure strain was selected for the creep tests. The PP sample for creep tests was cut from a solid block of virgin PP, which was supplied by Sabic Inc. (grade code: 575P, Sittard, The Netherlands). The melt flow rate of PP sample is 10.5 g/10min at 230 °C and 2.16 kg (ISO 1133).

Specimens were 13±1 mm wide and the testing length was fixed at 35 mm. The KPNC specimens were 3.0±0.2 mm thick and solid virgin PP plastics were 1.9±0.1 mm thick. In each test, the specimens were heated to the desired temperature and were allowed to equilibrate for 5 minutes prior to the test. Each test was repeated twice. The averaged values were reported. The KPNC and PP samples are shown in Figure 5.3.

Figure 5.3 Specimens for DMA tests: (left) KPNC and (right) solid virgin PP

The maximum nominal normal stress (MPa) in the dual-cantilever deformation mode is calculated using Equation 5.13 and the maximum nominal normal strain (%) is expressed using Equation 5.14:

$$\sigma_x = \frac{3 \cdot P \cdot L}{w \cdot t^2} \tag{5.13}$$

$$\varepsilon_x = \frac{3 \cdot \delta \cdot t \cdot F_c}{L^2 \cdot [1 + \frac{12}{5} \cdot (1 + \upsilon) \cdot \left(\frac{t}{L}\right)^2]}, \tag{5.14}$$

where L is the length (mm) between clamps (17.5 mm in this study); w is the sample width (mm); t is the sample thickness (mm); P is half of the applied force (N); F_c is the

clamping correction factor; and υ is the material Poisson's ratio. For KPNC υ is 0.3 and for virgin PP υ is 0.45 (Tscharnuter et al., 2011).

5.2.2.1 Temperature Determination in Creep Tests

To determine the temperature steps to perform creep test, sample 5/230/60 was heated from 40 to 200 °C and the virgin PP sample was heated from 40 to 180 °C at a heating rate of 5 °C/min. The samples were deformed in the dual-cantilever mode at 0.05% strain. Loading frequency was 1.0 Hz.

5.2.2.2 Linear Viscoelastic Limit (LVL)

Strain sweep tests of the KPNC and PP samples up to the maximum force level of the instrument (i.e., 18 N) were performed at a frequency of 1 Hz and at the temperatures of 40, 60, 80, 100, 120 and 140 °C. The strain rate was 2.28×10^{-5} s^{-1}.

5.2.2.3 Thirty-minute Creep Tests

The 30 min creep tests were performed at a frequency of 1 Hz at the temperatures of 40, 60, 80, 100, 120, and 140 °C for KPNC and at the temperatures of 40, 60, 80, and 100°C for PP. After equilibrating at the desired temperature, a stress of 1 MPa (the LVL value obtained in 5.2.2.2) was applied and held constant for thirty minutes while the creep strain was measured, followed by a 30 min recovery.

5.2.2.4 Three-day Creep Tests

Three-day creep tests were also performed at 40 °C for both the KPNC and PP samples at the stress level of 1 MPa. After 72 hours, the stress was released and the sample was allowed to recover for 24 hours. The three-day creep test results were compared with the TTS prediction from the master curves.

5.2.2.5 Stress Effects

The 30 min creep tests were performed at a frequency of 1 Hz at 40 °C for both KPNC and PP. After equilibrating, five stress levels of 0.5, 1, 1.5, 2.5, 3.5 MPa were applied and held constant for thirty minutes while the creep strains were measured.

5.2.2.6 Cyclic Creep Tests

The 30 min creep test in 5.2.2.3 was repeated for a total of ten cycles at 40–140°C for KPNC and at 40–100°C for the PP sample. The recovery rate for each cycle was calculated.

5.2.3 Creep Molding and Recovery Analysis

Non-linear regression was used to estimate E_M, η_M and η_K values in Equation 5.1. Least-square estimates of the regression parameters were calculated by minimizing the sum of squares. The correlation coefficient value r^2 is defined as model sum of squares divided by total sum of squares. A better goodness-to fit is obtained when r^2 is closer to 1. Statistical Analysis System (SAS) version 9.2 (SAS Inc, Cary, NC) was used to perform this non-linear regression analysis on the experimental data. The Gauss-Newton iterative method was implemented in estimating the parameters and minimizing the sum of squares.

5.3 RESULTS AND DISCUSSION

5.3.1 Tensile Tests at Various Strain Rates

Figure 5.4 (A) and Figure 5.3 (B) show that the stress and strain behavior varied with three strain rates at 2.2×10^{-5}, 10^{-4} and 10^{-3} s^{-1} for samples 7/230/60 and 5/230/60. The mechanical characteristics dependent upon the strain rate were calculated and compared. Composite failure stress, failure strain and Young's modulus all increased

with the strain rate, as a result of viscoelasticity of KPNC. The strain rate had a statistically significant effect on the failure strains for samples 7/230/60 and 5/230/60 (one-way ANOVA, $p<0.05$).

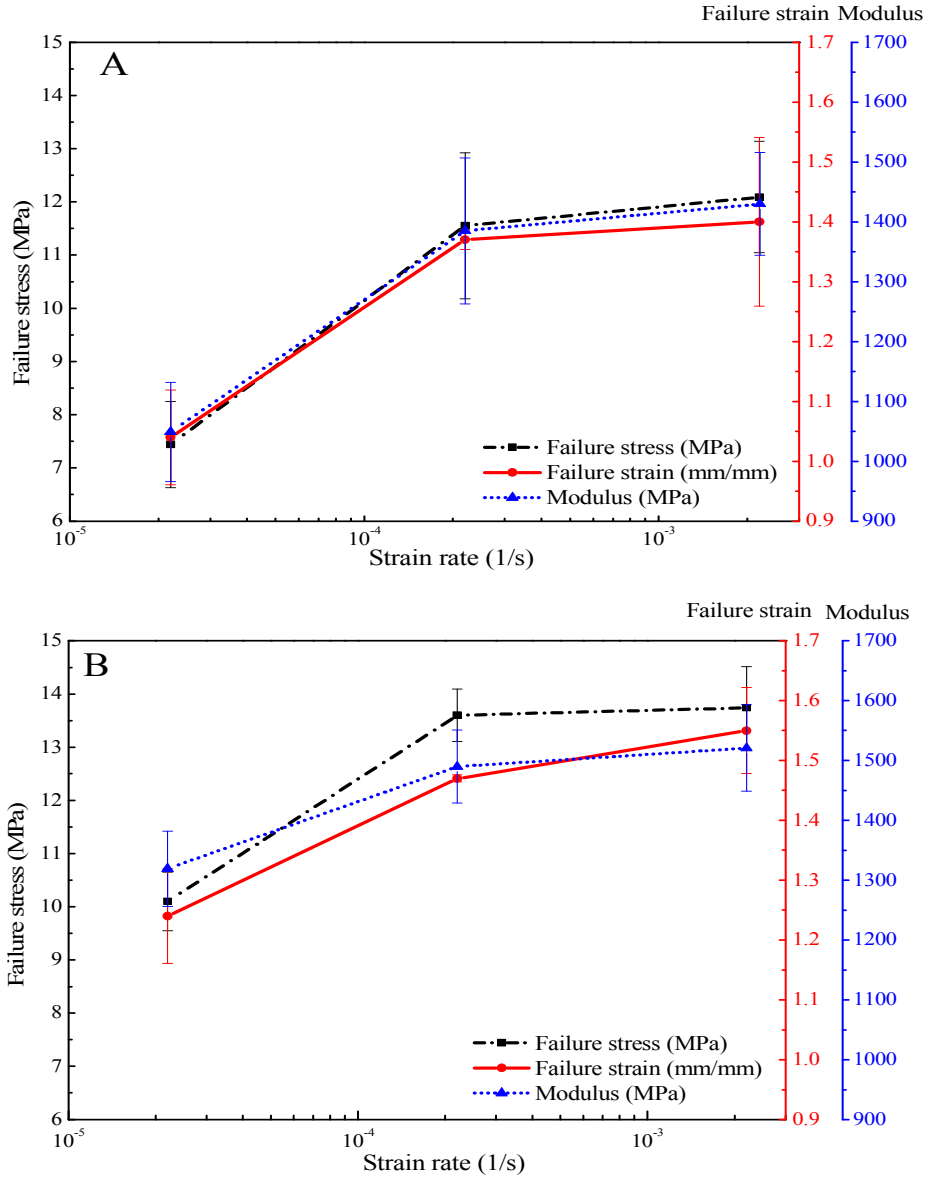

Figure 5.4 Tensile test of sample (A) 7/230/60 and (B) 5/230/60 at three strain rates (crosshead speeds): (low) $2.2\times10^{-5}s^{-1}$ (0.2 mm/min), (standard) $2.2\times10^{-4}s^{-1}$ (2 mm/min), (high) $2.2\times10^{-3}s^{-1}$ (20 mm/min)

5.3.2 Creep Tests

5.3.2.1 Temperature Determination in Creep Tests

As seen in Figure 5.5, the glass transition of KPNC occurred within 40–60 °C and melting of KPNC occurred within 150–160 °C. Therefore, the creep test temperature steps of KPNC were selected from 40 to 140 °C with an increment of 20 °C. In addition, the reference temperature (T_{ref}) in the TTS prediction was selected as 40 °C, because it is desirable to set T_{ref} close to T_g. For virgin PP, an abnormal storage modulus bump occurred when temperature exceeded 100 °C. Because PP exhibited a very low viscosity above 100 °C, the dimensional changes of the PP samples were very significant. Storage modulus calculations assume that the sample behaves in a linearly elastic manner. The creep strain caused by sample gravity was higher than the true strain applied by the instrument. Therefore, valid creep data for the PP sample was obtained by the DMA method only up to 100 °C. The creep test temperature steps of PP were thus selected from 40 to 100 °C, with an increment of 20 °C.

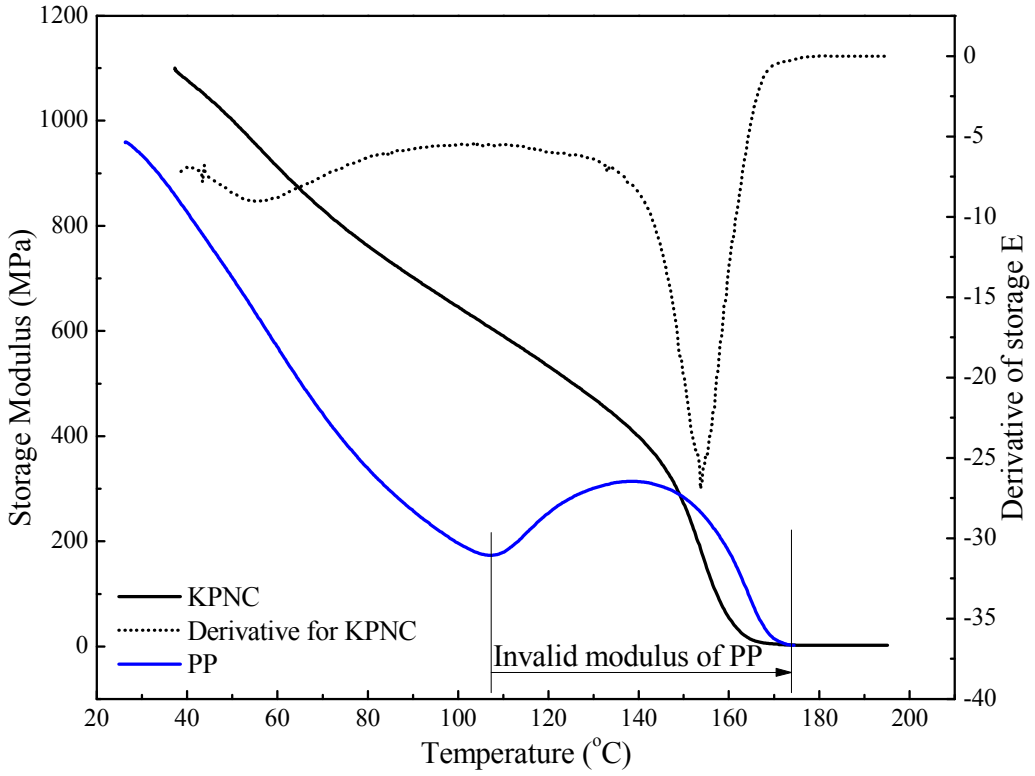

Figure 5.5 Storage moduli of KPNC and PP as a function of temperature

5.3.2.2 Linear Viscoelastic Limit (LVL)

Figure 5.6 shows the strain sweep test results for KPNC at 40–140 °C and of PP at 40–100 °C. The stress-strain curve for KPNC showed a good linear relationship in the testing region up to about 3.5 MPa at 40 °C, The LVL of KPNC was shortened to about 1 MPa when the temperature increased to 140 °C. This phenomenon resulted from the viscous behavior of KPNC and was not apparent during the test at 40 °C. But the mobility of polymer molecular chains (mainly PP matrix) increased with increasing temperature. Therefore, a stress of 1 MPa was used in the creep tests to ensure that the creep deformations were within the LVL.

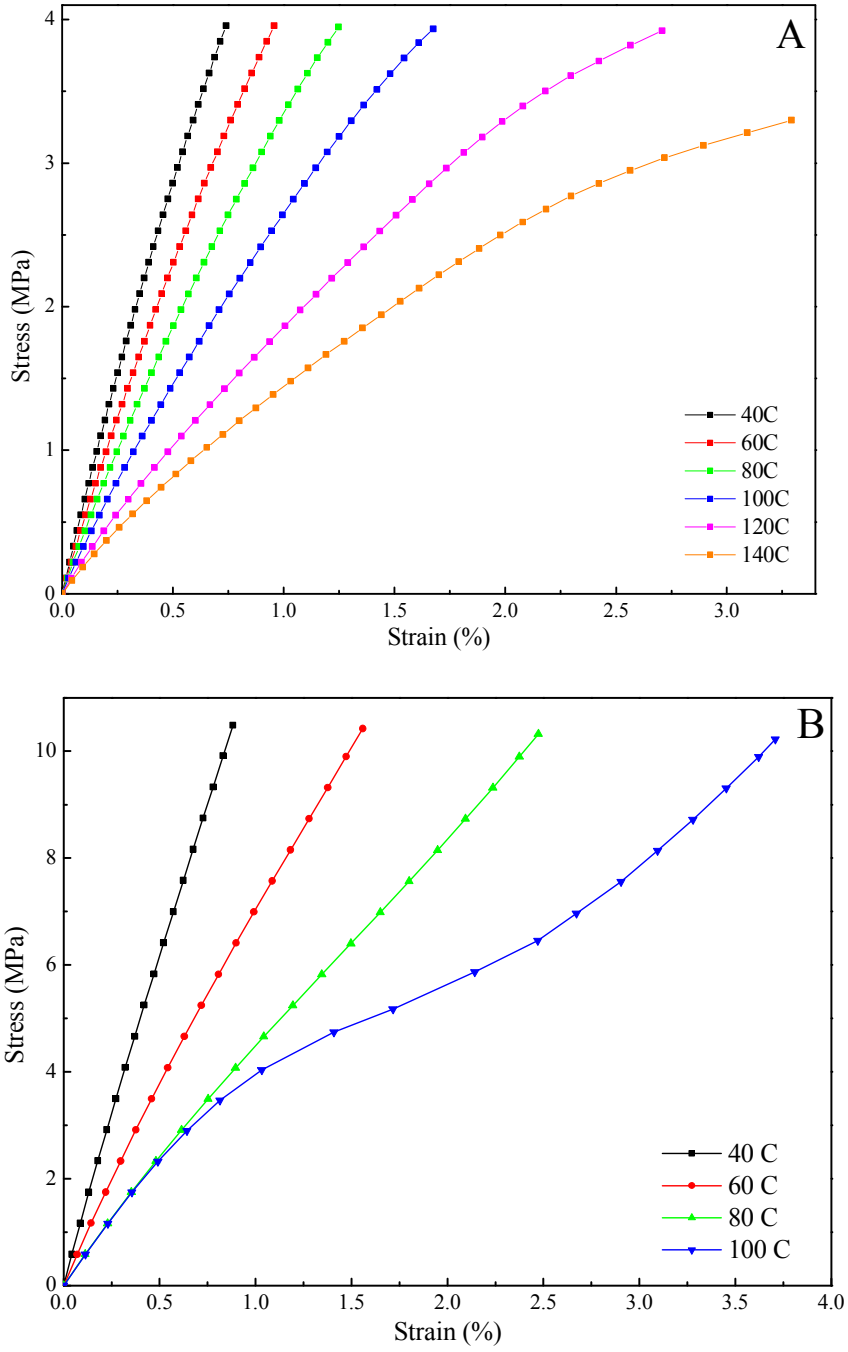

Figure 5.6 Stress-strain curves for (A) KPNC and (B) PP at various temperatures at a strain rate of 2.28×10^{-5} s^{-1}. The solid lines are interpolations between the data points

5.3.2.3 Temperature Effects

Figure 5.7 shows the experimental creep strains as a function of time for KPNC at 40–140 °C and for PP at 40–100 °C when a constant stress of 1 MPa was applied. The fitted curves from the four-element Burgers model are drawn as solid lines, for the purpose of comparison. Overall, the temperature had a statistically significant effect on the creep strains for KPNC and PP (one-way ANOVA, $p<0.05$). The creep strains for KPNC and PP increased at elevated temperatures. KPNC had a lower creep strain than the virgin PP at each temperature step. The creep strain differences between KPNC and PP were greater at higher temperatures. Therefore, KPNC showed a better creep resistance than the virgin PP, especially in a high temperature environment. Banik (Banik et al., 2008) found that the 30 min creep strains for cross-ply all-PP laminates were 0.48% at 40 °C, 0.62% at 60 °C and 0.78% at 80 °C in three-point bending deformation mode. These findings were consistent with our results on creep strains for solid virgin PP at 40, 60 and 80 °C.

Generally speaking, the four-element Burgers model simulation showed good agreement with experimental data at each temperature step, demonstrating that the parameters for the four-element Burgers model were applicable to the characterization of KPNC creep properties. However, some discrepancy occurred at the end of the 30 min creep tests. Moreover, the discrepancy became larger at higher temperatures especially for PP at 100 °C. The creep rate calculated with the four-element Burgers model parameters based on Equation 5.2 are presented in Figure 5.8, for a comparison with the experimental creep rate. The four-element Burgers model over-estimated the long-term creep rate. The four-element Burgers model could be improved by incorporating more Kelvin units to make six-, eight-, or high-element Burgers models.

The complete four-element Burgers modeling parameters are listed in Table 5.1 As a general trend, all four parameters (E_M, E_K, η_K, and η_M) of KPNC and PP decreased as temperature increased. The decreasing tendency of the E_M and η_M values resulted from a decreased material stiffness with respect to diminished instantaneous modulus and a lower viscosity of the bulk materials at elevated temperatures. The decreasing E_K and η_K values exhibited a higher molecular chain mobility of KPNC and PP at elevated temperatures. KPNC showed a smaller creep rate [$\varepsilon'(\infty)$] than PP, indicating that KPNC had lower long-term creep strain and less temperature dependency than PP.

According to Equation 5.1, E_M is the instantaneous elastic modulus that is determined by the Maxwell spring. It can be immediately recovered once the stress is removed. E_M also corresponds to the elasticity of the crystallized zones in a semi-crystallized polymer. Compared to the amorphous regions, the crystallized zones are subject to immediate stress due to their higher stiffness. The viscosity of the Maxwell unit η_M represents the non-recoverable creep deformation and is related to the long-term creep rate. At the molecular level, η_M corresponds to damage in the crystallized zones and irreversible deformation in the amorphous regions. The decrease in η_M implies an increasing deformation of the Maxwell unit at elevated temperatures. The retardant elasticity E_k is associated with the stiffness and the retardant viscosity η_k is coupled with the viscosity of the amorphous regions in the semi-crystallized polymer. In this study, it was also found that the elasticity E_k and viscosity η_k of the Kelvin unit decreased with temperature, indicating that the deformation of the Kelvin unit became larger at higher temperatures. As shown in Table 5.1, the η_M values are more than ten times higher than the η_k values. The predicted parameters for the four-element Burgers model are consistent with those published in the literature (Lee et al., 2004; Nuñez et al., 2004; Shi et al., 2012; Xu et al., 2011; Xu et al., 2010).

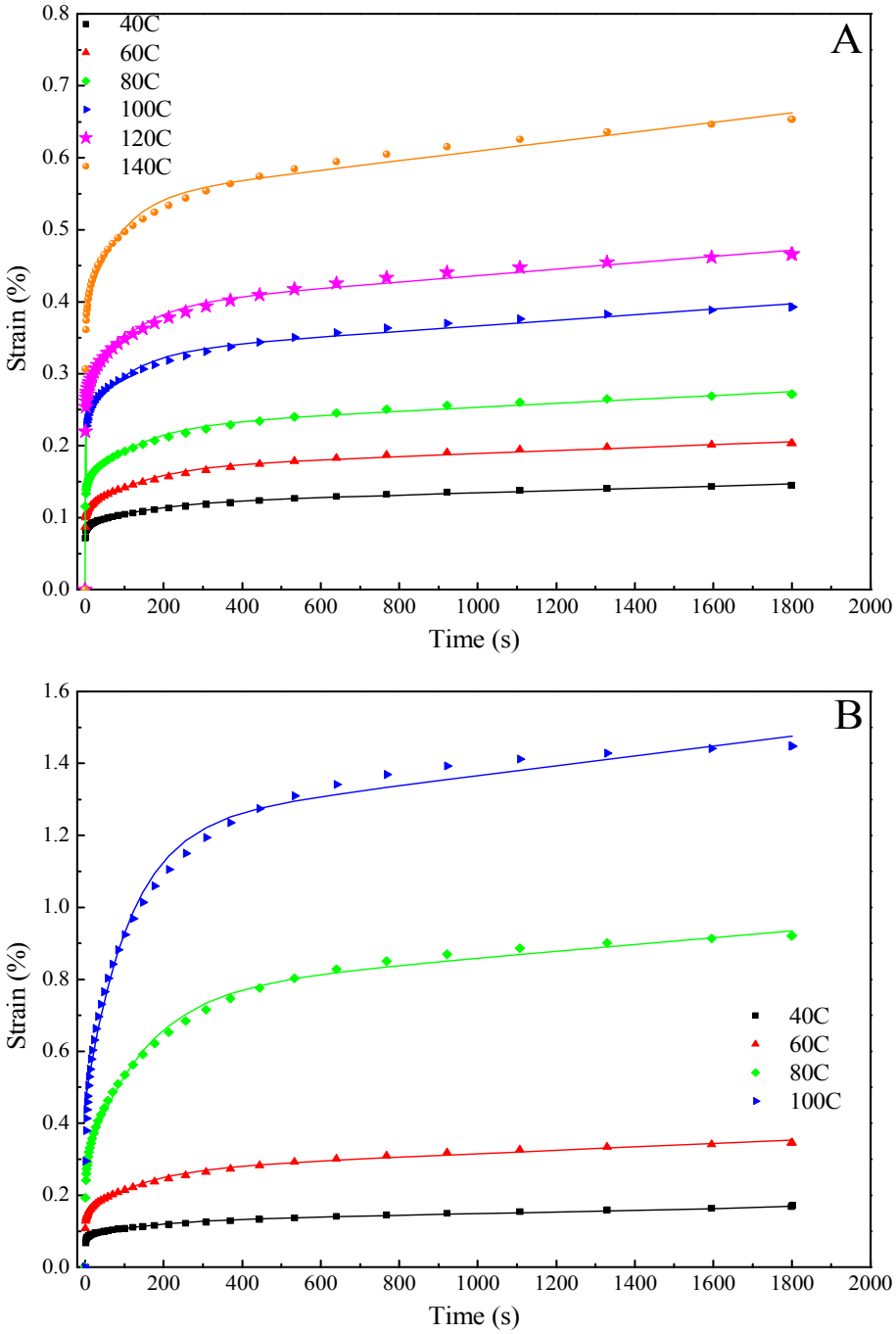

Figure 5.7 30 min creep strain for (A) KPNC and (B) PP at various temperatures when σ= 1 MPa. Symbols represent experimental data and solid lines represent the 4-element Burgers model fits

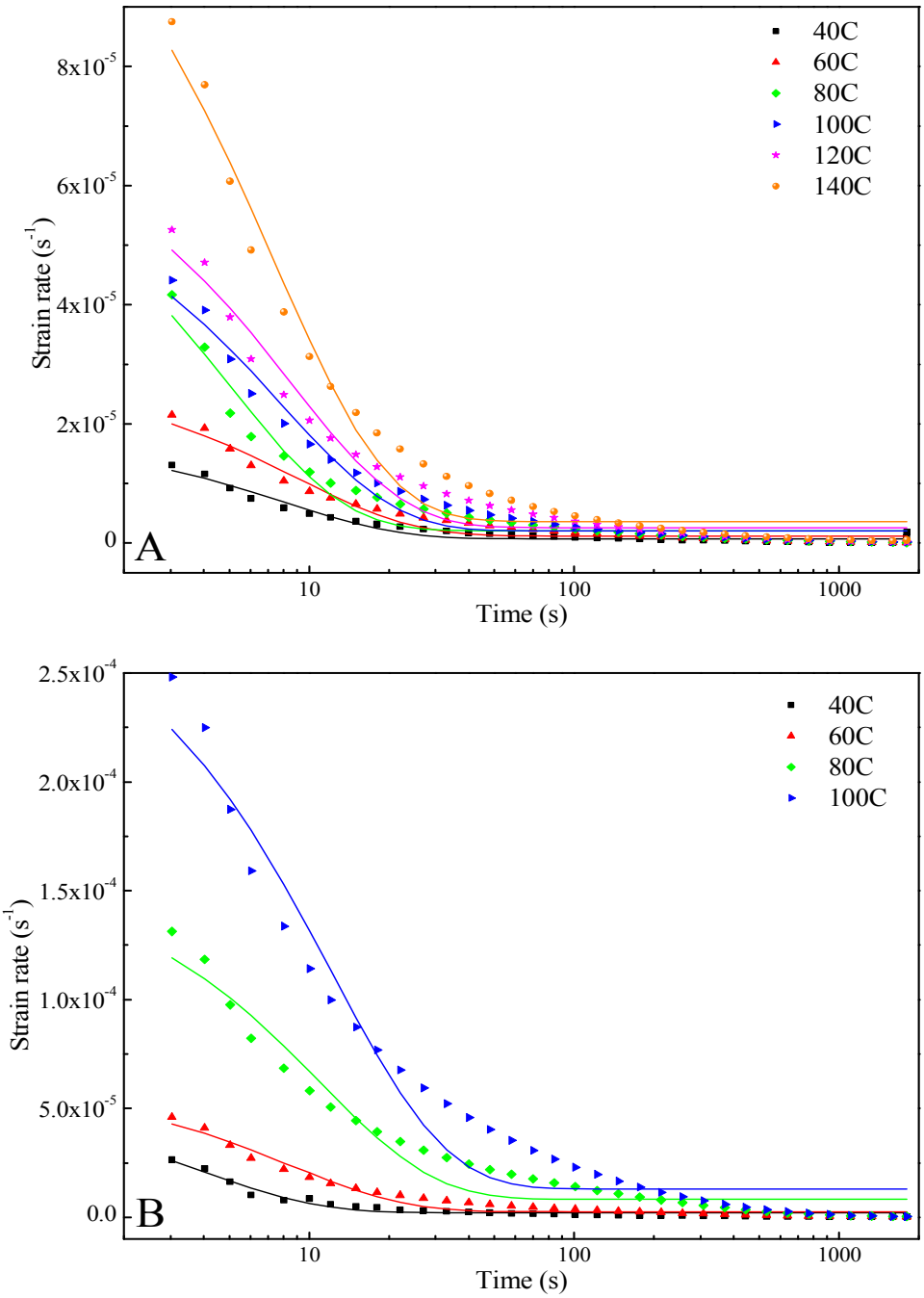

Figure 5.8 30 min creep strain rate for (A) KPNC and (B) PP at various temperatures when σ= 1 MPa. Symbols represent experimental data and solid lines represent the 4-element Burgers model fits

Table 5.1 The fitted parameters obtained from the four-element Burgers model at σ= 1 MPa

Sample	T (^{o}C)	E_M (MPa)	E_K (MPa)	η_K (GPa·s)	η_M (GPa·s)	r^2	τ (s)	ε' (∞) ($10^{-7}s^{-1}$)
KPNC	40	1161	3058	429	6250	0.995	140.3	1.6
	60	928	1653	224	4762	0.995	135.6	2.1
	80	681	1264	164	3704	0.992	130.0	2.7
	100	422	1096	115	2564	0.991	105.3	3.9
	120	368	834	89	2273	0.992	107.1	4.4
	140	257	652	56	1515	0.990	86.4	6.6
PP	40	978	1996	227	3333	0.992	113.8	3.0
	60	686	818	112	2128	0.993	136.7	4.7
	80	347	210	31	1068	0.995	149.5	9.4
	100	218	130	15	730	0.993	112.1	13.7

Figure 5.9 shows the experimental creep strains as a function of time for KPNC at 40–140 °C and for PP at 40–100 °C when a constant stress of 1 MPa was applied. The fits from the Findley power law model are drawn as solid lines. The complete Findley power law modeling parameters are listed in Table 5.2. The results reveal that the Findley power law model also fit well the experimental data within the whole range of testing temperature. The creep amplitude (ε_c) increased and time exponent (n) decreased as temperature increased. The linear relationship of ε_c vs. T and n vs. T of KPNC and PP are illustrated in Figure 5.10. This suggests that the Findley power law model would also be feasible in predicting KPNC creep behavior. However, the initial strain (ε_0) values showed an inconsistent trend. The ε_0 values should increase as temperature increases for both KPNC and PP. Since this is non-physical model, the ε_0 should not be a negative value for PP at 80 and 100 °C. The fit could be improved by attaching a built-in penalty in loss-function when performing the curve fitting (Narula & Wellington, 1982).

For the four-element Burgers model, the initial quick and unstable creep deformation in the primary stage is represented by the Maxwell spring and the steady-state creep in the secondary state is represented by the Kelvin unit. The creep rates based on these two units are different. Therefore, the predictions from the four-element Burgers model within the transition zone (100–600 s) were faster than the experimental creep rates. In contrast, the Findley power law does not use four parameters to predict the primary and secondary creep stages of materials. Therefore, the predictions from the Findley power law within the transition zone were slower than the experimental creep rates.

The creep rates for the four-element Burgers model at infinite time [$\varepsilon'(\infty)$] reached a constant value (σ/η_K), as listed in Table 5.1. In contrast, the $\varepsilon'(\infty)$ values predicted using the Findley power law model asymptotically reached zero. In the 30 min

creep test, the Findley power law model fits the experimental data for KPNC better than PP as seen in Figure 5.9. Comparing to the four-element Burgers model, the Findley power law is more effective in predicting the creep behavior of polymers that have no significant transition from primary to secondary creep stage. The predicted parameters for the Findley power law model are consistent with those reported by other researchers (Banik et al., 2008; Park & Balatinecz, 1998; Xu et al., 2010).

Table 5.2 The fitted parameters obtained from the Findley power law model at σ= 1 MPa

Sample	T (^{o}C)	ε_0 (%)	ε_c (10^{-2} s^{-n})	n	r^2
KPNC	40	0.067	0.012	0.254	0.998
	60	0.056	0.037	0.189	0.997
	80	0.072	0.054	0.178	0.997
	100	0.142	0.070	0.171	0.999
	120	0.127	0.111	0.151	0.998
	140	0.172	0.174	0.137	1.000
PP	40	0.064	0.011	0.300	0.999
	60	0.050	0.066	0.204	0.997
	80	-0.264	0.422	0.142	0.990
	100	-2.058	2.255	0.061	0.989

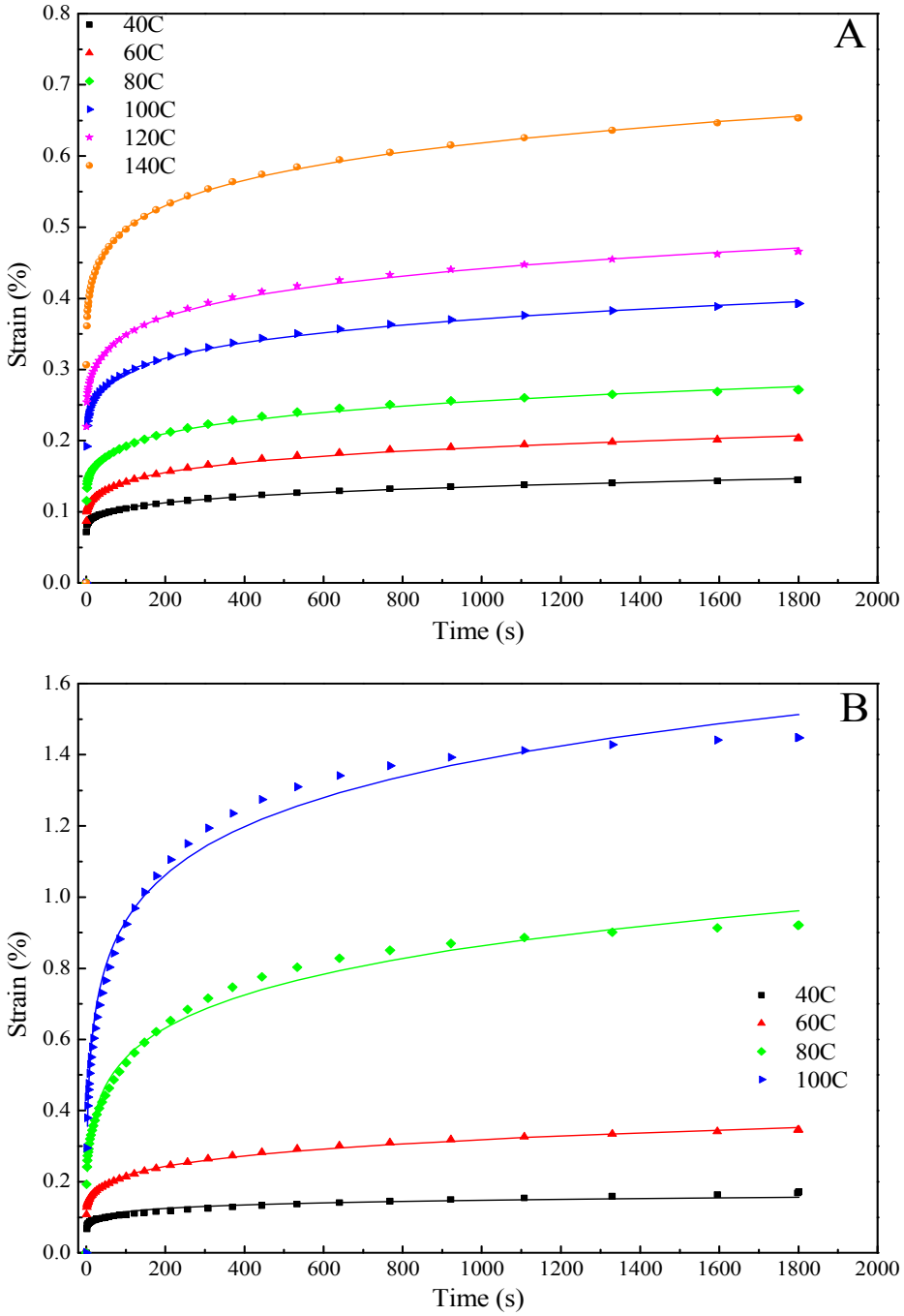

Figure 5.9 30 min creep strain for (A) KPNC and (B) PP at various temperatures when σ= 1 MPa. Symbols represent experimental data and solid lines represent the Findley power law model fits

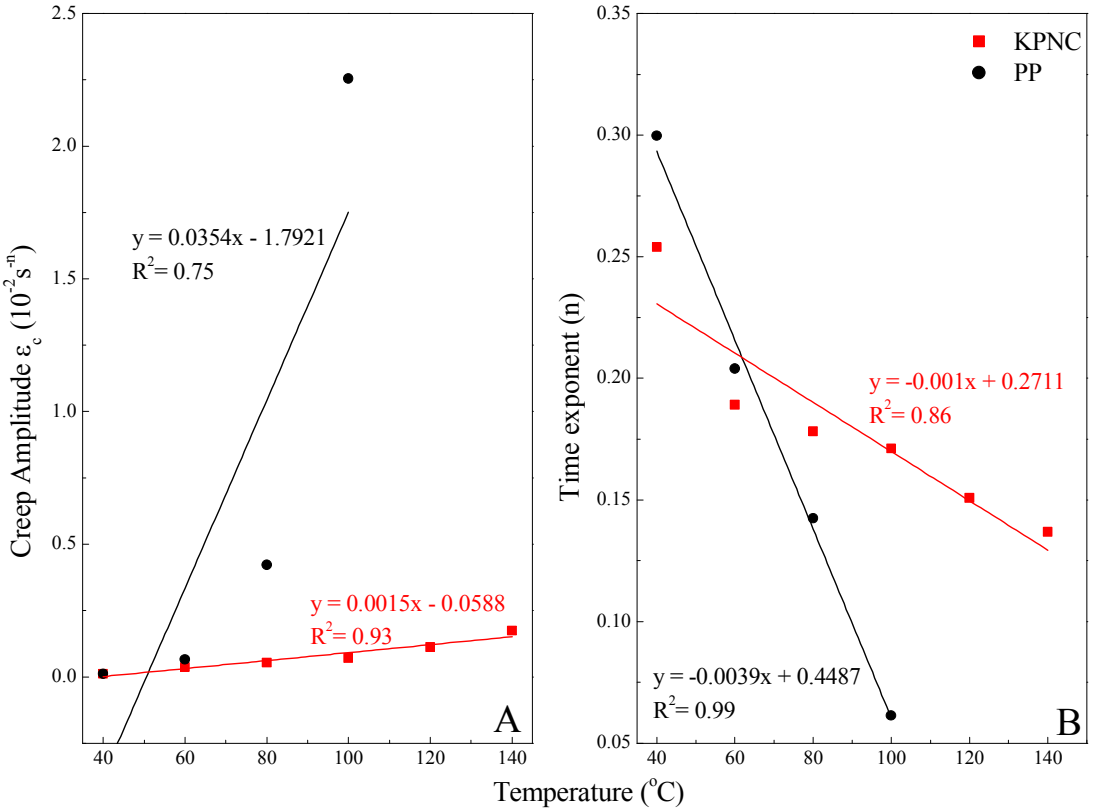

Figure 5.10 Relationship between (A) relative creep amplitude (ε_c) and temperature; (B) time exponent (n) and temperature

The TTS master curves were constructed from the 30 min creep tests for KPNC and PP. As seen in Figure 5.11, KPNC and PP had very similar initial creep strains at the beginning of the master curves. The creep strain differences became larger as time passed. The one year creep strain was extrapolated from the log creep strain at log time equals to 7.5 in Figure 5.11. It was estimated to be 0.32% for KNPC and 1.00% for virgin PP at 40 °C. KPNC showed both a lower long-term creep strain and a lower creep rate than PP. This resulted from the lower temperature-dependence of KPNC. The one-year

creep strain for cross-ply all-PP laminate at 30 °C was 0.87% predicted by Banik (Banik et al., 2008). It was consistent with our prediction on virgin PP plastics.

Figure 5.12 shows the comparison between the TTS prediction and the three-day creep data for KPNC and PP. The TTS prediction for PP fit the three-day experimental data well. It can be explained that the solid virgin PP sample had only one phase but KPNC had three phases (kenaf fiber, PP and air). Therefore PP was thermo-rheologically simpler than KPNC. A horizontal shifting was adequate to correctly superimpose the creep data of virgin PP. For KPNC the predicted values from the TTS model were lower than the experimental results. Tajvidi (Tajvidi et al., 2005), found that the long-term creep strain for 50 wt% kenaf/ HDPE composite was under-estimated by the TTS prediction. A better prediction was made by introducing vertical shifts. The difference between the TTS prediction and the experimental data indicated that the master curve needs to be verified before its application, because the creep behavior of polymers, especially semi-crystalline polymers, is complicated. They are affected by temperature, stress level, and service conditions.

Although the four-element Burgers model fit the 30 min creep test data very well as illustrated in Figure 5.7, this model can only be used for characterizing short-term creep behavior (30 min creep test in this study). As shown in Figure 5.12, the prediction of long-term creep behavior for KPNC and PP using the four-element Burgers model exhibited a large discrepancy with the three-day experimental data. In Xu's dissertation (Xu, 2009), the author also pointed out this large discrepancy between the predicted creep strain for 40 wt% bagasse/HDPE composite generated by the four-element Burgers model and the three-day creep data. In contrast, the Findley power law model, as expressed in Equation 5.4 with ε_0 and ε_c as material constants, showed very good agreement with the three-day experimental data. This indicated that the Findley power

law model was satisfactory for predicting the long-term creep performance of KPNC and PP at 40 °C.

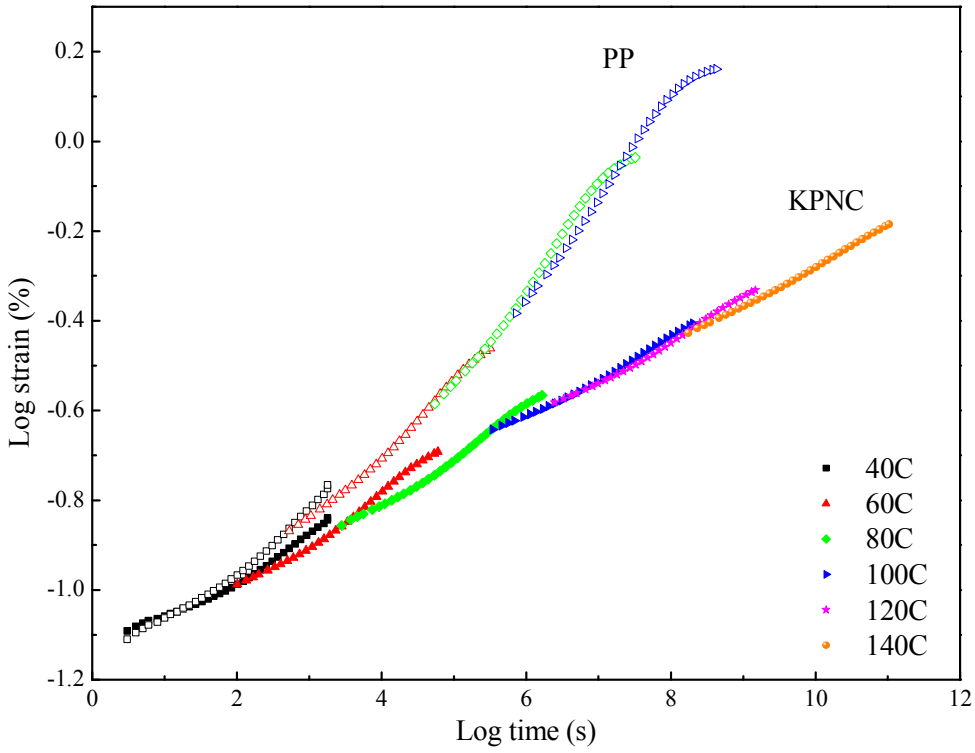

Figure 5.11 TTS master curves constructed from the 30 min creep data for KPNC (solid symbol) and PP (open symbol) at 40 °C, 60 °C, 80 °C, 100 °C, 120 °C and 140 °C (T_{ref} = 40 °C)

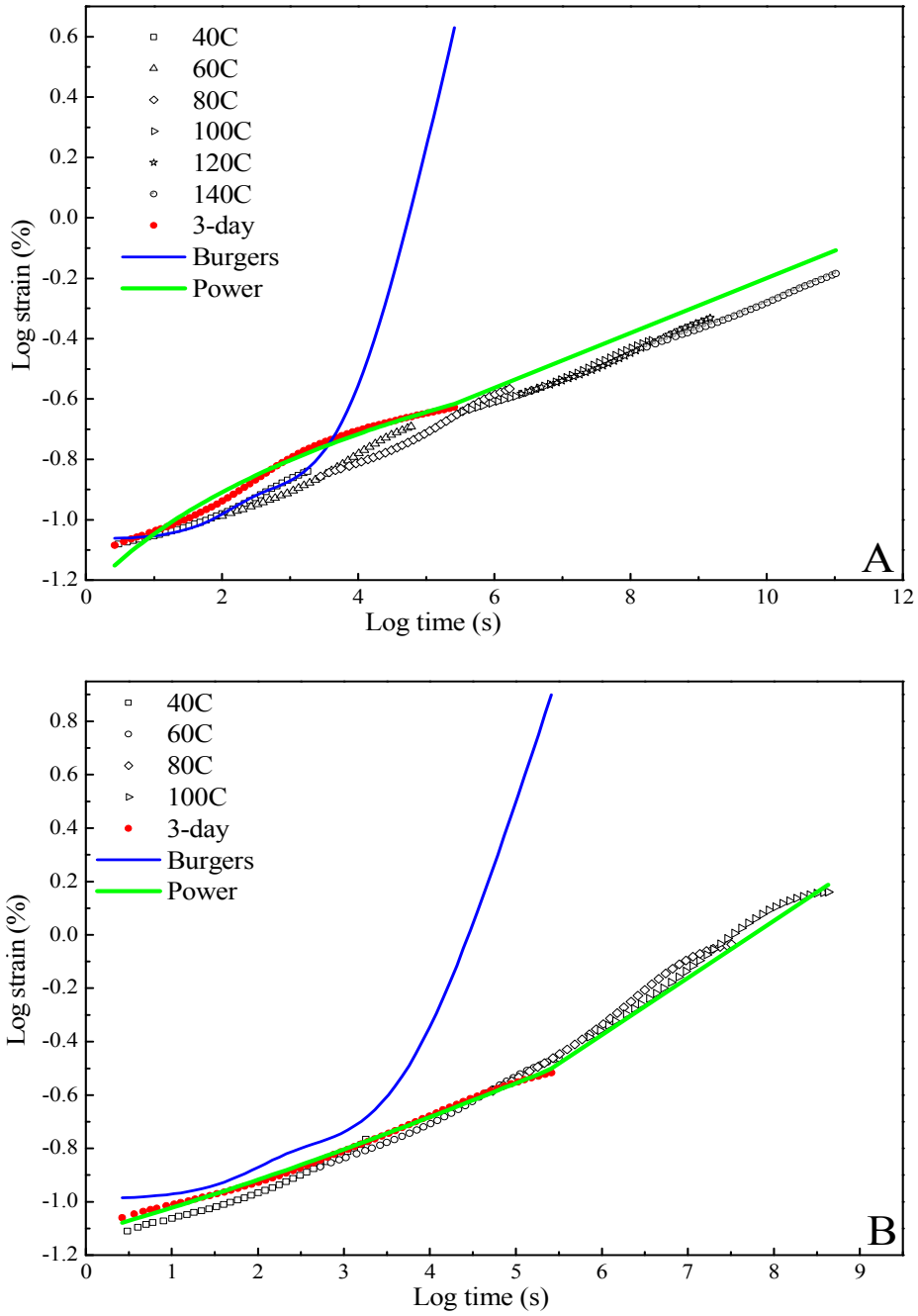

Figure 5.12 Comparison of three-day creep data with TTS and predictions at 40 °C (A) KPNC and (B) PP. Symbols represent experimental data; solid lines represent fits using the 4-element Burgers model and the Findley power law model

Figure 5.13 shows the creep (C), recovery (R), and non-recovery (NR) strains for KPNC and PP based on the 30 min creep tests. The recovery rate denoted as RR (1) at each temperature step is also listed in Table 5.5. The NR deformation started from 0 for KPNC at all temperature steps and for PP at 40 and 60 °C, indicating that the instantaneous creep deformation was fully recovered for KPNC and for PP at low temperatures. Based on the four-element Burgers model, the dashpot in the Maxwell unit created the NR strain, which was proportional to creep time as expressed in Equation 5.8. However, the NR curves failed to follow this linear trend, suggesting that the four-element Burgers model cannot be applied for recovery prediction. Comparatively, KPNC had lower NR deformation than PP at each temperature step. The NR deformation was less than the R deformation at each temperature step for KPNC. However, the NR deformation was larger than R deformation starting at 80 °C for PP. The higher recoverability of KPNC makes it a better choice for a high-temperature working environment.

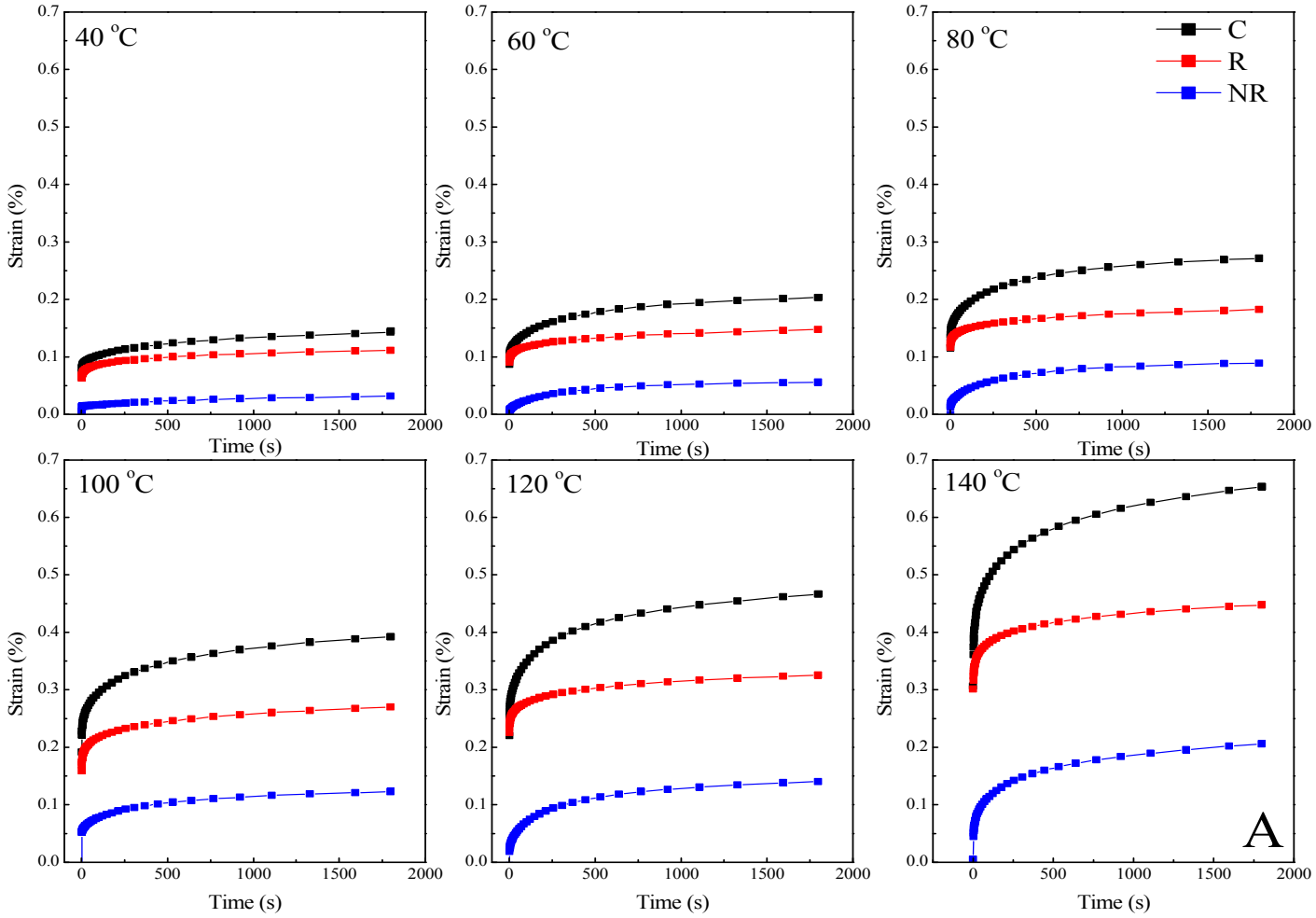

Figure 5.13 Creep (C), recoverable strain (R), and non-recoverable (NR) strain for (A) KPNC and (B) PP. The solid lines are interpolations between the data points

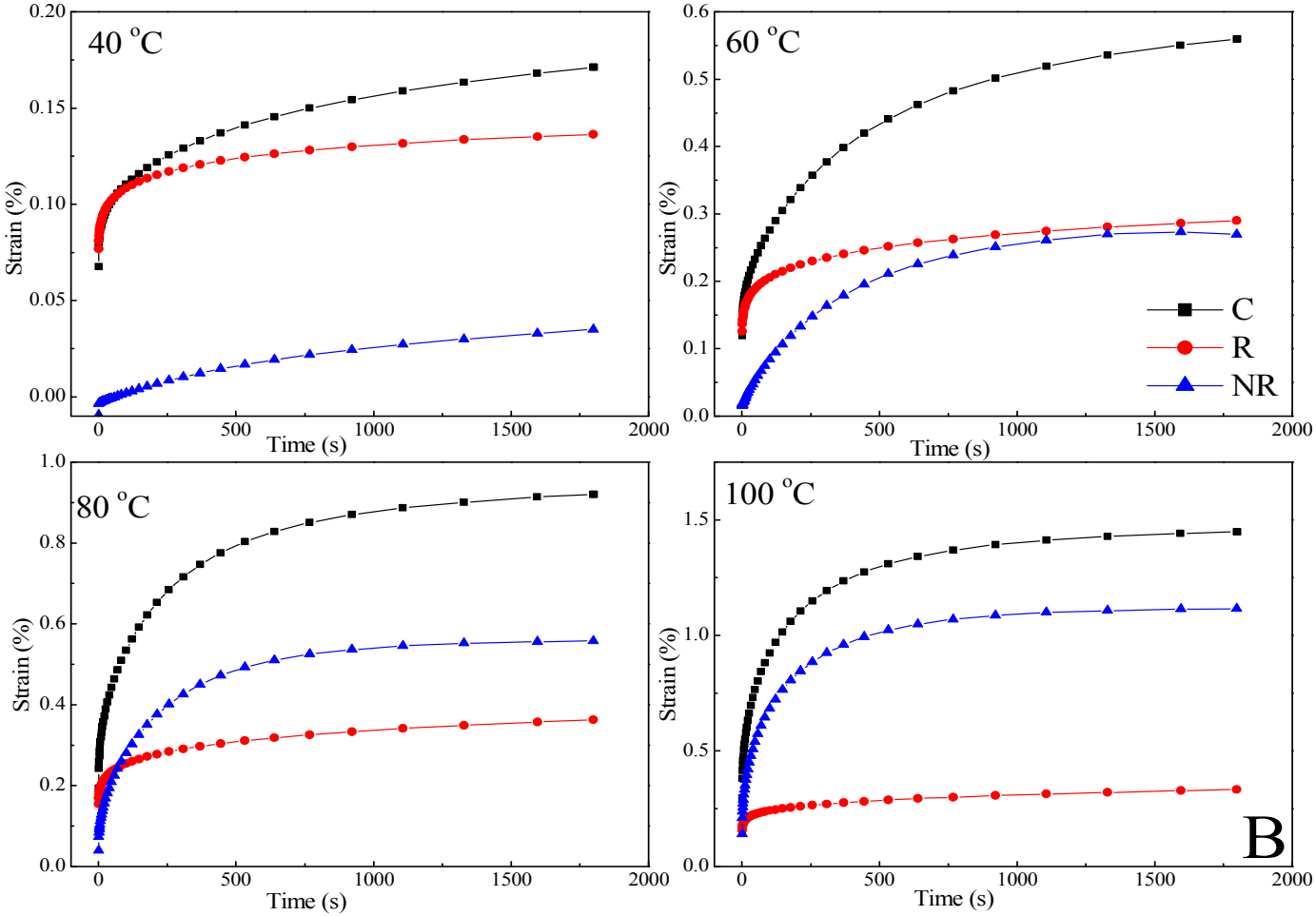

Figure 5.13 Cont.

5.3.2.4 Stress Effects

Figure 5.14 shows the experimental data for creep strains as a function of time for KPNC and PP when subjected to stress levels of 0.5, 1.0, 1.5, 2.5, and 3.5 MPa at 40 °C. The predictions from the four-element Burgers model are drawn as solid lines. Overall, the stress had a statistically significant effect on the creep strains for KPNC and PP (one-way ANOVA, $p<0.05$). The creep strains for KPNC and PP increased at elevated stress levels. The virgin PP had higher creep strain than KPNC at each stress level. KPNC had better creep resistance than the virgin PP under higher stresses. From Figure 5.14, it can also be observed that for both KPNC and PP the creep strain difference was increased corresponding to the stress increase.

Nunez (Nuñez et al., 2004) found that the 30 min creep strain for PP was 1.00% at 40 °C under 10 MPa stress in three-point bending deformation mode, which is consistent with our results that the 30 min creep strain for PP was 0.52 % at 40 °C under 3.5 MPa stress. Xu (Xu, 2009) found that the 30 min creep strain for 50 wt% Bagasse reinforced PVC composite was 0.10% at 45 °C under 2 MPa stress. This is lower than the creep strain (0.17–0.28%) for KPNC at 40 °C under 2 MPa stress in this study. A possible explanation is that the injection-molded composites had lower creep strains than nonwoven composites due to the large number of voids in nonwoven composites that are not present in the injection-molded composites.

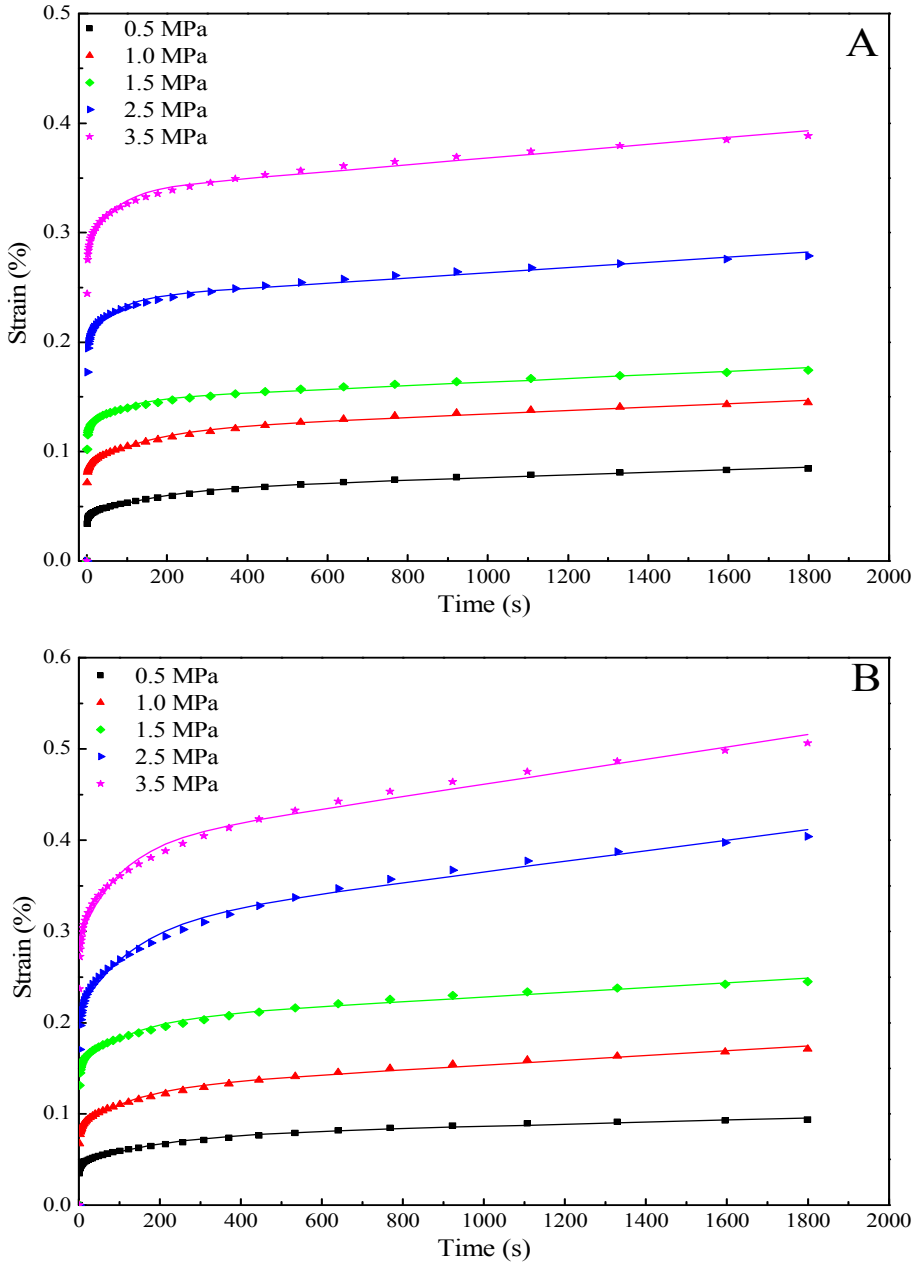

Figure 5.14 30 min creep strain for (A) KPNC and (B) PP at various stresses when T= 40 °C. Symbols represent experimental data and solid lines represent the 4-element Burgers model fits

The complete four-element Burgers modeling parameters are listed in Table 5.3. This model showed good agreement with the experimental data at each stress level. As a general trend, all four parameters (E_M, E_K, η_K, and η_M) of KPNC and PP decreased as temperature increased. One exception is PP at 1.0 and 1.5 MPa. The E_K, η_K, and η_M values at 1.0 and 1.5 MPa did not have statistically significant differences (t-test, $p>0.1$). It is possible that the stress difference of 1.0 and 1.5 MPa is too small to distinguish, considering the fact that the stresses of 1.0 and 1.5 MPa correspond to the forces of 1.9 and 2.8 N applied on the PP sample. At each stress level, KPNC had higher E_M values than PP. KPNC also showed a smaller creep rate [$\varepsilon'(\infty)$] than the virgin PP, indicating that the long-term creep strain of KPNC was lower and less stress-dependent than PP. However, the creep rates of KPNC and PP were insensitive to the stress level of 0.5 MPa at 40 °C.

The E_M values of KPNC and PP decreased with increasing stress levels at 40 °C. A significant reduction was found at the stresses of 2.5 and 3.5 MPa Compared to PP, KPNC had a larger E_M value, meaning a higher elasticity, at each temperature step. According to the predictions from the four-element Burgers model listed in Table 5.3, both E_K and η_K decreased with an increase in the stress level, indicating that the Kelvin unit had a very high stiffness and was very difficult to flow at low stress levels. With an increase in the stress levels, elastic deformation and viscous flow became larger, resulting in the reduced E_K and η_K values. The decreases in the E_K and η_K values for KPNC and PP demonstrate the effect of the stress levels on short-term creep resistance. In addition, the reduction of retardation time (τ) at elevated stress levels indicates that the higher stress levels accelerate the transition from primary to secondary creep. Table 5.3 also shows that the higher stress level lead to lower η_M values and higher $\varepsilon'(\infty)$ values, reflecting the effect of the stress levels on the long-term creep behavior of KPNC and PP.

Table 5.3 The fitted parameters obtained from the four-element Burgers model at T= 40 °C

Sample	Stress(MPa)	E_M (MPa)	E_K(MPa)	η_K (GPa·s)	η_M (GPa·s)	r^2	τ (s)	ε' (∞) ($10^{-7}s^{-1}$)
	0.5	2415	4292	725	8333	0.995	168.9	1.2
	1.0	1161	3058	429	6250	0.995	140.3	1.6
KPNC	1.5	830	3788	301	5882	0.990	79.4	1.7
	2.5	496	2639	175	4167	0.989	66.1	2.4
	3.5	351	1927	125	3226	0.991	64.6	3.1
	0.5	2252	3257	593	9091	0.992	182.2	1.1
	1.0	978	1996	227	3333	0.992	113.8	3.0
PP	1.5	651	2049	261	3846	0.993	127.5	2.6
	2.5	469	1062	143	1724	0.992	134.8	5.8
	3.5	343	978	98	1471	0.991	100.4	6.8

To evaluate the Findley power law model, Figure 5.15 illustrates the experimental data for creep strains as a function of time for KPNC and PP when subjected to the stress levels of 0.5, 1.0, 1.5, 2.5, and 3.5 MPa at 40 °C. The fits from the Findley power law model are drawn as solid lines. The complete Findley power law modeling parameters are listed in Table 5.4. This model exhibited good agreement with the experimental data at each stress level, demonstrating its applicability in analyzing composite creep behavior. The initial strain (ε_0) values increased as the stress levels increased, because the elastic strain increased when a higher stress was applied for both KPNC and PP. The creep amplitude (ε_c) increased and the time exponent (n) decreased for KPNC but remained constant for PP as stress increased. The linear relationship of ε_0 vs. T and ε_c vs. T for KPNC and PP are illustrated in Figure 5.16.

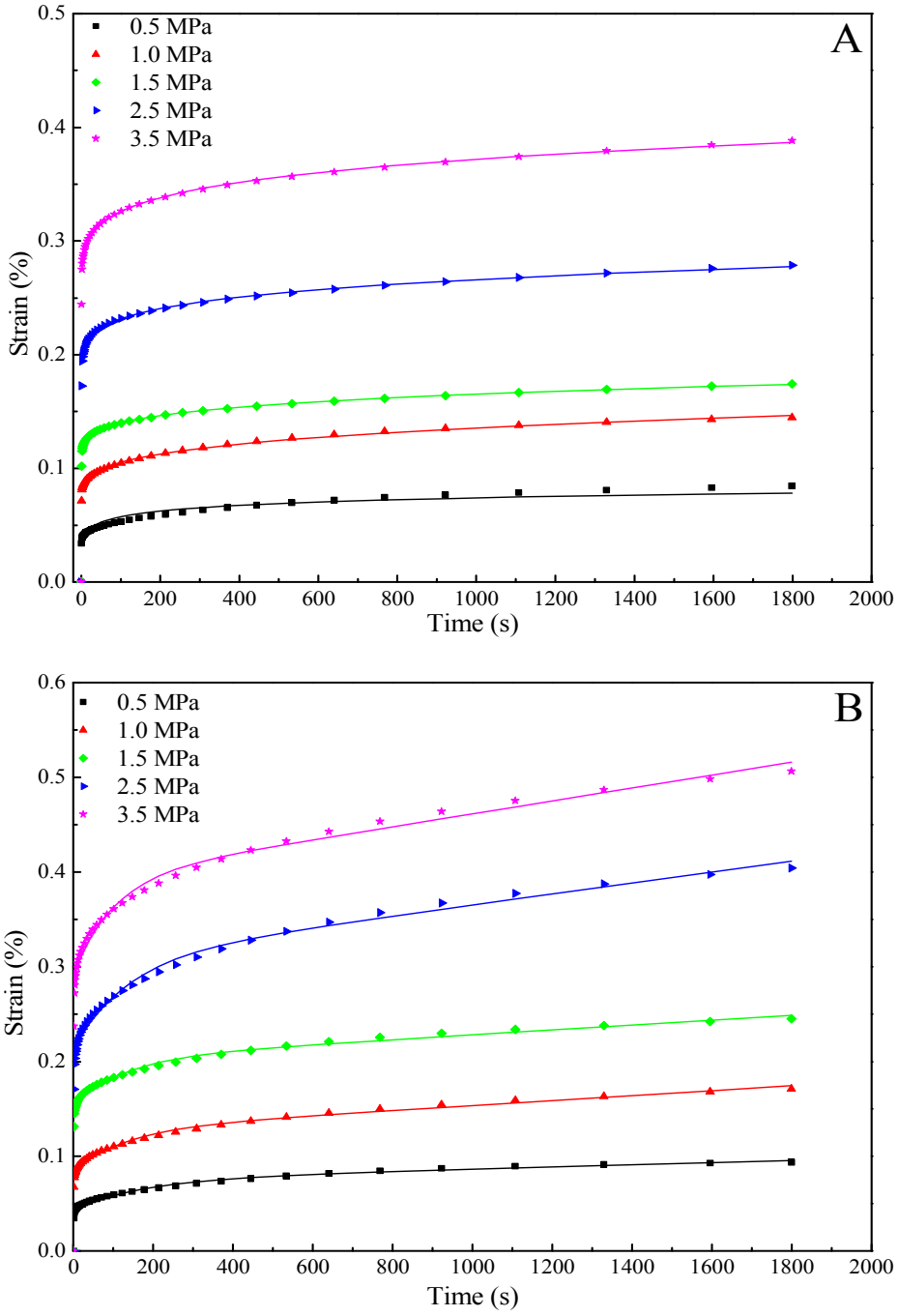

Figure 5.15 30 min creep strains for (A) KPNC and (B) PP at various stresses at 40 °C. Symbols represent experimental data and solid lines represent the Findley power law model fits

Table 5.4 The fitted parameters obtained from the Findley power law model at T= 40 °C

Sample	Stress (MPa)	ε_0 (%)	ε_c (10^{-2} s^{-n})	n	r^2
KPNC	0.5	0.032	0.005	0.309	0.998
	1.0	0.067	0.012	0.254	0.998
	1.5	0.098	0.017	0.204	0.999
	2.5	0.162	0.031	0.175	0.999
	3.5	0.224	0.049	0.161	0.999
PP	0.5	0.028	0.010	0.263	0.996
	1.0	0.064	0.011	0.300	0.999
	1.5	0.122	0.020	0.243	0.993
	2.5	0.165	0.028	0.290	0.993
	3.5	0.225	0.043	0.252	0.991

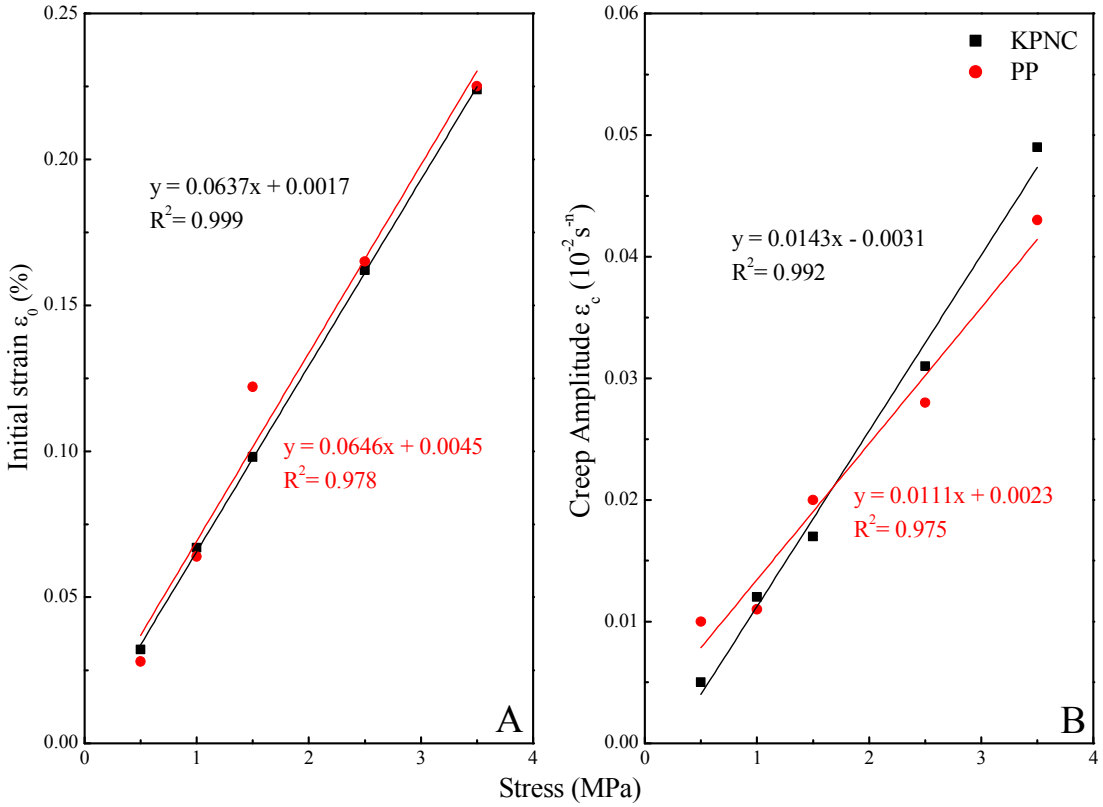

Figure 5.16 The linear relationship between (A) initial strain (ε_0) and temperature; (B) relative creep amplitude (ε_c) and temperature

The time-stress superposition (TSS) master curves were constructed from 30 min creep tests for KPNC and PP (Figure 5.17). The same method of horizontal shifting as applied to the TTS principle was also used for the TSS master curves by replacing temperature with stress. The effectiveness of the TSS principle has been reported in the literature (Hadid et al., 2004; Jazouli et al., 2005; Starkova et al., 2007; Urzhumtsev, 1972). A phenomenon similar to what was observed from the TTS master curves can be seen in Figure 5.17. KPNC and PP both exhibited a very similar initial creep strain at the beginning of the master curves. The difference in creep strains became larger as time passed. The extrapolated one-year creep strain is 0.25% for KNPC and 0.4% for PP at 1

MPa of the applied stress. KPNC showed a lower long-term creep strain and also a lower creep rate than PP. This resulted from the lower stress-dependence of KPNC.

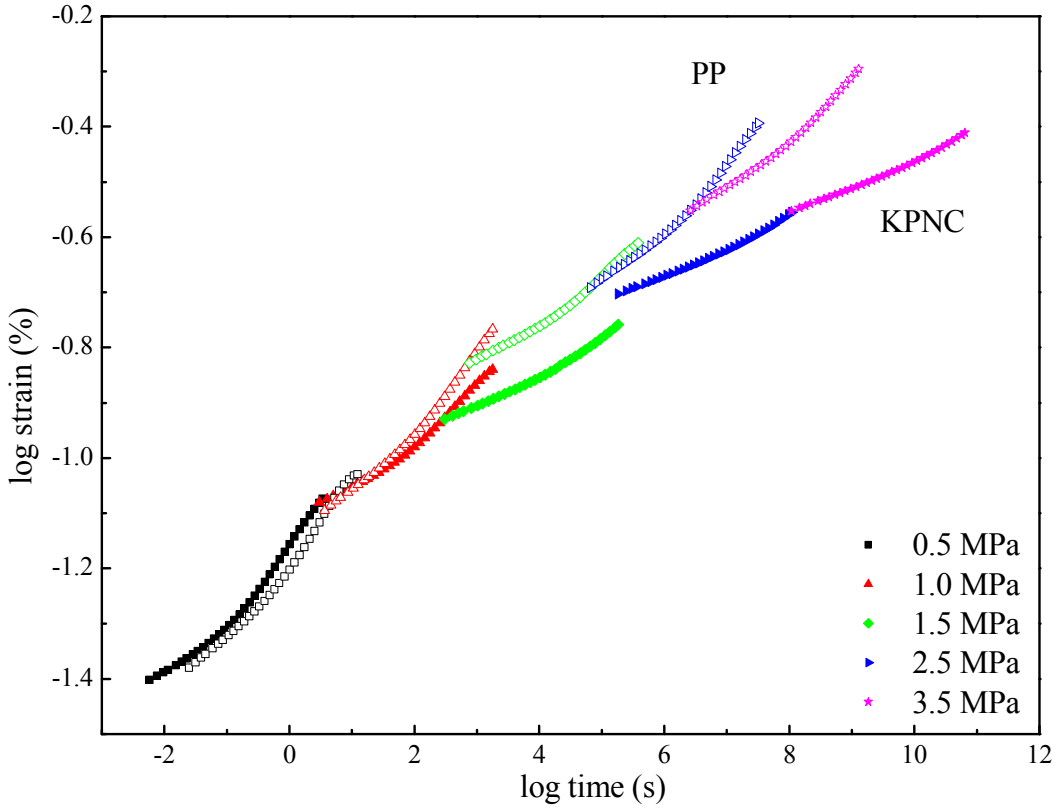

Figure 5.17 TSS master curves constructed from the 30 min creep data of KPNC (solid symbol) and PP (open symbol) at 0.5, 1.0, 1.5, 2.5 and 3.5 MPa (σ_{ref} = 1 MPa)

Figure 5.18 shows the comparison between the TSS prediction and the three-day creep data of KPNC and PP. The TSS prediction for PP fit the three-day experimental data better than that for KPNC, due to the thermo-rheologically simplicity of PP as discussed previously. The predicted strains for KPNC from the TSS prediction were lower than the experimental results.

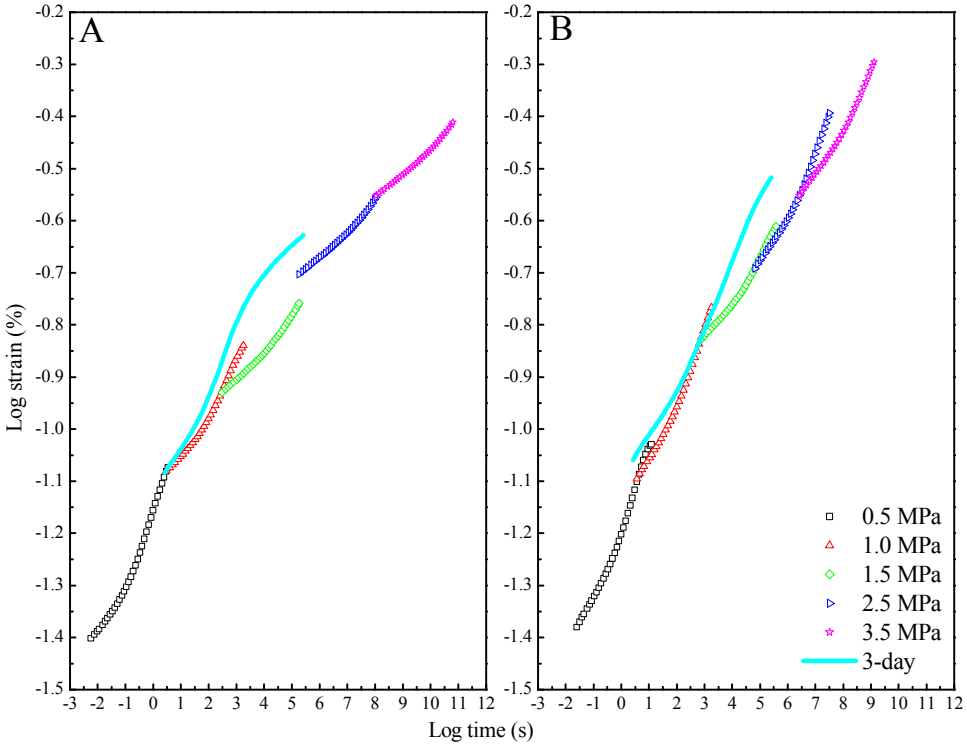

Figure 5.18 Comparison of three-day creep data with TSS prediction at 40 °C (A) KPNC and (B) PP

5.3.2.5 Cyclic Thirty-minute Creep Tests

Cyclic creep tests were conducted by performing creep tests for 30 min at 1 MPa followed by a 30 min recovery process for ten cycles. The recovery rate for each cycle was calculated according to Equation 5.9 and is listed in Figure 5.19. The exponential decay function expressed in Equation 5.10 was fit very well with the recovery rates from Cycle 1 to Cycle 10. As shown in Table 5.5, the predicted recovery rate of KPNC and PP after infinite numbers of cycles [RR (∞)] decreased at elevated temperatures. At each temperature step, the RR (∞) value of KPNC was higher than PP, indicating a better recoverability of KPNC than PP. X is defined as the ratio of RR (∞) over RR (1). A higher X value indicates a larger percent of recovery rate that materials can retain during

the cyclic creep process. KPNC was superior to PP because it maintained a higher recovery rate.

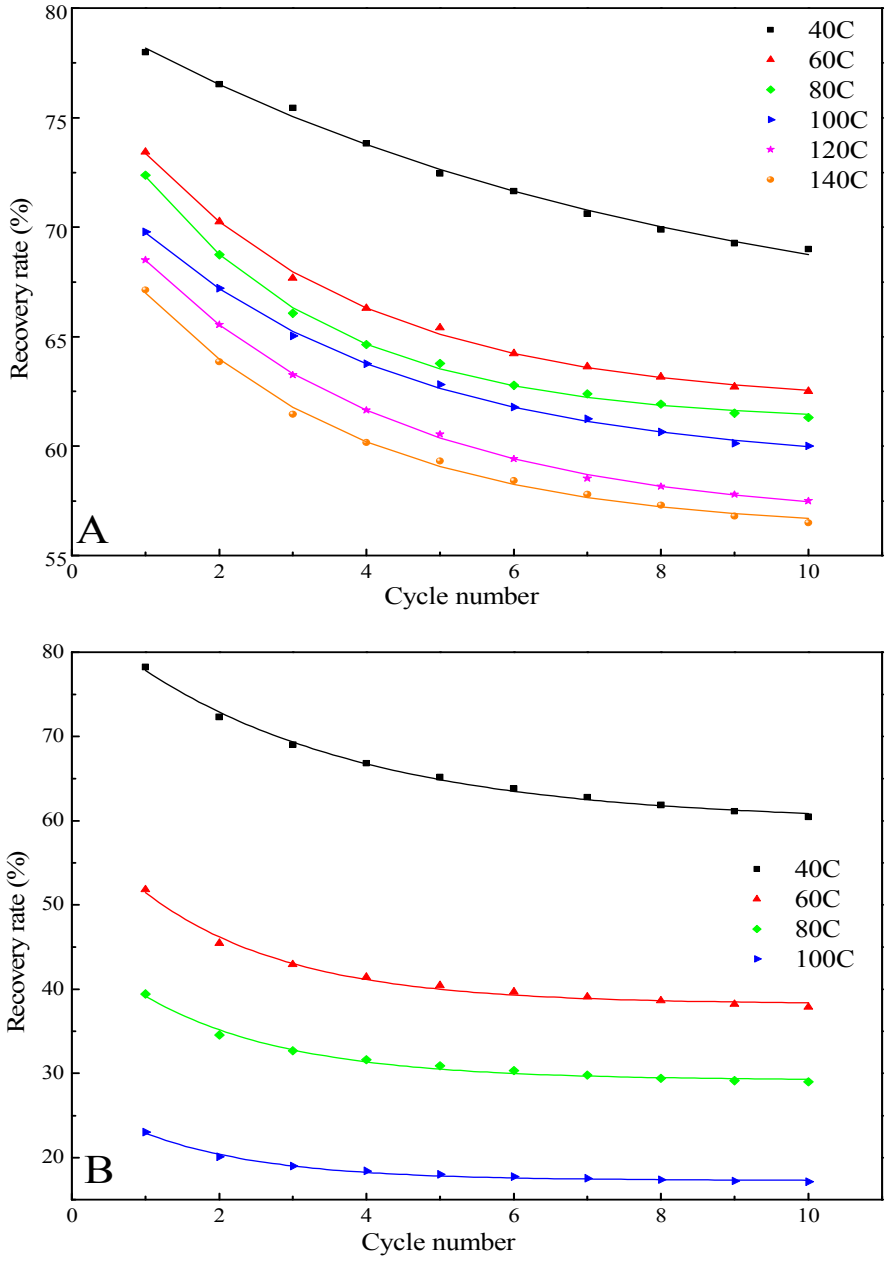

Figure 5.19 Recovery rate vs. cycle number for (A) KPNC and (B) PP. Symbols represent calculations from experimental data; solid lines represent the curve fitting results

Table 5.5 The fitting parameters for the cyclic creep recovery rate

Sample	T (°C)	RR (1) (%)	RR (∞) %	X	a	b	r^2
KPNC	40	77.78	64.49	0.829	15.58	7.71	0.995
	60	73.44	61.91	0.843	15.78	3.13	0.998
	80	72.38	61.09	0.844	16.44	2.62	0.998
	100	69.78	59.08	0.847	14.02	3.65	0.999
	120	68.50	56.54	0.825	15.89	3.52	0.999
	140	67.13	56.13	0.836	15.06	3.06	0.996
PP	40	78.24	59.87	0.765	24.74	3.13	0.995
	60	51.83	38.26	0.738	21.96	1.97	0.998
	80	39.44	29.22	0.741	16.56	1.96	0.996
	100	23.02	17.30	0.751	10.13	1.69	0.989

5.4 CONCLUSIONS

The mechanical responses of KPNCs demonstrated a sensitivity to strain rates when performing tensile tests at various loading rates. As the strain rates increased, the failure stress, failure strain and Young's modulus increased. The strain rate effects were the result of viscoelastic behavior of KPNCs, which were then studied by performing the creep tests.

Both temperature and stress had statistically significant effects on the creep strains for KPNC and PP. The creep strains for KPNC and PP increased at elevated temperatures. However, the creep strain for KPNC was lower than that of PP at each temperature step. The difference between creep strains for KPNC and PP became larger at higher temperatures, indicating that KPNC had a better creep resistance than PP at elevated temperatures. A similar trend was also found on the stress effects. The recovery analyses indicated that KPNC has a higher recovery rate than PP at every 30 min creep cycle.

The four-element Burgers model was found be only be appropriate for characterizing short-term creep behavior (30 min in this study). In contrast, the Findley power law model was satisfactory for predicting the long-term creep performance of KPNC and PP. Both models demonstrated their applicability in predicting composite creep behavior. However, some limitations of both models still exist.

The TTS master curves for KPNC and PP were established. The master curve for PP fit well with the three-day creep data, showing a better prediction accuracy. The master curve for KPNC under-estimated its long-term creep performance due to the multiphase thermo-rheological complexity of KPNC. Therefore, the accuracy of TTS

method needs to be verified by experiments (the three-day creep test in this study), especially for composites with multiple components.

5.5 ACKNOWLEDGEMENTS

I would like to thank Dr. Wei Li in the Department of Mechanical Engineering at University of Texas at Austin for the use of the DMA instrument. Appreciation is also extended to Mr. Yizhuo Chen, Department of Textiles at North Carolina State University for the valuable technical discussion on statistical analysis and curve fitting methods.

5.6 REFERENCES

Acha, B.A., Reboredo, M.M., Marcovich, N.E. 2007. Creep and dynamic mechanical behavior of PP–jute composites: Effect of the interfacial adhesion. *Composites Part A: Applied Science and Manufacturing*, **38**(6), 1507-1516.

Alvarez, V.A., Kenny, J.M., Vázquez, A. 2004. Creep behavior of biocomposites based on sisal fiber reinforced cellulose derivatives/starch blends. *Polymer Composites*, **25**(3), 280-288.

Banik, K., Karger‐Kocsis, J., Abraham, T. 2008. Flexural creep of all‐polypropylene composites: Model analysis. *Polymer Engineering & Science*, **48**(5), 941-948.

Bledzki, A.K., Faruk, O. 2004. Creep and impact properties of wood fibre–polypropylene composites: influence of temperature and moisture content. *Composites Science and Technology*, **64**(5), 693-700.

Bueno, B., Costanzi, M., Zornberg, J. 2005. Conventional and accelerated creep tests on nonwoven needle-punched geotextiles. *Geosynthetics International*, **12**(6), 276-287.

Cyras, V., Martucci, J., Iannace, S., Vazquez, A. 2002. Influence of the fiber content and the processing conditions on the flexural creep behavior of sisal-PCL-starch composites. *Journal of Thermoplastic Composite Materials*, **15**(3), 253-265.

Das, A., Kothari, V., Kumar, A., Mehta, M. 2005. Study on anisotropic creep behavior of nonwoven geotextiles. *Fibers and Polymers*, **6**(4), 313-317.

Findley, W.N., Davis, F.A. 1989. *Creep and relaxation of nonlinear viscoelastic materials*. Dover Publications.

Hadid, M., Rechak, S., Tati, A. 2004. Long-term bending creep behavior prediction of injection molded composite using stress–time correspondence principle. *Materials Science and Engineering: A*, **385**(1–2), 54-58.

Holbery, J., Houston, D. 2006. Natural-fiber-reinforced polymer composites in automotive applications. *Jom*, **58**(11), 80-86.

Jazouli, S., Luo, W., Bremand, F., Vu-Khanh, T. 2005. Application of time–stress equivalence to nonlinear creep of polycarbonate. *Polymer Testing*, **24**(4), 463-467.

Knauss, W. 2008. The sensitivity of the time-temperature shift process to thermal variations—A note. *Mechanics of Time-Dependent Materials*, **12**(2), 179-188.

Krempl, E., Khan, F. 2003. Rate (time)-dependent deformation behavior: an overview of some properties of metals and solid polymers. *International Journal of Plasticity*, **19**(7), 1069-1095.

Lee, S.-Y., Yang, H.-S., Kim, H.-J., Jeong, C.-S., Lim, B.-S., Lee, J.-N. 2004. Creep behavior and manufacturing parameters of wood flour filled polypropylene composites. *Composite Structures*, **65**(3–4), 459-469.

Liqing, X., Hongdi, Z., Lei, Z. 2001. Measurement and Analysis of Creep Property of Nonwoven Geotextiles by Photic Leverage [J]. *Technical Textiles*, **2**, 012.

Narula, S.C., Wellington, J.F. 1982. The minimum sum of absolute errors regression: A state of the art survey. *International Statistical Review/Revue Internationale de Statistique*, 317-326.

Nayak, S.K., Mohanty, S., Samal, S.K. 2009. Influence of short bamboo/glass fiber on the thermal, dynamic mechanical and rheological properties of polypropylene hybrid composites. *Materials Science and Engineering: A*, **523**(1), 32-38.

Nielsen, L.E., Landel, R.F. 1993. *Mechanical properties of polymers and composites*. CRC.

Nuñez, A.J., Marcovich, N.E., Aranguren, M.I. 2004. Analysis of the creep behavior of polypropylene-woodflour composites. *Polymer Engineering & Science*, **44**(8), 1594-1603.

Park, B.-D., Balatinecz, J.J. 1998. Short term flexural creep behavior of wood-fiber/polypropylene composites. *Polymer Composites*, **19**(4), 377-382.

Pooler, D.J., Smith, L.V. 2004. Nonlinear Viscoelastic Response of a Wood–Plastic Composite Including Temperature Effects. *Journal of Thermoplastic Composite Materials*, **17**(5), 427-445.

Pothan, L.A., Oommen, Z., Thomas, S. 2003. Dynamic mechanical analysis of banana fiber reinforced polyester composites. *Composites Science and Technology*, **63**(2), 283-293.

Rouison, D., Sain, M., Couturier, M. 2006. Resin transfer molding of hemp fiber composites: optimization of the process and mechanical properties of the materials. *Composites Science and Technology*, **66**(7–8), 895-906.

Scott, D.W., Lai, J.S., Zureick, A.-H. 1995. Creep behavior of fiber-reinforced polymeric composites: a review of the technical literature. *Journal of reinforced plastics and composites*, **14**(6), 588-617.

Shi, A., Wang, L., Li, D., Adhikari, B. 2012. Characterization of starch films containing starch nanoparticles. Part 2: Viscoelasticity and creep properties. *Carbohydrate Polymers*.

Starkova, O., Yang, J., Zhang, Z. 2007. Application of time–stress superposition to nonlinear creep of polyamide 66 filled with nanoparticles of various sizes. *Composites Science and Technology*, **67**(13), 2691-2698.

Sullivan, J.L. 1990. Creep and physical aging of composites. *Composites Science and Technology*, **39**(3), 207-232.

Tajvidi, M., Falk, R.H., Hermanson, J.C. 2005. Time–temperature superposition principle applied to a kenaf-fiber/high-density polyethylene composite. *Journal of Applied Polymer Science*, **97**(5), 1995-2004.

Tscharnuter, D., Jerabek, M., Major, Z., Lang, R.W. 2011. Time-dependent poisson's ratio of polypropylene compounds for various strain histories. *Mechanics of Time-Dependent Materials*, **15**(1), 15-28.

Urzhumtsev, Y.S. 1972. Prediction of the deformation and fracture of polymeric materials. *Polymer Mechanics*, **8**(3), 438-450.

Ward, I.M. 1983. *Mechanical properties of solid polymers*. Wiley.

Xu, Y. 2009. Creep Behavior Of Natural Fiber Reinforced Polymer Composites, Louisiana State University.

Xu, Y., Lee, S.Y., Wu, Q. 2011. Creep analysis of bamboo high‐density polyethylene composites: Effect of interfacial treatment and fiber loading level. *Polymer Composites*, **32**(5), 692-699.

Xu, Y., Wu, Q., Lei, Y., Yao, F. 2010. Creep behavior of bagasse fiber reinforced polymer composites. *Bioresource Technology*, **101**(9), 3280-3286.

Chapter 6: Conclusions and Future Work

6.1 CONCLUSIONS

Three natural fibers: kenaf, jute, sunn hemp and treated sunn hemp were compared in terms of the physical, thermal, and mechanical properties. Sunn hemp fiber was not selected for the subsequent research, although USDA was interested in this fiber, because sun hemp fiber did not show higher thermal stability or better mechanical properties than jute or kenaf fibers. Besides, the price of sunn hemp fiber is much higher than kenaf and jute fibers. Kenaf fiber was used in the following research. The reasons to select kenaf are: (1) kenaf fiber has a porous structure that can result in higher energy absorption of kenaf fiber reinforced composites; and (2) kenaf fiber has a higher specific modulus, a moderate price, and available kenaf crop within the US.

Based on the study of surface modification on sunn hemp fiber, chemical surface modification on kenaf fiber was not applied for the subsequent research. After the alkaline treatment, the sunn hemp fiber surface appearance improved. The sunn hemp moisture content, glass-transition temperature, and decomposition temperature also increased, indicating that the thermal stability was enhanced by the fiber modification. However, these improvements were not significant. Considering the time, energy and money spent for modification, it was not cost-effective or practical for industrial mass production. Therefore, kenaf fiber without surface modification was selected for subsequent research.

The influence of manufacturing conditions was investigated by evaluating the mechanical and thermal performance of KPNCs. It was found that temperature and time were the most significant processing factors for 6 mm thick KPNCs and the interaction between temperature and time was also a significant factor for 3 mm thick KPNCs. Although the overall effect of pressure was not found significant, post-hoc comparisons

showed significant differences in moduli attributable to pressure within the same levels of temperature and time.

For the 3 mm thick KPNCs, sample 7/230/60 had the highest tensile modulus. Because more fiber bondings are formed at higher temperature; the degradation of kenaf fiber is less at shorter time; and samples are more compact at higher pressing pressure. The manufacturing conditions at higher temperature (230 °C) and shorter time (60 s) are recommended in order to achieve best mechanical performance among eight samples studied in this research.

For the 6 mm thick KPNCs, longer processing time was needed since the sample thickness was doubled comparing to the 3 mm thick samples. Processing at 230 °C for 120 s (sample 5/230/120 or 7/230/120) gave the best mechanical properties among eight samples studied in this chapter. In contrast, samples 5/200/60 and 7/200/60, having the lowest moduli, were the best impact energy absorbers due to their panel-felt-panel sandwich structure.

The manufacturing conditions did not significantly affect the composite thermo-mechanical properties. KPNCs were more thermally stable than virgin PP plastics by adding kenaf fiber as reinforcement.

The notch effects on the tensile properties of KPNCs were evaluated by performing OHT and pin FHT tests. Three W/D ratios of 6, 3 and 2 were compared. The OHT test showed that the strength-reducing effect of stress concentration was mitigated greatly by the ductile-like behavior of KPNCs. Therefore, KPNCs were relatively insensitive to notch effects. The FHT test showed that the pins had little effect on the initial stiffness of the specimen. As to the strength and failure, the effects of pin tended to be dependent on the W/D ratios. After inserting the pin, the specimen with W/D= 3 showed more ductile behavior, while the specimen with W/D= 2 exhibited the lowest

breaking strength and strain. This may provide a basic understanding on the pin joint effects for KPNC materials used for automotive interior parts.

The predictions of the load-displacement curves by the XFEM model showed good agreement with experimental data for the OHT and FHT tests with the two W/D ratios. The crack propagation pattern predicted by XFEM also matched the experimental crack path very well. It indicated the applicability of XFEM in predicting the failure strength and simulating crack propagation of natural fiber reinforced composites with an open hole or pin filled hole.

The mechanical responses of KPNCs demonstrated a sensitivity to strain rates when performing tensile tests at various loading rates. As the strain rates increased, the failure stress, failure strain and Young's modulus increased. The strain rate effects were the result of viscoelastic behavior of KPNCs, which were then studied by performing the creep tests.

Both temperature and stress had statistically significant effects on the creep strains for KPNC and PP. The creep strains for KPNC and PP increased at elevated temperatures. However, the creep strain for KPNC was lower than that of PP at each temperature step. The difference between creep strains for KPNC and PP became larger at higher temperatures, indicating that KPNC had a better creep resistance than PP at elevated temperatures. A similar trend was also found on the stress effects. The recovery analyses indicated that KPNC has a higher recovery rate than PP at every 30 min creep cycle.

The four-element Burgers model was found be only be appropriate for characterizing short-term creep behavior (30 min in this study). In contrast, the Findley power law model was satisfactory for predicting the long-term creep performance of

KPNC and PP. Both models demonstrated their applicability in predicting composite creep behavior. However, some limitations of both models still exist.

The TTS master curves for KPNC and PP were established. The master curve for PP fit well with the three-day creep data, showing a better prediction accuracy. The master curve for KPNC under-estimated its long-term creep performance due to the multiphase thermo-rheological complexity of KPNC. Therefore, the accuracy of TTS method needs to be verified by experiments (the three-day creep test in this study), especially for composites with multiple components.

In summary, this research has three major accomplishments:

(1) The best manufacturing conditions among the eight combinations studied in this research were recommended for industrial mass production.

(2) The notch effects can provide a basic understanding for composite pin joint design in automobile interior application. The XFEM successfully predicted the composite strength and simulated the crack propagation.

(3) The creep behavior of KPNC comparing to virgin PP plastics has been studied extensively in this research. The long-term end-use performance of KPNC was predicted. The major contribution of this original work is to provide a comprehensive set of data and analyses of the creep behavior of a typical natural fiber nonwoven composite for other researchers to compare their work on nonwoven composites in the future.

6.2 SUGGESTED FUTURE WORK

In this research, manufacturing conditions were studied using a 2^3 factorial design with the objective of identifying acceptable combinations. Future research should focus on an experimental design with more than 2 levels of each processing factor, in order to

better understand the interactions suggested by our results. A response surface design of experiment would also enable a more accurate and thorough identification of the optimal processing conditions.

A laminate structure or a fiber-fiber structure could be introduced when establishing the XFEM model, instead of using an isotropic homogeneous material assumption in simulating the OHT and FHT tests. A better fit can be achieved when a more accurate structure assumption is used. More experimental parameters are needed to support the suggested models. This research can be further developed into the manufacture of 3D composite parts. The application of the validated XFEM model from 2D panels for 3D parts prediction could be explored.

In the study of creep properties, one more kenaf/PP fiber weight ratio of 70/30 could be made and compared with ratio of 50/50 in the long-term creep behavior of KPNCs.

Bibliography

ABAQUS. 2009a. ABAQUS/CAE User's Manual Daussalt Systemes, Inc., Vélizy-Villacoublay, France

ABAQUS. 2009b. Extended Finite Element Method (XFEM) in Abaqus http://www.simulia.com/download/rum11/UK/Advanced-XFEM-Analysis.pdf, Vol. 2013.

Acha, B.A., Reboredo, M.M., Marcovich, N.E. 2007. Creep and dynamic mechanical behavior of PP–jute composites: Effect of the interfacial adhesion. *Composites Part A: Applied Science and Manufacturing*, **38**(6), 1507-1516.

Agarwal, B. 1979. Static strength prediction of bolted joint in composite material. *Structures, Structural Dynamics, and Materials Conference, 20 th, St. Louis, Mo*. pp. 303-309.

Alvarez, V.A., Kenny, J.M., Vázquez, A. 2004. Creep behavior of biocomposites based on sisal fiber reinforced cellulose derivatives/starch blends. *Polymer Composites*, **25**(3), 280-288.

Aronsson, C.-G., Backlund, J. 1986. Tensile fracture of laminates with cracks. *Journal of Composite Materials*, **20**(3), 287-307.

Aziz, S.H., Ansell, M.P. 2004. The effect of alkalization and fibre alignment on the mechanical and thermal properties of kenaf and hemp bast fibre composites: Part 1 – polyester resin matrix. *Composites Science and Technology*, **64**(9), 1219-1230.

Backlund, J. 1981. Fracture analysis of notched composites. *Computers & Structures*, **13**(1), 145-154.

Bais-Singh, S., Biggers, S.B., Goswami, B.C. 1998. Finite Element Modeling of the Nonuniform Deformation of Spun-Bonded Nonwovens. *Textile Research Journal*, **68**(5), 327-342.

Banik, K., Karger‐Kocsis, J., Abraham, T. 2008. Flexural creep of all‐polypropylene composites: Model analysis. *Polymer Engineering & Science*, **48**(5), 941-948.

Basak, R.K., Saha, S.G., Sarkar, A.K., Saha, M., Das, N.N., Mukherjee, A.K. 1993. Thermal Properties of Jute Constituents and Flame Retardant Jute Fabrics. *Textile Research Journal*, **63**(11), 658-666.

Belytschko, T., Black, T. 1999. Elastic crack growth in finite elements with minimal remeshing. *International journal for numerical methods in engineering*, **45**(5), 601-620.

Bledzki, A.K., Faruk, O. 2004. Creep and impact properties of wood fibre–polypropylene composites: influence of temperature and moisture content. *Composites Science and Technology*, **64**(5), 693-700.

Bledzki, A.K., Reihmane, S., Gassan, J. 1996. Properties and modification methods for vegetable fibers for natural fiber composites. *Journal of Applied Polymer Science*, **59**(8), 1329-1336.

Brockmann, W., Geiß, P.L., Klingen, J., Schröder, K.B. 2008. *Adhesive bonding: materials, applications and technology*. Wiley-VCH.

Bueno, B., Costanzi, M., Zornberg, J. 2005. Conventional and accelerated creep tests on nonwoven needle-punched geotextiles. *Geosynthetics International*, **12**(6), 276-287.

Camanho, P.P., Lambert, M. 2006. A design methodology for mechanically fastened joints in laminated composite materials. *Composites Science and Technology*, **66**(15), 3004-3020.

Chang, F.-K., Scott, R.A., Springer, G.S. 1984. Failure of composite laminates containing pin loaded holes—method of solution. *Journal of Composite Materials*, **18**(3), 255-278.

Chapman, R.A. 2010. Applications of nonwovens on technical textiles. in: *Nonwoven textiles in automotive interiors*, (Ed.) Y. Chen, CRC Press LLC. Boca Raton.

Chen, J., Liu, F. 2010. Bast fibers: from plants to products 1ed. in: *Industrial Crops and Uses*, (Ed.) B.P. Singh, CABI. Cambridge, UK, pp. 308-325.

Chen, Y., Chiparus, O., Sun, L., Negulescu, I., Parikh, D.V., Calamari, T.A. 2005a. Natural fibers for automotive nonwoven composites. *Journal of Industrial Textiles*, **35**(Compendex), 47-62.

Chen, Y., Sun, L., Negulescu, I., Wu, Q., Henderson, G. 2007. Comparative Study of Hemp Fiber for Nonwoven Composites. *Journal of Industrial Hemp*, **12**(1), 27 - 45.

Chen, Y., Sun, L.F., Chiparus, O., Negulescu, I., Yachmenev, V., Warnock, M. 2005b. Kenaf/ramie composite for automotive headliner. *Journal of Polymers and the Environment*, **13**(2), 107-114.

Choi, J.-H., Chun, Y.-J. 2003. Failure load prediction of mechanically fastened composite joints. *Journal of Composite Materials*, **37**(24), 2163-2177.

Collings, T. 1982. On the bearing strengths of CFRP laminates. *Composites*, **13**(3), 241-252.

Cook, C.G., White, G.A. 1996. *Crotalaria juncea: a potential multi-purpose fiber crop*. ASHS Press, Arlington, VA.

Cook, J.G. 1984. *Handbook of textile fibers*. Merrow Publishing Co. Ltd.

Crews, J.H.J., Hong, C., Raju, I. 1981. Stress-Concentration Factors for Finite Orthotropic Laminates with a Pin-Loaded Hole. DTIC Document.

Cyras, V., Martucci, J., Iannace, S., Vazquez, A. 2002. Influence of the fiber content and the processing conditions on the flexural creep behavior of sisal-PCL-starch composites. *Journal of Thermoplastic Composite Materials*, **15**(3), 253-265.

Das, A., Kothari, V., Kumar, A., Mehta, M. 2005. Study on anisotropic creep behavior of nonwoven geotextiles. *Fibers and Polymers*, **6**(4), 313-317.

Das, M., Chakraborty, D. 2004. Reinforcing action of mercerization on bamboo fibers. *International Conference on Polymers for Advanced Technologies*, December 15-16, 2004, Thiruvananthapuram, India.

Davoodi, M.M., Sapuan, S.M., Ahmad, D., Ali, A., Khalina, A., Jonoobi, M. 2010. Mechanical properties of hybrid kenaf/glass reinforced epoxy composite for passenger car bumper beam. *Materials & Design*, **31**(10), 4927-4932.

Dolbow, J., Belytschko, T. 1999. A finite element method for crack growth without remeshing. *International journal for numerical methods in engineering*, **46**(1), 131-150.

Dornburg, V., Lewandowski, I., Patel, M. 2003. Comparing the land requirements, energy savings, and greenhouse gas emissions reduction of biobased polymers and bioenergy. *Journal of Industrial Ecology*, **7**(3 - 4), 93-116.

Edeerozey, A.M.M., Akil, H.M., Azhar, A.B., Ariffin, M.I.Z. 2007. Chemical modification of kenaf fibers. *Materials Letters*, **61**(10), 2023-2025.

Eichhorn, S.J., Baillie, C.A., Zafeiropoulos, N., Mwaikambo, L.Y., Ansell, M.P., Dufresne, A., Entwistle, K.M., Herrera-Franco, P.J., Escamilla, G.C., Groom, L., Hughes, M., Hill, C., Rials, T.G., Wild, P.M. 2001. Review: Current international research into cellulosic fibres and composites. *Journal of Materials Science*, **36**(9), 2107-2131.

El-Sabbagh, S., El-Hariri, D., El-Ghaffar, M. 2001. Effect of kenaf fibres on the properties of natural rubber vulcanizates. *Polymers & polymer composites*, **9**(8), 549-560.

EngineeringToolBox. 2013. Frictional Coefficients for some Common Materials and Materials Combinations http://www.engineeringtoolbox.com/friction-coefficients-d_778.html.

Findley, W.N., Davis, F.A. 1989. *Creep and relaxation of nonlinear viscoelastic materials*. Dover Publications.

Fisher, F.T., Brinson, L.C. 2001. Viscoelastic interphases in polymer–matrix composites: theoretical models and finite-element analysis. *Composites Science and Technology*, **61**(5), 731-748.

Flynn, J.H., Wall, L.A. 1966. A quick, direct method for the determination of activation energy from thermogravimetric data. *Journal of Polymer Science Part B: Polymer Letters*, **4**(5), 323-328.

Gassan, J., Bledzki, A.K. 1999a. Alkali treatment of jute fibers: relationship between structure and mechanical properties. *Journal of Applied Polymer Science*, **71**(4), 623-629.

Gassan, J., Bledzki, A.K. 1997. The influence of fiber-surface treatment on the mechanical properties of jute-polypropylene composites. *Composites Part A: Applied Science and Manufacturing*, **28**(12), 1001-1005.

Gassan, J., Bledzki, A.K. 1999b. Possibilities for improving the mechanical properties of jute/epoxy composites by alkali treatment of fibres. *Composites Science and Technology*, **59**(9), 1303-1309.

George, J., Sreekala, M., Thomas, S. 2004. A review on interface modification and characterization of natural fiber reinforced plastic composites. *Polymer Engineering & Science*, **41**(9), 1471-1485.

Gledhill, R., Kinloch, A. 1974. Environmental failure of structural adhesive joints. *The Journal of Adhesion*, **6**(4), 315-330.

Hadid, M., Rechak, S., Tati, A. 2004. Long-term bending creep behavior prediction of injection molded composite using stress–time correspondence principle. *Materials Science and Engineering: A*, **385**(1–2), 54-58.

Hao, A., Geng, Y., Xu, Q., Lu, Z., Yu, L. 2008a. Study of different effects on foaming process of biodegradable PLA/starch composites in supercritical/compressed carbon dioxide. *Journal of Applied Polymer Science*, **109**(4), 2679-2686.

Hao, A., Jiang, W., Chen, J. 2010. Sunn hemp fiber physical and thermal properties in comparison with kenaf and jute fibers. in: *Plant Fibers as Renewable Feedstocks for Biofuel and Bio-based Products*, (Ed.) F. Liu, CCG International Inc., pp. 2-15.

Hao, A., Sun, B., Qiu, Y., Gu, B. 2008b. Dynamic properties of 3-D orthogonal woven composite T-beam under transverse impact. *Composites Part A: Applied Science and Manufacturing*, **39**(7), 1073-1082.

Hao, A., Yuan, L., Zhao, H., Jiang, W., Chen, J.Y. 2012a. Notch effects on the tensile property of kenaf/polypropylene nonwoven composites in: *American Society of Mechanical Engineers IMECE2012-87108* Houston, TX.

Hao, A., Zhao, H., Jiang, W., Chen, J.Y. 2012b. Kenaf fiber nonwoven composites as automotive interior material: mechanical, thermal, and acoustical performance. in: *Society for the Advancement of Material and Process Engineering (SAMPE)*. May 21-24, Baltimore, MD.

Hao, A., Zhao, H., Jiang, W., Yuan, L., Chen, J. 2012c. Mechanical properties of kenaf/polypropylene nonwoven composites. *Journal of Polymers and the Environment*, **20**(4), 959-966.

Hart-Smith, L.J. 1986. Design and analysis of bolted and riveted joints in fibrous composite structures. *Douglas Paper 7739*, 1-15.

Hart-Smith, L.J. 1980. Mechanically-fastened joints for advanced composites-phenomelogical considerations and simple analysis. in: *Fibrous composites in structural design*, (Ed.) O.D. Leneo EM, Burke JJ Plenum Press. New York.

Hashin, Z. 1980. Failure criteria for unidirectional fiber composites. *Journal of applied mechanics*, **47**, 329.

Heikal, S.O., El‐Kalyoubi, S.F. 1982. Graft copolymerization of acrylonitrile onto bagasse and wood pulps. *Journal of Applied Polymer Science*, **27**(8), 3027-3041.

Herrera-Franco, P.J., Valadez-González, A. 2004. Mechanical properties of continuous natural fibre-reinforced polymer composites. *Composites Part A: Applied Science and Manufacturing*, **35**(3), 339-345.

Herrera-Franco, P.J., Valadez-González, A. 2005. A study of the mechanical properties of short natural-fiber reinforced composites. *Composites Part B: Engineering*, **36**(8), 597-608.

Holbery, J., Houston, D. 2006. Natural-fiber-reinforced polymer composites in automotive applications. *Jom*, **58**(11), 80-86.

Hollmann, K. 1996. Failure analysis of bolted composite joints exhibiting in-plane failure modes. *Journal of Composite Materials*, **30**(3), 358-383.

Hou, X., Acar, M., Silberschmidt, V.V. 2009. 2D finite element analysis of thermally bonded nonwoven materials: Continuous and discontinuous models. *Computational Materials Science*, **46**(3), 700-707.

IJSG. 2013. International Jute Study Group. Available from: http://www.jute.org/index.php Access on January 27, 2013.

Jacob, M., Thomas, S., Varughese, K.T. 2004. Mechanical properties of sisal/oil palm hybrid fiber reinforced natural rubber composites. *Composites Science and Technology*, **64**(7–8), 955-965.

Jazouli, S., Luo, W., Bremand, F., Vu-Khanh, T. 2005. Application of time–stress equivalence to nonlinear creep of polycarbonate. *Polymer Testing*, **24**(4), 463-467.

Jiang, W., Sun, L., Hao, A., Chen, J.Y. 2011. Regenerated cellulose fibers from waste bagasse using ionic liquid. *Textile Research Journal*, **81**(18), 1949-1958.

Jiang, W., Sun, L., Hao, A., Lynch, V., Chen, J.Y. 2012. Nano-particles modified cellulose films regenerated from ionic liquid solutions. *Journal of Nanostructured Polymers and Nanocomposites*, **8**(3), 71-77.

Jones, R. 1998. *Mechanics of composite materials*. CRC.

Joshi, S., Drzal, L., Mohanty, A., Arora, S. 2004. Are natural fiber composites environmentally superior to glass fiber reinforced composites? . *Composites Part A: Applied Science and Manufacturing*, **35**(3), 371-376.

Kador, A.F., Karlgren, C., Verwest, H.K. 1990. A Fast Growing Fiber Source for Papermaking. *Tappi Journal*, **73**(11), 205-209.

Kanninen, M., Rybicki, E., Brinson, H. 1977. A critical look at current applications of fracture mechanics to the failure of fibre-reinforced composites. *Composites*, **8**(1), 17-22.

Karnani, R., Krishnan, M., Narayan, R. 1997. Biofiber-reinforced polypropylene composites. *Polymer Engineering & Science*, **37**(2), 476-483.

KEFI. Properties of principal fibers, Available from: http://www.kenaf-fiber.com/en/infotec-tabella10.asp Access on January 13, 2013.

Keller, A. 2003. Compounding and mechanical properties of biodegradable hemp fibre composites. *Composites Science and Technology*, **63**(9), 1307-1316.

Knauss, W. 2008. The sensitivity of the time-temperature shift process to thermal variations—A note. *Mechanics of Time-Dependent Materials*, **12**(2), 179-188.

Kozlowski, R., Mieleniak, B., Helwig, M., Przepiera, A. 1999. Flame resistant lignocellulosic-mineral composite particleboards. *Polymer Degradation and Stability*, **64**(3), 523-528.

Kozłowski, R., Władyka-Przybylak, M. 2008. Flammability and fire resistance of composites reinforced by natural fibers. *Polymers for Advanced Technologies*, **19**(6), 446-453.

Krempl, E., Khan, F. 2003. Rate (time)-dependent deformation behavior: an overview of some properties of metals and solid polymers. *International Journal of Plasticity*, **19**(7), 1069-1095.

Kretsis, G., Matthews, F. 1985. The strength of bolted joints in glass fibre/epoxy laminates. *Composites*, **16**(2), 92-102.

Lee, S.-Y., Yang, H.-S., Kim, H.-J., Jeong, C.-S., Lim, B.-S., Lee, J.-N. 2004. Creep behavior and manufacturing parameters of wood flour filled polypropylene composites. *Composite Structures*, **65**(3–4), 459-469.

Lewin, M. 2006. *Handbook of fiber chemistry*. CRC, Boca Raton, FL

Li, X., Tabil, L., Panigrahi, S. 2007. Chemical Treatments of Natural Fiber for Use in Natural Fiber-Reinforced Composites: A Review. *Journal of Polymers and the Environment*, **15**(1), 25-33.

Liao, T., Adanur, S. 1999. Computerized Failure Analysis of Nonwoven Fabrics Based on Fiber Failure Criterion. *Textile Research Journal*, **69**(7), 489-496.

Liqing, X., Hongdi, Z., Lei, Z. 2001. Measurement and Analysis of Creep Property of Nonwoven Geotextiles by Photic Leverage [J]. *Technical Textiles*, **2**, 012.

Loh, W., Crocombe, A., Abdel Wahab, M., Ashcroft, I. 2002. Environmental degradation of the interfacial fracture energy in an adhesively bonded joint. *Engineering fracture mechanics*, **69**(18), 2113-2128.

Maldas, D., Kokta, B.V., Raj, R.G., Daneault, C. 1988. Improvement of the mechanical properties of sawdust wood fibre--polystyrene composites by chemical treatment. *Polymer*, **29**(7), 1255-1265.

Mazumder, B.B., Ohtani, Y., Cheng, Z., Sameshima, K. 2000. Combination treatment of kenaf bast fiber for high viscosity pulp. *Journal of wood science*, **46**(5), 364-370.

Mohanty, A., Misra, M., Drzal, L. 2002. Sustainable bio-composites from renewable resources: opportunities and challenges in the green materials world. *Journal of Polymers and the Environment*, **10**(1), 19-26.

Mohanty, A.K., Misra, M., Hinrichsen, G. 2000. Biofibres, biodegradable polymers and biocomposites: An overview. *Macromolecular Materials and Engineering*, **276-277**(1), 1-24.

Mueller, D.H., Kochmann, M. 2004. Numerical Modelling of Thermobonded Nonwovens. *International Nonwovens Journal*, **13**(1), 56-62.

Mwaikambo, L.Y., Ansell, M.P. 2002. Chemical modification of hemp, sisal, jute, and kapok fibers by alkalization. *Journal of Applied Polymer Science*, **84**(12), 2222-2234.

Nair, K.C.M., Diwan, S.M., Thomas, S. 1996. Tensile properties of short sisal fiber reinforced polystyrene composites. *Journal of Applied Polymer Science*, **60**(9), 1483-1497.

Narula, S.C., Wellington, J.F. 1982. The minimum sum of absolute errors regression: A state of the art survey. *International Statistical Review/Revue Internationale de Statistique*, 317-326.

Nayak, S.K., Mohanty, S., Samal, S.K. 2009. Influence of short bamboo/glass fiber on the thermal, dynamic mechanical and rheological properties of polypropylene hybrid composites. *Materials Science and Engineering: A*, **523**(1), 32-38.

Nielsen, L.E., Landel, R.F. 1993. *Mechanical properties of polymers and composites*. CRC.

Nuñez, A.J., Marcovich, N.E., Aranguren, M.I. 2004. Analysis of the creep behavior of polypropylene-woodflour composites. *Polymer Engineering & Science*, **44**(8), 1594-1603.

Ouajai, S., Shanks, R.A. 2005. Composition, structure and thermal degradation of hemp cellulose after chemical treatments. *Polymer Degradation and Stability*, **89**(2), 327-335.

Park, B.-D., Balatinecz, J.J. 1998. Short term flexural creep behavior of wood-fiber/polypropylene composites. *Polymer Composites*, **19**(4), 377-382.

Pearl, I.A. 1967. *The chemistry of lignin*. Marcel Dekker, New York.

Pervaiz, M., Sain, M.M. 2003. Carbon storage potential in natural fiber composites. *Resources, Conservation and Recycling*, **39**(4), 325-340.

Pooler, D.J., Smith, L.V. 2004. Nonlinear Viscoelastic Response of a Wood–Plastic Composite Including Temperature Effects. *Journal of Thermoplastic Composite Materials*, **17**(5), 427-445.

Pothan, L.A., Oommen, Z., Thomas, S. 2003. Dynamic mechanical analysis of banana fiber reinforced polyester composites. *Composites Science and Technology*, **63**(2), 283-293.

Ray, D., Sarkar, B.K., Basak, R.K., Rana, A.K. 2002. Study of the thermal behavior of alkali-treated jute fibers. *Journal of Applied Polymer Science*, **85**(12), 2594-2599.

Rösler, J., Harders, H., Bäker, M. 2007. *Mechanical behaviour of engineering materials: metals, ceramics, polymers, and composites*. Springer.

Rouison, D., Sain, M., Couturier, M. 2006. Resin transfer molding of hemp fiber composites: optimization of the process and mechanical properties of the materials. *Composites Science and Technology*, **66**(7–8), 895-906.

Rowlands, R., Rahman, M., Wilkinson, T., Chiang, Y. 1982. Single-and multiple-bolted joints in orthotropic materials. *Composites*, **13**(3), 273-279.

Saheb, D.N., Jog, J. 1999. Natural fiber polymer composites: a review. *Advances in Polymer Technology*, **18**(4), 351-363.

Scott, D.W., Lai, J.S., Zureick, A.-H. 1995. Creep behavior of fiber-reinforced polymeric composites: a review of the technical literature. *Journal of reinforced plastics and composites*, **14**(6), 588-617.

Sellers Jr, T., Miller, G.D., Fuller, M.J. 1993. Kenaf core as a board raw material. *Forest products journal*, **43**(7-8), 69-71.

Sgriccia, N., Hawley, M., Misra, M. 2008. Characterization of natural fiber surfaces and natural fiber composites. *Composites Part A: Applied Science and Manufacturing*, **39**(10), 1632-1637.

Shahkarami, A., Vaziri, R. 2007. A continuum shell finite element model for impact simulation of woven fabrics. *International Journal of Impact Engineering*, **34**(1), 104-119.

Sherman, L. 1999. Natural fibers: the new fashion in automotive plastics. in: *Plastics Technology*, Vol. 45, Gardner Publications, Inc., pp. 62-68.

Shi, A., Wang, L., Li, D., Adhikari, B. 2012. Characterization of starch films containing starch nanoparticles. Part 2: Viscoelasticity and creep properties. *Carbohydrate Polymers*.

Shibata, S., Cao, Y., Fukumoto, I. 2008. Flexural modulus of the unidirectional and random composites made from biodegradable resin and bamboo and kenaf fibres. *Composites Part A: Applied Science and Manufacturing*, **39**(4), 640-646.

Shinji, O. 2008. Mechanical properties of kenaf fibers and kenaf/PLA composites. *Mechanics of Materials*, **40**(4–5), 446-452.

Singh, B., Gupta, M. 2005. Natural fiber composites for building applications. in: *Natural Fibers, Biopolymers, and Biocomposites*, CRC Press.

Singh, B., Gupta, M., Verma, A. 1996. Influence of fiber surface treatment on the properties of sisal-polyester composites. *Polymer Composites*, **17**(6), 910-918.

Song, F., Zhao, H., Hu, G. 2012. Explicit cross-link relations between effective elastic modulus and thermal conductivity for fiber composites. *Computational Materials Science*, **51**(1), 353-359.

Starkova, O., Yang, J., Zhang, Z. 2007. Application of time–stress superposition to nonlinear creep of polyamide 66 filled with nanoparticles of various sizes. *Composites Science and Technology*, **67**(13), 2691-2698.

Sukumar, N., Moës, N., Moran, B., Belytschko, T. 2000. Extended finite element method for three‐dimensional crack modelling. *International journal for numerical methods in engineering*, **48**(11), 1549-1570.

Sullivan, J.L. 1990. Creep and physical aging of composites. *Composites Science and Technology*, **39**(3), 207-232.

Sydenstricker, T.H.D., Mochnaz, S., Amico, S.C. 2003. Pull-out and other evaluations in sisal-reinforced polyester biocomposites. *Polymer Testing*, **22**(4), 375-380.

Tajvidi, M., Falk, R.H., Hermanson, J.C. 2005. Time–temperature superposition principle applied to a kenaf-fiber/high-density polyethylene composite. *Journal of Applied Polymer Science*, **97**(5), 1995-2004.

Thoppul, S.D., Finegan, J., Gibson, R.F. 2009. Mechanics of mechanically fastened joints in polymer–matrix composite structures–a review. *Composites Science and Technology*, **69**(3), 301-329.

Toriz, G., Denes, F., Young, R.A. 2002. Lignin-polypropylene composites. Part 1: Composites from unmodified lignin and polypropylene. *Polymer Composites*, **23**(5), 806-813.

Treadwell, D.D., Alligood, M. 2008. Sunn hemp (Crotalaria juncea L.): A summer cover crop for Florida vegetable producers, HS 1126, Horticultural Sciences Department, University of Florida, Gainesville, FL.

Tscharnuter, D., Jerabek, M., Major, Z., Lang, R.W. 2011. Time-dependent poisson's ratio of polypropylene compounds for various strain histories. *Mechanics of Time-Dependent Materials*, **15**(1), 15-28.

Tserpes, K., Labeas, G., Papanikos, P., Kermanidis, T. 2002. Strength prediction of bolted joints in graphite/epoxy composite laminates. *Composites Part B: Engineering*, **33**(7), 521-529.

Ueng, C., Zhang, K.-D. 1985. Strength prediction of a mechanically fastened joint in laminated composites. *AIAA journal*, **23**(11), 1832-1834.

Urzhumtsev, Y.S. 1972. Prediction of the deformation and fracture of polymeric materials. *Polymer Mechanics*, **8**(3), 438-450.

Valadez-Gonzalez, A., Cervantes-Uc, J., Olayo, R., Herrera-Franco, P. 1999. Effect of fiber surface treatment on the fiber–matrix bond strength of natural fiber reinforced composites. *Composites Part B: Engineering*, **30**(3), 309-320.

Van de Velde, K., Baetens, E. 2000. Thermal and mechanical properties of flax fibers for composites reinforcement. in: *3rd International Wood and Natural Fiber Composites Symposium*. Kassel, Germany.

Vodicka, R. 2006. Thermoplastics for Airframe Applications-A Review of the Properties and Repair Methods for Thermoplastic Composites. *Thermoplastics for Airframe Applications: A Review of the Properties and Repair Methods for Thermoplastic Composites*.

Wambua, P., Ivens, J., Verpoest, I. 2003. Natural fibres: can they replace glass in fibre reinforced plastics? *Composites Science and Technology*, **63**(9), 1259-1264.

Wang, Y. 1999. Effect of Consolidation Method on the Mechanical Properties of Nonwoven Fabric Reinforced Composites. *Applied Composite Materials*, **6**(1), 19-34.

Wang, Y., Li, J. 1995. Properties of Composites Reinforced With E-Glass Nonwoven Fabrics. *Journal of Advanced Materials*, **26**(3), 28-34.

Ward, I.M. 1983. *Mechanical properties of solid polymers*. Wiley.

Whitney, J., Nuismer, R. 1974. Stress fracture criteria for laminated composites containing stress concentrations. *Journal of Composite Materials*, **8**(3), 253-265.

Xie, X.L., Fung, K.L., Li, R.K.Y., Tjong, S.C., Mai, Y.W. 2002. Structural and mechanical behavior of polypropylene/ maleated styrene-(ethylene-co-butylene)-styrene/sisal fiber composites prepared by injection molding. *Journal of Polymer Science Part B: Polymer Physics*, **40**(12), 1214-1222.

Xu, Y. 2009. Creep Behavior Of Natural Fiber Reinforced Polymer Composites, Louisiana State University.

Xu, Y., Lee, S.Y., Wu, Q. 2011. Creep analysis of bamboo high‐density polyethylene composites: Effect of interfacial treatment and fiber loading level. *Polymer Composites*, **32**(5), 692-699.

Xu, Y., Wu, Q., Lei, Y., Yao, F. 2010. Creep behavior of bagasse fiber reinforced polymer composites. *Bioresource Technology*, **101**(9), 3280-3286.

Xue, Y., Du, Y., Elder, S., Wang, K., Zhang, J. 2009. Temperature and loading rate effects on tensile properties of kenaf bast fiber bundles and composites. *Composites Part B: Engineering*, **40**(3), 189-196.

Yan, U., Sun, H., Wei, W., Chang, F. 1998. Response and Failure of Composite Plates With a Bolt-Filled Hole. DTIC Document.

Yancey, R.N., Pindera, M.-J. 1990. Micromechanical analysis of the creep response of unidirectional composites. *Journal of Engineering Materials and Technology*, **112**(2), 157-163.

Yang, H., Yan, R., Chen, H., Lee, D.H., Zheng, C. 2007. Characteristics of hemicellulose, cellulose and lignin pyrolysis. *Fuel*, **86**(12–13), 1781-1788.

Ye, C., Shi, J., Cheng, G.J. 2012. An eXtended Finite Element Method (XFEM) study on the effect of reinforcing particles on the crack propagation behavior in a metal–matrix composite. *International Journal of Fatigue*, **44**(0), 151-156.

Yu, L., Waisman, H., Shi, J., Liu, P., Jum, L. 2008. Pre-processing Toolkit for Three-dimensional X-FEM. *Aerospace and Electronics Conference, 2008. NAECON 2008. IEEE National*, 16-18 July 2008. pp. 265-272.

Yuan, X., Jayaraman, K., Bhattacharyya, D. 2004. Effects of plasma treatment in enhancing the performance of woodfibre-polypropylene composites. *Composites Part A: Applied Science and Manufacturing*, **35**(12), 1363-1374.

Yussuf, A.A., Massoumi, I., Hassan, A. 2010. Comparison of polylactic acid/kenaf and polylactic acid/rise husk composites: the influence of the natural fibers on the mechanical, thermal and biodegradability properties. *Journal of Polymers and the Environment*, **18**(3), 422-429.

Zampaloni, M., Pourboghrat, F., Yankovich, S.A., Rodgers, B.N., Moore, J., Drzal, L.T., Mohanty, A.K., Misra, M. 2007. Kenaf natural fiber reinforced polypropylene composites: A discussion on manufacturing problems and solutions. *Composites Part A: Applied Science and Manufacturing*, **38**(6), 1569-1580.